DIELECTRIC BARRIER DISCHARGE (DBD) PLASMA STERILIZATION: AN IN-DEPTH STUDY OF THE FACTORS CONTRIBUTING TO AND ENHANCING THE STERILIZATION PROCESS

By

NAVYA MASTANAIAH

A DISSERTATION PRESENTED TO THE GRADUATE SCHOOL
OF THE UNIVERSITY OF FLORIDA IN PARTIAL FULFILLMENT
OF THE REQUIREMENTS FOR THE DEGREE OF
DOCTOR OF PHILOSOPHY

UNIVERSITY OF FLORIDA

2013

© 2013 Navya Mastanaiah

To the one person who believed in me with her whole heart.
Mom
Ad Astra Per Aspera

ACKNOWLEDGMENTS

This thesis has seen the light of day, because of the direct support and encouragement of a number of people as well as the indirect inspiration and guidance provided by a vast number of people, whose names if I listed here, would make for a separate dissertation-sized document!

First and foremost, heartfelt gratitude is due to my advisor, Dr. Subrata Roy. I have learnt a tremendous amount from his thoughtful input, his patience and encouragement and his constant reminder to “think about the physics of the problem”.

An equally heartfelt note of thanks is due to Dr.Judith Johnson, who has provided me, a student with an engineering background, a functional and tremendously helpful understanding in the biological aspects of my research. Her enthusiasm and readiness in helping me plan my experiments truly inspired me to give my best.

Thanks are also due to my committee members, Dr.David Hahn, Dr. Renwei Mei and Dr.Tommy Angelini. Their valuable suggestions and expert guidance helped me better understand many facets of the work that has gone into this dissertation.

I have been blessed with a fun group of lab mates and would be highly remiss if I did not thank James, Mark, Tomas, Ryan, Jignesh, Ariel, Moses, Arnob, Pengfei and Ankush for the high-spirited discussions, the thoughtful suggestions and for the memorable lab get-togethers. Especially James for cheerfully guiding me in my initial days at APRG. Of course, my work in plasma sterilization would be incomplete if I did not thank Raul A. Chinga for his invaluable work in optimizing the electrical circuit used for plasma generation. It is truly a pleasure to work with and learn from someone so patient and meticulous

Words are not enough to express gratitude to all my wonderful friends, throughout my time here, for all the late night discussions, the potlucks, the gator nights and for so much more. Especially Navina and Vaishnavi, who've been there for me through the roughest of times and Siddhesh and Ajeta, who have a wonderful way of cheering me up every time.

Last, but definitely not the least, this dissertation and every other success I have been and will be fortunate enough to see in the future is dedicated to and solely because of the constant love, support and strength provided by the three most important people in my life: Mom, Dad and Kutty. I am nothing if not for you three.

TABLE OF CONTENTS

ACKNOWLEDGMENTS 4

LIST OF TABLES 8

LIST OF FIGURES 9

ABSTRACT 14

CHAPTER

1 INTRODUCTION 16

1.1 Sterilization- Current State of the Art 16
1.2 What is Plasma? 21
1.3 DBD Plasma Sterilization 27
1.3.1 Factors involved in Plasma Sterilization- Parametric studies 29
1.3.2 Mechanism of Plasma Sterilization 36
1.3.3 Plasma interaction with biofilms 44
1.3.4 Numerical modeling of Plasma Sterilization 45

2 RESEARCH MOTIVATION 48

3 METHODS & MATERIALS 50

3.1 Experimental setup used for plasma sterilization experiments 50
3.2 Design of the Plasma Device 52
3.3 The portable sterilization setup 56
3.4 Description of Biological Pathogens Tested 57
3.5 Experimental Protocols Followed 61
3.5.1 Preparation of bacterial biological test samples for experiments: 62
3.5.2 Post-processing of bacterial samples after experiments 63
3.5.3 Ozone Safety Protocol 64

4 PARAMETRIC STUDIES IN DBD SURFACE PLASMA STERILIZATION 67

4.1 Type of Microorganism 67
4.2 Inoculation Volume 79
4.3 Nature of Dielectric Material 81
4.4 Input power and frequency 92
4.5 Operating pressure 97
4.6 Discussion 101

5 UNDERSTANDING THE MECHANISM OF DBD SURFACE PLASMA STERILIZATION 106

5.1 Spectroscopic studies 107

5.2 Ozone studies 114
5.2.1 Characterization of ozone production and decay during DBD plasma generation 115
5.2.2 The effect of ozone produced during DBD plasma generation on *E. coli* 125
5.3 Temperature Studies 134
5.4 Microbiological analysis 142
5.4.1 Evaluation of membrane damage by Live/Dead® BacLight™ Assay. 143
5.4.2 Mutation Studies. 148
5.4.3 Microscopic analysis of plasma interaction with *B. subtilis* biofilms... 149
5.5 Discussion 152

6 CONCLUDING REMARKS & RECOMMENDATIONS FOR FUTURE WORK 160

6.1 Scope of Technology 163
6.2 Further analysis of the mechanism of plasma sterilization 164
6.3 Numerical modeling in plasma sterilization 165

REFERENCES 168

BIOGRAPHICAL SKETCH 178

LIST OF TABLES

Table 1-1. A comparison of various factors of an ideal sterilant for different sterilization methods [16] 20

Table 1-2. Micro-discharge properties in air at atmospheric pressure [24] 25

Table 3-1. Listing of all the microorganisms tested 58

Table 3-2. Description of organelles and essential proteins in different types of microorganisms 60

Table 4-1. Results obtained from Plasma Sterilization Experiments with BSL-II pathogens 78

Table 4-2. Description of protocols that the different devices were subjected to, prior to SEM Testing. 85

Table 5-1. Values of the constants used in Equation (5-5)-(5-6) 119

LIST OF FIGURES

Figure 1-1. Schematic of A) Sterrad ® and B) Plazlyte ™ Plasma Sterilization Systems [14] 19

Figure 1-2. Plasma temperatures and number densities [21] 21

Figure 1-3. Dependence of voltage on current for various DC discharges [23] 23

Figure 1-4. A) Volume Plasma DBD configuration used in most experimental setups. Schematic based on a similar schematic shown in [25] B) DBD configuration used in this study 24

Figure 1-5. End-on-view of micro-discharges in atmospheric pressure air [24] 26

Figure 1-6. Schematic of an apparatus used earlier on for plasma sterilization [39] 28

Figure 1-7. Various Factors involved in DBD Plasma sterilization 30

Figure 1-8. Comparison of spore mortality [log10(No/N)] in MW and RF O2/CF4 plasmas, after 5 minutes of exposure (P=200W, p= 80 mTorr, F= 80sccm, [CF4]= 12%) [59] 33

Figure 1-9. Results of inactivation of E. coli on the agar surface by direct (a,b) and indirect (c,d) plasma treatment [63] As is evident, direct plasma leads to a clean spot in the center with no bacterial growth, while indirect plasma leads to incomplete inactivation. 34

Figure 1-10. Wavelength and energy of radiation in the UV and visible portion of the spectrum [59] 36

Figure 1-11. UV spectrum of a DBD in air in the 200-300 nm wavelength range [68] .. 39

Figure 1-12. Increase of sample temperature vs. plasma dissipated power for a DBD volume plasma in air at atmospheric pressure [68]. 42

Figure 1-13. Schematic illustration of the different phases in a plasma sterilization survival curve [67] 43

Figure 1-14. A) Computational Model used, depicting the breakup of the skin into different layers as well as the plasma source placement B) Electric field inside the epidermal layer, at different simulation time-points [86] 46

Figure 3-1. Schematic of the experimental setup used 50

Figure 3-2. Three ‘powered’ electrode configurations considered (All dimensions in’mm’). ‘Black’ denotes powered while ‘grey’ denotes grounded (*on the opposite side of the dielectric surface*). 53

Figure 3-3. The three electrode configurations, shown in Figure 3-2, when powered .. 54

Figure 3-4. Stamp Test (at 60s) for three different electrode designs A) Sawtooth B) π-electrode C) comb-like electrode design 55

Figure 3-5. Portable experimental setup, using devices made of Rogers® 3003C semi-ceramic dielectric 57

Figure 3-6. The bacterial cell wall (a) The Gram-positive envelope (b) The Gram-negative envelope 58

Figure 3-7. Structure of the yeast cell wall. The wall is primarily composed of mannoproteins and β-glucan that is linked (1->3) and (1->6). Ergosterol is the major lipid component of the underlying plasma structure. [88] 59

Figure 3-8. Typical growth curve for a bacterial population in a batch culture [89] 61

Figure 4-1. Survival curves obtained using FR4 plasma devices and *S. cerevisiae* (Yeast) and *E. coli* as test pathogens. Complete sterilization is obtained within 90-120s. 72

Figure 4-2. Survival curves, using FR4 devices for *B. subtilis* cells grown in LB and MSgg medium 74

Figure 4-3. Survival curves, using FR4 devices for G*. stearothermophilus* spores 76

Figure 4-4. Comparison of D-values for the different test microorganisms, using FR4 devices 77

Figure 4-5. Survival curves for inoculation volume= 40 µl of E. coli 80

Figure 4-6. Survival curves comparing FR4 and SC plasma devices for A) *S. cerevisiae and B) E. coli* 83

Figure 4-7. Comparison of D-values for the different (dielectric, test pathogen) 83

Figure 4-8. SEM images of FR4 devices at 2000x magnification. Images A-E and Images F-J correspond to the SEM images of the dielectric and electrode surface respectively of the devices used for Protocols#1-5. 87

Figure 4-9. SEM images of SC devices at 2000x magnification. Images A-E and Images F-J correspond to the SEM images of the dielectric and electrode surface respectively of the devices used for Protocols#1-5. 87

Figure 4-10. EDS analysis of the A) dielectric surface B) electrode surface for a FR4 device 89

Figure 4-11 EDS analysis of the A) dielectric surface B) electrode surface for a SC device 90

Figure 4-12. Comparison between a FR4 device and a PMMA device. A and B depict the unpowered FR4 and PMMA devices respectively. C and D depict the same device, powered. 91

Figure 4-13. Comparison of the temporal variation of input power for clean and inoculated devices in the case of FR4 and SC dielectric. 92

Figure 4-14. Comparison of the average measured input power (W) for each input voltage (kV p-p) 93

Figure 4-15. Temporal variation of input power for different input voltages using inoculated devices for A) FR4 and B) SC. 94

Figure 4-16. Dependence of sterilization effectiveness on input voltage (V) 95

Figure 4-17. A) Temporal variation of input power for an inoculated FR4 and SC device (f= 60 kHz, V= 9-10 kV p-p) B) Dependence of sterilization on input voltage at f= 60 kHz, for FR4 and SC 96

Figure 4-18. Images of the devices at A) 760 Torr B) 500 Torr C) 400 Torr 98

Figure 4-19. Sterilization behavior at reduced pressures for A) FR4 and B) SC plasma devices. Two sterilization times (t= 60s and 120s) were tested, using *E. coli* at the reduced pressures. 100

Figure 5-1. Spectral signature of A) a clean FR4 device and B) an inoculated FR4 device. Y-axis lists emission intensity in arbitrary unit. 107

Figure 5-2. Spectral signature of A) a clean SC device and B) an inoculated SC device. Y-axis lists emission intensity in arbitrary unit. 108

Figure 5-3. Expanded version of (A) Spectral signature of a clean FR4 device (B) Spectral signature of an inoculated FR4 device. 110

Figure 5-4. Expanded version of (A) Spectral signature of a clean SC device (B) Spectral signature of an inoculated SC device. 110

Figure 5-5. Spectroscopic comparison of (A) FR4 devices and (B) SC devices at reduced pressure 112

Figure 5-6. Schematic of Chamber#4. The grey square in the middle represents the plasma device. The black short lines represent the different locations at which ozone measurements are taken. These locations are uniformly spaced (4” apart), along the X- and Y- axis. 116

Figure 5-7. (A) Spatial variation of ozone distribution along the X-axis in the sterilization chamber (B) Spatial variation of ozone distribution along the Y-axis in the sterilization chamber..... 117

Figure 5-8 (A) and (B) showing the two different configurations in which the device is placed. 118

Figure 5-9. Comparison of ozone concentrations in all four chambers. The plasma device is powered at 0 min and turned off at 2 minutes, after which the setup is allowed to sit for another 5 minutes 120

Figure.5-10. Correlation of the ozone levels with the corresponding chamber volumes. The different time points (60,120,240,360,420s) represent ozone measurements in each chamber at that particular time point. 121

Figure 5-11. Correlation of the total number of ozone molecules present in each chamber at t= 60,120,240,360,420s) to the respective chamber volumes. The X-axis is plotted on a $\log_2$scale for easier comparison. #1-#4 represents the different chambers. 123

Figure 5-12. Comparison of ozone production during 7 minutes for FR4 versus SC. The plasma device is powered at 0 min and turned off at 2 minutes, after which the setup is allowed to sit for another 5 minutes..... 124

Figure 5-13. Experimental schematic for the ozone exposure tests. 125

Figure 5-14: Inactivation plots due to ozone exposure with (A) FR4 plasma generator and (B) SC plasma generator..... 127

Figure 5-15. Inactivation plots due to ozone exposure in the different chambers using a FR4 plasma generator and an inoculated FR4 substrate..... 129

Figure 5-16. Comparison of ozone production with and without charcoal for Chamber#1. Plasma is turned off at 2 min. 130

Figure 5-17. Inactivation plots due to ozone exposure in Chamber#1 with and without charcoal. A clean FR4 device was used as the ozone generator and covered with charcoal when needed. The device was powered for 2 minutes. 131

Figure 5-18. DBD Surface Plasma Sterilization, comparing air and nitrogen as the discharge gas. Two sterilization times (60s and 120s) are tested, using *E, coli* as the test pathogen..... 133

Figure 5-19. Variation of temperatures at t= 30s, 60s,90s, 120s for Clean FR4 device (A-D) and Inoculated FR4 device (E-H)..... 137

Figure 5-20. Variation of temperatures at t= 30s, 60s,90s, 120s for Clean SC device (A-D) and Inoculated SC device (E-H)..... 138

Figure 5-21. Comparison of average surface temperatures during plasma generation for clean and inoculated FR4 and SC devices, measured using an infrared camera. 139

Figure 5-22. Sterilization plots analyzing the effect of temperature on inoculated FR4 and SC devices. In each case, the inoculated devices were heated up to the average temperature measured during plasma generation. 140

Figure 5-23. Sterilization plots analyzing the effect of temperature on inoculated FR4 and SC devices. In each case, the inoculated devices were heated up to the maximum temperature measured during plasma generation..... 141

Figure 5-24. Fluorescence Images obtained of the different cell suspensions after exposure to plasma for t= 0,30,60,90 and 120s respectively. A-E correspond to t= 0-120s respectively..... 144

Figure 5-25. An example of the calibration curve calculated by measuring $Ratio_{G/R}$ for cell suspensions with different proportions of live/dead cells. 145

Figure 5-26. Plot of the $Ratio_{G/R}$ calculated after different plasma exposure times 147

Figure 5-27. Images of bio-films before, during and after plasma exposure. CFP indicates motile cells and YFP indicates matrix-producing cells. A-E indicates the imaging order of the biofilms. 151

Figure 5-28. Mean intensity variation in CFP and YFP modes for imaging order A-E. On the Y-axis is plotted the % reduction in intensity (-ve because of the reduction). Points 1-5 correspond to frames A-E..... 151

Figure 5-29. Plot of pH values, obtained by rinsing devices with Millipore water after plasma generation and measuring the pH value of this water in each case. Both FR4 and SC dielectrics are compared. 157

Figure 6-1. Scheme of reactions used for Lipid Peroxidation [114] 167

Abstract of Dissertation Presented to the Graduate School
of the University of Florida in Partial Fulfillment of the
Requirements for the Degree of Doctor of Philosophy

Dielectric Barrier Discharge (DBD) Plasma Sterilization: An in-depth study of the factors contributing to and enhancing the sterilization process

By

NAVYA MASTANAIAH

August, 2013

Chair: Subrata Roy
Major: Aerospace Engineering

Plasma is an ionized gas comprised of charged particles, neutrals and UV photons. Sterilization is defined as any process that kills all micro-organisms on a surface. Plasma based sterilization or plasma sterilization is a method in which plasma is used for sterilization. It offers a fast, low-temperature, versatile alternative to conventional sterilization methods. Plasma sterilization can be divided into two regimes: volume and surface plasma sterilization. While a lot of research has been done in understanding the former, the latter is yet to be fully explored. The purpose of this study is to identify and understand the key contributors controlling the process of surface plasma sterilization under atmospheric conditions.

This is accomplished by a two-pronged approach of parametric studies and diagnostic studies. The plasma used for the purpose of this study is known as dielectric barrier discharge (DBD) plasma. DBD plasma generation is influenced by numerous factors such as input power, frequency, dielectric material used etc. In parametric studies some of these factors are selectively controlled to help us understand their effect on the sterilization process.

Diagnostic equipment is used to characterize the DBD plasma in terms of spectroscopic signature, ozone levels produced and surface temperatures of the dielectric surface during plasma generation. Diagnostic studies help us identify the role of these different plasma features for a better insight into the process of plasma sterilization. Plasma interaction with the cell has also been visualized using both high-resolution microscopy as well as fluorescence microscopy. Fluorescent staining of the supernatant obtained from bacterial samples treated with plasma helps identify which cell component has been affected by plasma exposure.

The goal of this dissertation is to help explain the key mechanisms of surface plasma sterilization, understanding of which will allow access to many life-critical medical technologies including self-sterilizing operating tables and food counters, and even portable kits to provide fast, accessible sterilization for triage situations.

CHAPTER 1
INTRODUCTION

Plasma sterilization is quickly evolving into a sought after method of sterilization in multiple industries: food preparation, healthcare, medicine etc. Specifically, DBD plasma sterilization is an interesting topic to pursue due to its ability to operate at atmospheric conditions, as well as its operational simplicity. It finds application in a wide-variety of real-world scenarios. However, a deeper understanding of the fundamentals of plasma sterilization is required before this technology can be transplanted from research to reality. This study is an effort in that direction.

1.1 Sterilization- Current State of the Art

Sterilization destroys all micro-organisms [1]. It is the certainty that everything is killed. The term ‘micro-organisms’ covers a broad spectrum of pathogens, including bacteria, fungi, viruses, endospores and prions. Of these, endospores and prions deserve a special mention, because of the challenge they pose to existing methods of sterilization. Endospores are tough, dormant, reproductive cells, produced by some bacteria as a survival mechanism when threatened by harsh conditions. In times of stress, this bacterium replicates its DNA and develops a double membrane and thick cell wall around it, forming what is called an endospore. Once the harmful conditions tide over, the endospore re-germinates. Endospores are particularly resistant to most of the current sterilization methods. In fact, spores are often used as biological indicators to test the sterilization efficiency of techniques such as autoclaving. One factor for this resistance is attributed to the lower water content of the spore [2]-[3].

Prions are infectious agents composed of proteins in a mis-folded form. They differ from other infectious agents, which contain nucleic acids. When a prion enters a

healthy organism, it acts as a template to guide the misfolding of more proteins into prion forms. Sterilizing prions therefore involves the 'denaturation' of the protein to such a state that it is no longer capable of inducing protein mis-folding in molecules containing normal proteins. Prions are usually highly resistant to proteases (enzymes capable of abolishing a protein's function), heat, radiation and chemical treatments, although their infectivity can be reduced by such treatments. All known prion-diseases affect structures of the brain or other neural tissues, and are all currently untreatable and universally fatal [4].

Conventional sterilization methods consist of moist and dry heat sterilization [5]-[6]; chemical sterilization using ethylene oxide and glutaraldehyde [7]-[8]; irradiation by high energetic rays like γ-irradiation and UV irradiation and more recently, gas plasma sterilization[9-11]. A brief description of each of these methods is given below. It is to be noted that for all these methods, effective sterilization can be achieved *only* when the object to be sterilized is initially wiped clean, so that any organic matter remaining on the instrument is removed.

Heat sterilization: This primarily consists of two techniques: moist heat sterilization and dry heat sterilization. Moist heat sterilization (autoclaving) uses high pressure and temperature to achieve complete sterilization. Unwrapped objects are exposed to steam at 121^{o}C for 20 minutes or at 137^{o}C for 15 minutes. Dry heat sterilization comprises exposing unwrapped objects to intense heat (170^{o}C) for 1 hour and then cooling them down for 2-2.5 hours. In both moist and dry heat sterilization, cycles begin only when the objects being sterilized reach the specified sterilization temperature and significant amounts of time are required for cooling before use. In

addition to the time required, the major drawback to heat sterilization methods is that they damage many heat-sensitive materials.

Chemical sterilization: This technique utilizes common disinfectants such as Ethylene oxide (EtO), glutaraldehyde or formaldehyde. Objects need to be soaked at least for 10 hours in 2-4% glutaraldehyde solution or for 24 hours in 8% formaldehyde solution. EtO sterilization is a much more complex procedure, requiring a chamber in which the contaminated objects are exposed to EtO vapor for at least 2 hours and thereafter the chamber is aerated for a long period to dispel any toxic vapor.

Irradiation: This process uses highly energetic gamma (γ) rays. Gamma irradiation is the irradiation of contaminated matter using photons in the gamma part of the electromagnetic spectrum (wavelength<10^{-12} m). Radiation is obtained through radio-isotopes such as cobalt-60 or cesium-137. It is used to sterilize medical devices used in operations and other healthcare treatmenets. Gamma-irradiation is also used for sterilization in food, pharmaceutical, cosmetic, horticultural and automotive industries. However owing to the inherent hazards of such a technique, the main radioactive source has to be shielded for the safety of the operators [12]

UV irradiation is another disinfection method that uses at short wavelengths (~254 nm) to kill micro-organisms. At this wavelength, it is effective in destroying the nucleic acids in micro-organisms by a process known as dimerization [13].

Gas plasma sterilization: Commercial plasma sterilization systems, called Sterrad® and Plazlyte ™ were introduced a couple of years ago. Schematics of both systems are shown in Figure 1-1.

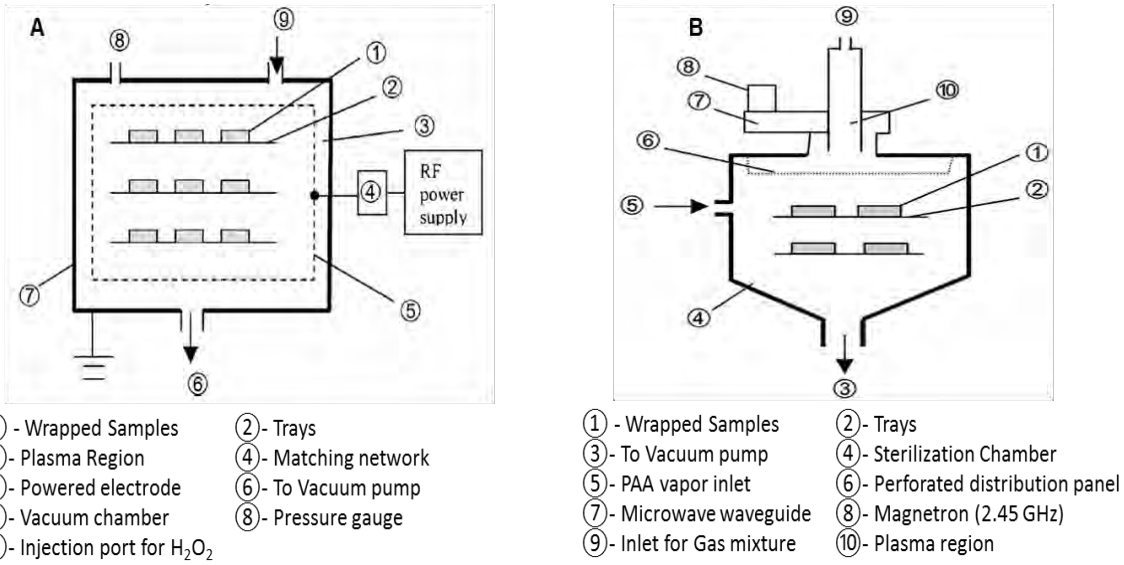

Figure 1-1. Schematic of A) Sterrad ® and B) Plazlyte ™ Plasma Sterilization Systems [14] .

The Sterrrad®, shown in Figure 1-1(A), consists of a vacuum chamber in which wrapped items were placed on trays and exposed to hydrogen peroxide (H_2O_2) gas for 45 minutes. Following this, 300 W of RF power at 13.56 MHz was applied at very low pressure to create plasma inside the chamber. The system's efficacy has been shown to be mainly due to the H_2O_2 vapor with the plasma primarily removing the toxic residue. Similarly, the Plazlyte^{TM}, shown in Figure 1-1(B) consisted of a vacuum chamber in which wrapped items were placed. Peracetic acid (PAA) vapor was pumped into the chamber upstream of where the wrapped items were placed. Plasma treatment consisted of excitation of a mixture of oxygen, hydrogen and argon at low-pressure, using a microwave (MW) plasma at 2.45 GHz. The Plazlyte treatment consisted of alternate cycles of the vapor treatment and plasma treatment. Note that both of these sterilization systems are not plasma sterilizers, in the strict sense of the term, as the objects being sterilized do not come into contact with the plasma [15]. Eventually in

1998, the FDA issued an alert on using the Plazlyte™ system for ophthalmic instruments. The problem appeared to be the deposition of copper and zinc salts on devices sterilized with this system, which caused serious eye injuries in some patients (FDA talk paper T98-17, 1998).

An ideal sterilant as defined by Moisan et al. [16] should provide (a) short sterilization times (b) low processing temperatures (c) versatility of operation and (d) harmless for patients, operators and materials. Table 1-1 provides a comparison of all these factors for the different sterilization methods discussed.

Table 1-1. A comparison of various factors of an ideal sterilant for different sterilization methods [16]

Sterilization Method	COMPARISON			
	Sterilization time	Processing Temperatures	Toxicity/Handling Hazard	Versatility
Autoclaving	50-60 min	121°C- 137°C	Cooling down time required	Cannot be used for heat-sensitive polymers
Dry Heat Ovens	3-4 hours	160°C- 170°C	Cooling down time required	Same limitations as autoclaving
EtO Sterilization	1-2 hours	55 °C	Toxic vapors, possibility of chemical residue on objects	Can damage certain sensitive polymers
UV Irradiation	Dependent on UV dosage	Low temperatures	Exposure to UV rays can burn the skin and eyes	Can effectively irradiate the topmost layer of cells only. Dependent on object geometry
γ-Irradiation	Short times, but requires a longer standing time for radiation levels to reduce to safe levels.	High temperature	Operation requires thick concrete shields and safety measures for handlers.	Used only in some facilities due to low availability of radioactive isotopes

DBD plasma at atmospheric conditions meets all of the above requirements for an ideal sterilant. The time scales of plasma sterilization range from 2-20 minutes. Since it is generated from air, once the plasma is turned off, ionized species recombine into components of air, which are non-toxic. Finally, because it is low-temperature and non-toxic, it can be used with a wide variety of materials, even heat-sensitive polymers.

There is an abundant cache of literature on experimental methods of plasma sterilization, wherein different plasma sources, using different plasma parameters, have been used to sterilize different standard bacterial samples [17]-[20]. Before this topic can be discussed further, a brief introduction to plasma, especially DBD plasma must be provided.

1.2 What is Plasma?

Plasma is known as the fourth state of matter. It makes up the majority of the universe. The best known natural plasma phenomenon in earth's atmosphere is lightning [21].

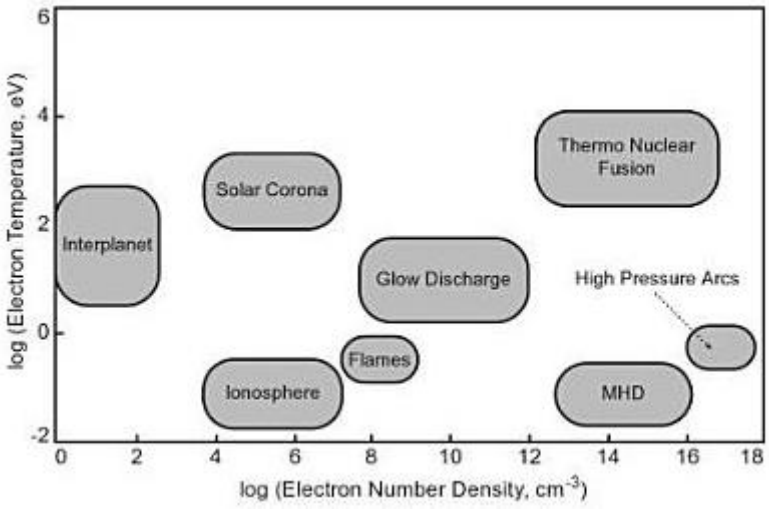

Figure 1-2. Plasma temperatures and number densities [21]

The seeds for this theory were first sown in about 1750, when Benjamin Franklin suspected that lightning is an electrical current and conducted experiments with a kite. Another natural phenomenon is the aurora borealis. Natural and man-made plasmas occur over a wide range of pressures, temperatures and electron number densities. Figure 1-2 above shows this diversity.

Apart from naturally occurring plasmas, plasmas can also be generated for industrial purposes. Plasma finds applications in electronics, lasers, fluorescent lamps, television screens, computer and cell-phone hardware and more recently, in medical applications.

Plasma is an ionized gas, made up of ions, electrons and neutrals. It is most commonly categorized either on the basis of temperature or electron-number density.

Temperature: Laboratory plasmas can be distinguished into two categories: high-temperature plasmas and low-temperature plasmas [22]. These plasmas can also be divided into local thermal equilibrium (LTE) plasmas and non-LTE plasmas. The heavy particles in plasmas (ions, atoms) are at a much lower temperature than the electrons, which are typically highly energetic particles. In a high-temperature plasma, the high temperature serves to equilibrate the high temperature of the electrons with the ion temperature, thus establishing LTE. In non-LTE plasma, this thermal equilibrium is not established. LTE discharges are typically used for high-temperature applications such as welding. Non-LTE plasmas are typically used for low-temperature applications such as etching or plasma deposition.

Degree of ionization of plasmas**:** A common condition in plasma chemistry is for the gases to be only partially ionized [21]. The ionization degree (ratio of density of

major charged species to neutral species) for most conventional plasma-chemical systems is in the range of 10^{-7}-10^{-4}. Plasmas, with an ionization degree close to one are called fully ionized plasmas**.** Most thermo-nuclear and space plasma systems belong to this category. Weakly ionized plasmas**,** with a low degree of ionization, encompass most laboratory plasmas.

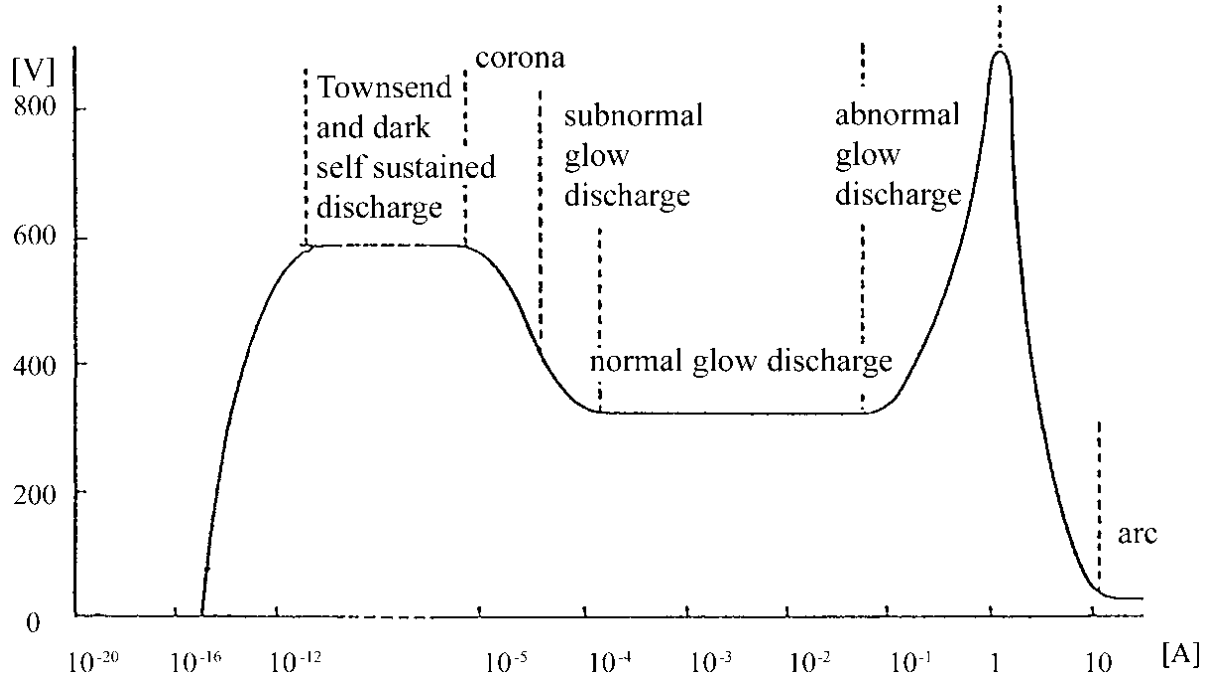

Figure 1-3. Dependence of voltage on current for various DC discharges [23]

In any volume of gas, there exist free electrons. If the electric field is high enough, these will accelerate and collide with molecules of the gas, releasing more electrons, which in turn will do the same, creating an electron avalanche. As long as net charge is not sufficient enough to distort the electric field, this electron avalanche moves with the electron drift velocity, applied to the electric field. If during this avalanche, secondary electrons are generated, then they create newer avalanches. This

mechanism, by which current grows exponentially, is known as the Townsend Breakdown Mechanism.

Different types of plasma discharges can be obtained, depending on the applied voltage and discharge current. Figure 1-3 shows this dependence. The Townsend discharge is a self-sustained dark discharge. The transition from the Townsend discharge to the sub-normal/normal dark discharge regime is accompanied by a decrease in voltage and a simultaneous increase in discharge current. A further increase in discharge current leads to an irreversible transitioning of the glow discharge into the arc regime. The DBD discharge occurs in the transition between the corona and normal glow discharge, which will be described in further detail in the next section.

Dielectric barrier discharge (DBD) plasma was known as early as 1857, when Werner Von Siemens reported experimental investigations wherein a flow of oxygen or air was subjected to the influence of a DBD maintained in a narrow annular gap between two coaxial electrodes, to which an alternating electric field was applied [24].

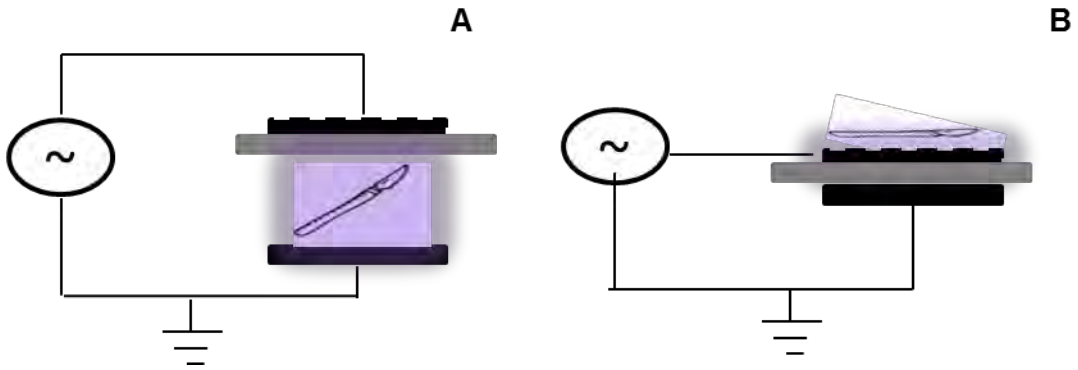

Figure 1-4. A) Volume Plasma DBD configuration used in most experimental setups. Schematic based on a similar schematic shown in [25] B) DBD configuration used in this study

In its simplest configuration, DBD is the gas-discharge between two electrodes, separated by one or more dielectric layers and a gas-filled gap. The most common

configurations are shown above in Figure 1-4. Figure 1-4 (B) shows the DBD configuration used in this thesis. It consists of two electrodes separated by a dielectric barrier. Plasma is seen on top of the electrode. This type of plasma is also known as 'surface plasma', as opposed to 'volume plasma' which is generated via the configuration shown in Figure 1-4 (A). In (A), a small scalpel that needs to be sterilized would be placed in the discharge gap between the dielectric barrier and grounded electrode since this is where plasma is generated. In (B), the same small scalpel would be placed on top of the dashed black surface, since this is where the plasma would be generated.

When high alternating-current (AC) voltage is applied to one of the electrodes, resulting electric field is adequate to produce ionization of the gas in/above the gap. The radicals, ions and electrons produced are attracted towards the electrodes of opposite polarity and form a charge layer on the surface of the dielectric. This accumulated charge cancels the charge on the electrodes, so that the electric field in the gap falls to zero and the discharge stops. Hence a low-current, low-power discharge is obtained.

Table 1-2. Micro-discharge properties in air at atmospheric pressure [24]

Duration:	10^{-9}-10^{-8}	Total Charge:	10^{-10}-10^{-9} C
Filament radius:	~10^{-4} m	Electron density:	10^{20}-10^{21} m^{-3}
Peak Current:	0.1 A	Mean Electron Energy:	1-10 eV
Current density:	10^{6}-10^{7} Am^{-2}	Filament Temp:	Close to gas temp.

When electric field is sufficiently high to cause breakdown of the discharge gas, a large number of micro-discharges can be observed emanating from the electrodes.

Micro-discharges are thin, conductive channels that are formed when a voltage difference is applied to the discharge gap, thus causing a critical stage in the electron avalanche, wherein extremely fast streamer formation is possible [24]. These micro-discharges spread uniformly along the surface of a dielectric and are shown in Figure 1-5.

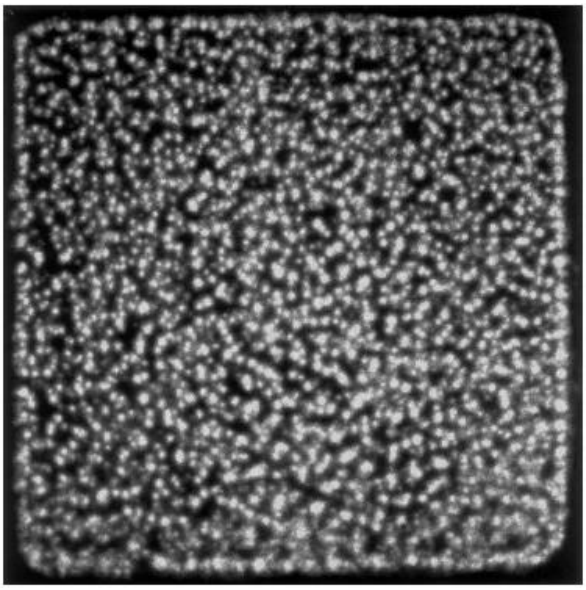

Figure 1-5. End-on-view of micro-discharges in atmospheric pressure air [24]

The gap width is of the order of a few millimeters. Since the dielectric layer in between cannot pass DC current, these devices requires AC voltage. The dielectric acts as ballast- it imposes an upper limit on the current density in the gap. Typically DBDs are operated at 1-100 kV and frequencies of 50 Hz-1 MHz. At higher frequencies, it becomes tougher to impose the dielectric limitation on the current density [24].

For a long time, DBDs were primarily utilized in industrial ozone generators [26]. Apart from this, DBDs are also implemented in surface modification [27], plasma chemical vapor deposition, pollution control [28], excitation of CO_2 laser and plasma display panels. More recently, DBD plasma at atmospheric pressure has found newer

applications in the medical and sterilization industries. Kalghatgi et al. [29] reported experiments testing the effect of DBD plasma on endothelial cells, reporting that low-power non-thermal plasma is relatively non-toxic to endothelial cells at short exposure times. This enables the application of plasmas to therapeutic applications such as wound healing [30] and blood coagulation [31]. However prolonged plasma exposure can also have an adverse effect on malignant cells [32]. Hence plasma also finds application in the sterilization industry[33];[34]. Dermatology [35] and dentistry [36]-[37] are two other areas wherein DBD plasma has been identified as an easily accessible, effective method of sterilization.

Plasma sterilization meets all criteria of an ideal sterilant, listed by Moisan et al.[16]. As a good alternative to conventional sterilization techniques, it has also sparked off a remarkable volume of research aimed at understanding its underlying mechanism. Understanding the mechanism of sterilization is vital to the successful implementation of this technology. Before discussing the possible mechanism, a brief summary of research in plasma sterilization is necessary.

1.3 DBD Plasma Sterilization

The origins of plasma sterilization can be traced all the way back to 1968 when Menashi [38] filed a patent for a high-temperature/ high pressure plasma sterilization process.

A separate patent was filed in 1972 for a low temperature plasma sterilization process. Further patents by Boucher and Bithell [39]- [40]cemented a growing interest in plasma sterilization.

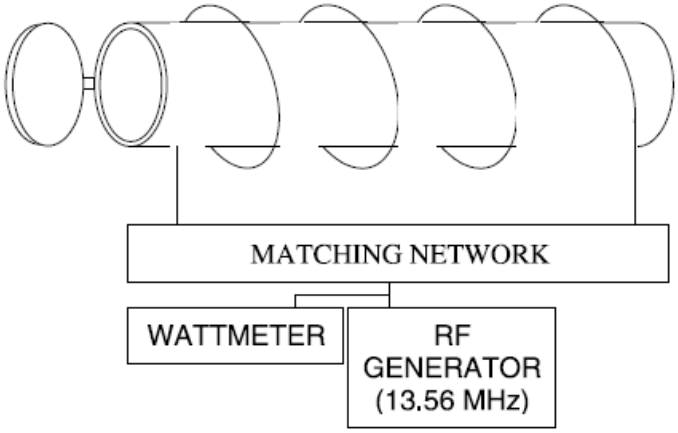

Figure 1-6. Schematic of an apparatus used earlier on for plasma sterilization [39]

Early experiments, during this decade, were conducted at low pressures of 0.1-10 Torr and mostly used Helium or Argon as discharge gases. Further experiments consisted of refining the experimental setup used and varying experimental parameters such as discharge gas used (Ratner et al. [41]showed that plasma sterilization is efficient with common discharge gases such as N_2, O_2, air etc.), input power density (Boucher also reported that sterilization efficacy increased with RF power density absorbed in the discharge) and type of micro-organism (difference between plasma sterilization times take for Gram-negative and Gram-positive pathogens was identified early on by Baier et al. [42]). Researchers also speculated on the role of UV radiation and oxygen atoms in the sterilization process. However while many were divided about whether UV radiation played a role[43]-[45], some experiments conclusively proved that sterilization via an O_2 plasma was much more effective[46].

The experiments during the 70s and 80s were mostly in the volume plasma range. The later part of the 20th century and early 21st century sparked off research in surface plasma sterilization at atmospheric pressure. Initial research was published by [47]. This was the time when sterilization using glow discharge at atmospheric pressure

and more, specifically, DBD sterilization was recognized as a much more accessible alternative to earlier low-pressure plasma sterilization systems. A flurry of publications followed from numerous research groups pursuing dielectric barrier discharge sterilization. [48]-[52]

. Research in plasma sterilization can be classified into two categories: (i) Parametric studies of the factors involved. (ii) Studies aimed at determining the underlying mechanism. The former involved researchers embarking upon an empirical path, varying each and every factor and noting its significance on the plasma sterilization time as well as the efficiency and efficacy of the process while the latter involved in-depth studies aimed at understanding the role of several plasma agents in the plasma sterilization process. Both categories of research were pursued using experimental methods primarily. Another area of research, that could potentially provide a more fundamental insight into the plasma sterilization process, is the numerical modeling of plasma sterilization. However numerically modeling the interaction of plasma with the biological cell is a highly complex process and is perhaps the reason why very little research exists in this area.

1.3.1 Factors involved in Plasma Sterilization- Parametric studies

Lerouge et al. [14] outlined a schematic of the numerous factors involved in plasma sterilization. This schematic, modified for DBD plasma sterilization is given below in Figure 1-7.

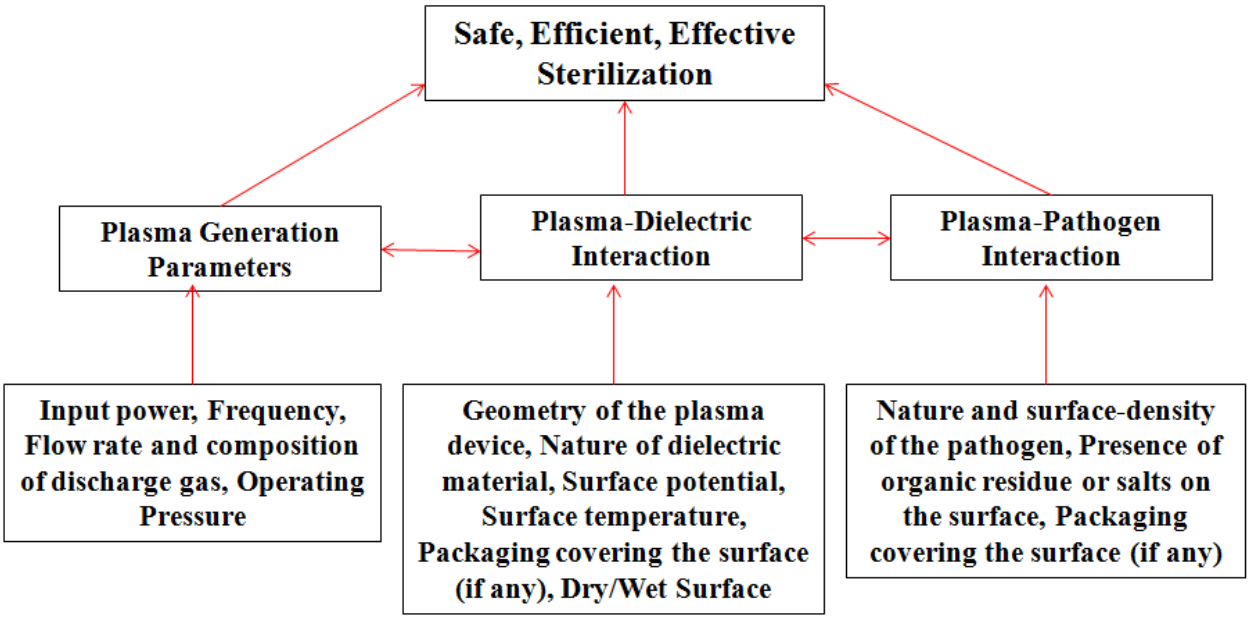

Figure 1-7. Various Factors involved in DBD Plasma sterilization

Given below is a brief summary of the research conducted by various authors in evaluating the various factors affecting plasma sterilization.

Gas Composition: Plasma can be generated using various discharge gases: Air, N_2, O_2, He, Ar, O_2+CF_4 etc. Over the decades, extensive research has been conducted in determining the best possible gas mixture for optimum plasma sterilization.Hury et al. [53] studied the destruction of *Bacillus subtilis* spores in oxygen(O_2) based plasmas sustained in the mTorr pressure range. They confirmed Boucher's assertion that O_2 plasma achieved more killing than Ar plasma. Similarly Lerouge et al. [54] conducted experiments, also in the mTorr range, wherein different gas compositions were compared in terms of destruction efficiency. They found that the O_2/CF_4 plasma was most effective, due to the combined etching action of both oxygen and fluorine atoms. Most of the O_2 tests were conducted in a low-pressure regime. However in 2006, Ying et al. [55] compared yeast inactivation in He, Air and N_2 DBD (volume) plasma at atmospheric pressure. Working at a frequency of 0-20 kHz and an input voltage of 40

kV p-p for a treatment time of 5 minutes, they reported a 10^5, 10^6 and 10^7 reduction in bacterial concentration using plasma generated in N_2, air and He respectively. They concluded that for their case, the electrostatic tension caused the rupture of the cell membrane, leading to cell death and that the effect of this electrostatic tension was exacerbated in the case of He plasma.

Gas Pressure: Moisan et al. state the three pressure regimes in which most plasma sterilization experiments have been conducted: low pressure (1-10 mTorr), medium pressure (0.1-10 Torr) and atmospheric pressure [16]. Until a couple of years ago, most reported experiments pertained to the medium pressure range. Using an RF discharge reactor operating at 13.56 MHz and a discharge gas mixture of O_2/CF_4, Wrobel et al. [56] concluded that rising pressure produced competing effects in plasma; upto a certain limit it increased residence time of the gas molecules, thus increasing the concentration of active species, possibly promoting sterilization effectiveness. However, beyond a certain point, increasing pressure decreased the plasma volume and increased the gas temperature. Chau et al. [57] noted that when exposed to a microwave (MW) plasma, complete inactivation of *Escherichia coli* was noted at lower pressures like 43-200 mTorr. However a higher pressure of 400 mTorr showed incomplete inactivation.

The effect of low pressure versus atmospheric pressure is still contested. It has been argued that low pressure allows the emission of Vacuum-UV (VUV) radiation (λ<200 nm). However the role of VUV radiation in inactivating bacteria is still debated. This will be discussed in detail in a later section. On the other hand, it is commonly agreed that at atmospheric pressure, the lethal UV photons/oxidizing atoms produced

are easily reabsorbed, thus eliminating the possibility of UV-irradiation or etching by oxidation.

Input Power & Frequency: The role of power has always been coupled with the role of surface temperature. Rising power leads to an increased concentration of active species in the plasma, which could lead to increased microbiocidal and sporicidal activity. Bol'shakov et al. [58] conducted experiments using an RF O_2 plasma source and *D.radiodurans* as the test pathogen, wherein they concluded that sterilization time depended inversely on plasma density and fluxes of active species (O and O_2*), whereas these fluxes increased linearly with input power but changed weakly with pressure under their conditions.

However increased power also implies increased heating of the substrate, which could be detrimental to the materials being sterilized. In discussing the effect of input frequency on plasma sterilization, the debate has always been about radio-frequency (RF) versus microwave (MW) plasma. RF frequencies belong to the range of 3 kHz- 300 GHz, while MW frequencies occupy the upper range of RF frequencies (0.3-300 GHz). Lerouge et al. [59] have reported experiments wherein they noted high sporicidal activity of MW plasma (2.45 GHz) as compared to its RF counterpart (13.56 MHz).

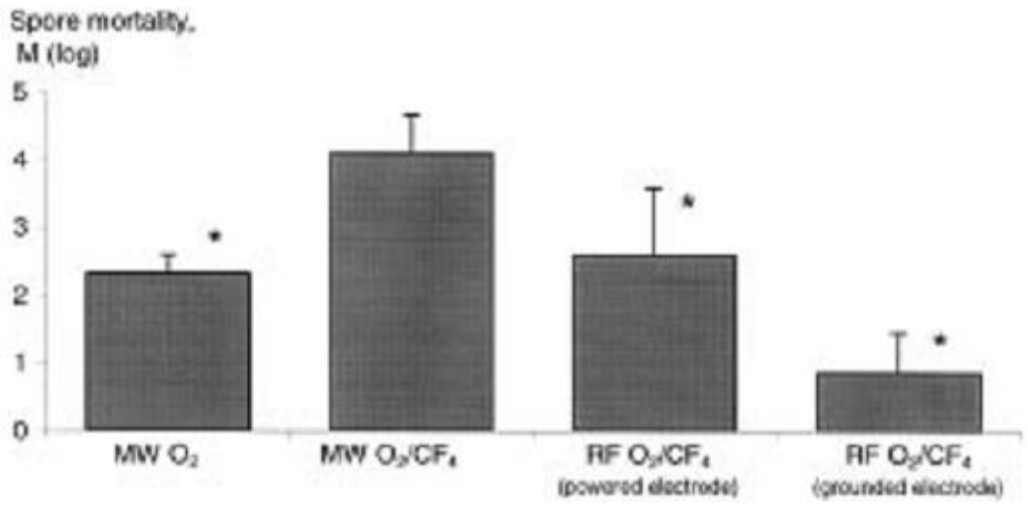

Figure 1-8. Comparison of spore mortality [log10(No/N)] in MW and RF O2/CF4 plasmas, after 5 minutes of exposure (P=200W, p= 80 mTorr, F= 80sccm, [CF4]= 12%) [59]

Figure 1-8 above shows this comparison of RF and MW plasmas using O_2/CF_4. Authors concluded that the frequency determined the Electron Energy Density Function (EEDF), which determined the concentration of high energy electrons in MW plasma, as compared to its RF counterpart. This was hypothesized as the reason for the higher sporicidal activity observed with MW plasma.

Effect of Afterglow: Direct plasma sterilization refers to experiments in which the bacterial sample is directly exposed to the generated plasma. Afterglow-based sterilization, on the other hand, indicates experiments in which plasma is generated and the bacterial sample is exposed downstream of the reactive chemical species produced during plasma generation (afterglow). Microwave experiments using the afterglow of N_2-O_2 plasma to achieve complete inactivation of *B. subtilis* spores within 40 min with an absorbed power of 100 W were also reported [60]. However, authors noted that the efficacy of such a system was highly dependent on the gas flow reaching all parts of the object to be sterilized and on short-lived active species being transported with sufficient

rapidity. Experiments using the afterglow of non-thermal plasma at atmospheric pressure to inactivate *E. coli* and *B. cereus* (within 15 minutes) and *P. aeruginosa* (within 10 minutes) have also been reported [61].

In the case of afterglow, the bacterial concentrations are in essence being exposed to the reactive chemical species produced during plasma generation i.e. neutrals and charged species. Experiments using the reduced pressure afterglow stemming from discharge in a N_2-O_2 mixture were reported [62] wherein it was concluded that sterilization time was the shortest when the O_2 percentage in the mixture was set to maximize UV emission intensity. This was an example of sterilization being influenced by the UV photons in the plasma afterglow.

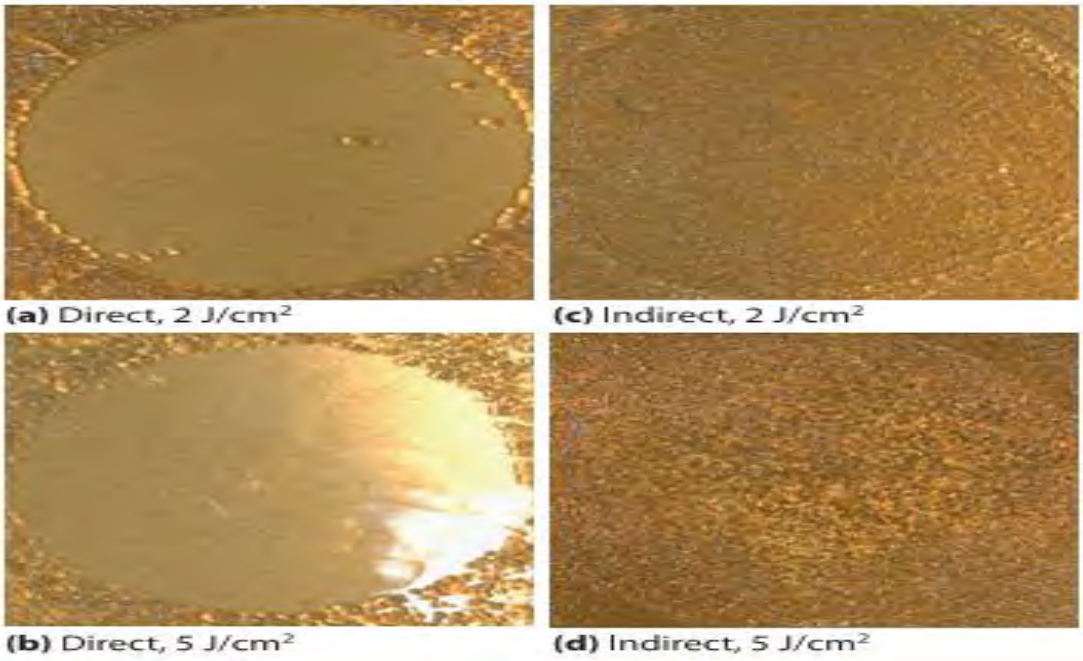

Figure 1-9. Results of inactivation of E. coli on the agar surface by direct (a,b) and indirect (c,d) plasma treatment [63] As is evident, direct plasma leads to a clean spot in the center with no bacterial growth, while indirect plasma leads to incomplete inactivation.

Dobrynin et al. [63] also reported experiments wherein they compared bacterial samples exposed to direct plasma (discharge is ignited on the treated surface) to those exposed

to indirect plasma (a grounded metal mesh is used as a second electrode, thus cutting off charged species. The mesh was corrected to produce the same amount of UV radiation). They concluded that direct plasma was more effective than indirect plasma due to the combined action of charged species, neutrals and UV photons. This comparison is shown above in Figure 1-9. Thus, with the use of a plasma afterglow for sterilization, the agent responsible for sterilization in such a case remains highly debated. In general, a review of literature commonly indicates greater sterilization times using the afterglow, as compared to when using direct plasma.

Miscellaneous Factors: Various other factors have also been debated: nature and surface density of test pathogens, packaging, geometrical factors involved in the design of the sterilization reactor, gas flow rate etc. For instance, the type and surface density of test pathogens is a huge factor in determining efficiency of plasma sterilization. Vegetative pathogens (*E. coli*, yeast) are usually less resistant than bacterial or fungal spores (*G. steaothermophilus, B. subtilis)*. Hury et al.[53] also concluded that the surface density of spores used was an important factor in determinng plasma sterilization efficiency i.e. higher the surface density of spores, longer the sterilization time. Presence of absence of packaging material was another factor considered to determine the effectiveness of a plasma sterilization process. In order to ensure that an object sterilized using plasma remains sterile until use, an alternative method could be to enclose the object in a polymeric package and expose it to plasma. However Lerouge et al. [14] demonstrated that this led to negligible reduction in spore population, due to the reduced number of active species passing through the package material. To date, it

is suggested that any object be first plasma sterilized and then immediately inserted into sterile sealed packages until further use.

It is evident from the volume of research reviewed above that a plethora of factors influence plasma sterilization. While the role of some factors (nature and surface spore density of test pathogen, role of packaging) has been clearly identified, the role of others (discharge gas, power, pressure) still continues to be debated. However one thing is clear: All the debatable factors in plasma sterilization are coupled, meaning that more often than not, for efficient plasma sterilization, a trade-off between the different factors will have to be considered.

1.3.2 Mechanism of Plasma Sterilization

DBD plasma is a soup of UV photons and reactive chemical species at a slightly elevated temperature. In understanding the mechanism of plasma sterilization, it is necessary to evaluate the roles of each of these components. This section reviews the majority of the literature published in evaluating these roles.

UV photons: The UV radiation spectrum is given below in Figure 1-10 below.

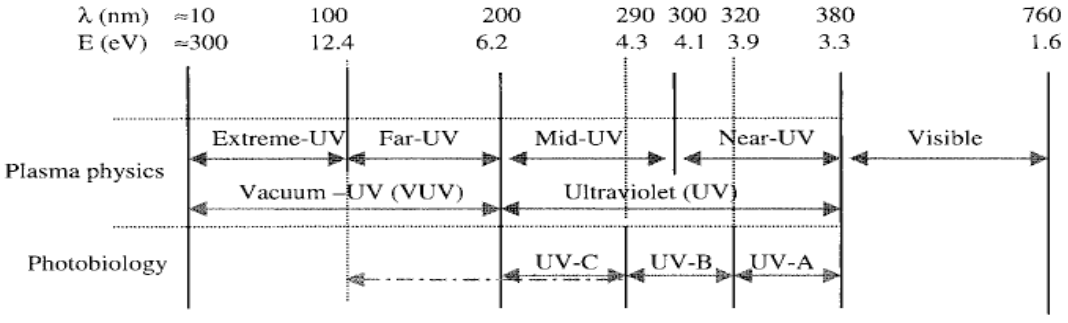

Figure 1-10. Wavelength and energy of radiation in the UV and visible portion of the spectrum [59]

The vacuum ultra-violet (VUV) ranges from 10-200 nm while the UV portion of the spectrum ranges from 200-380 nm. At atmospheric pressure, emitted VUV radiation is usually absorbed by atmospheric oxygen. Of the VUV range, Far-UV radiation (100 nm< λ<200 nm) is capable of breaking bonds in the protective membranes of micro-organisms.

The UV portion of the spectrum (200<λ<380 nm) is further broken up into UV-C, UV-B and UV-A. There are two main mechanisms for UV damage (a) direct effects of UV radiation that are based on UV energy absorption by cellular macromolecules. Typically, UV-C and UV-B are capable of inducing a reaction between two pyrimidine molecules (thymine and cytosine, adjacent to each other on the same strand of DNA) causing them to form a dimer. The presence of this dimer affects base pairing and causes mutations during DNA replication [64] (b) DNA, protein and lipid alterations caused by the UV-A induced disturbance in the cellular redox state. UV-A can induce the release of intracellular reactive species (RS), causing oxidative degradation of lipids and DNA [65].

The role of UV radiation in plasma sterilization has often been closely connected to the operating pressure. Low pressure facilitates the emission of VUV radiation (λ<200 nm), which has been argued to be one of the key factors in influencing plasma sterilization. Lerouge et al. [59] hypothesized that very energetic VUV photons emitted in a glow discharge plasma may have a greater effect on spores by attacking not only DNA but also the spore membranes. However, in conducting experiments at low pressure using both RF and MW plasmas, they noted that VUV radiation in the range 115-170 nm required more than a 5 minute exposure to kill 90% of the micro-organisms.

From their observations, they concluded that VUV radiation did not appear very promising, since it was not more efficient in killing micro-organisms than UV-C (254 nm). On the contrary, Halfmann et al. [66] conducted experiments wherein they determined that the wavelength range of 235-300 nm played a major role in sterilizing spores of *Bacillus atrophaeus.* They also concluded that active species played a minor role but were not negligible. Most of the earlier work reported in plasma sterilization has been reported in the low and medium pressure regimes.

The more recent body of work in plasma sterilization concentrates on sterilization due to glow discharge and dielectric barrier discharge volume plasma at atmospheric pressure. It has often been speculated that in higher pressure regimes (such as atmospheric pressure) the more reactive VUV photons and oxidizing atoms produced during plasma generation often recombine instantly or are re-absorbed instantly [67], thus making them unavailable for sterilization. Authors have reported experiments confirming that the role of UV radiation in plasma sterilization at atmospheric pressure is minimal. Experiments were conducted in which the spectroscopic signature of DBD volume plasma in air at atmospheric pressure was measured [68]. Their results (Figure 1-11 below) showed that no significant UV emission occurs below 285 nm, which led them to conclude that UV might not play a significant direct role in the sterilization process by low-temperature air plasmas.

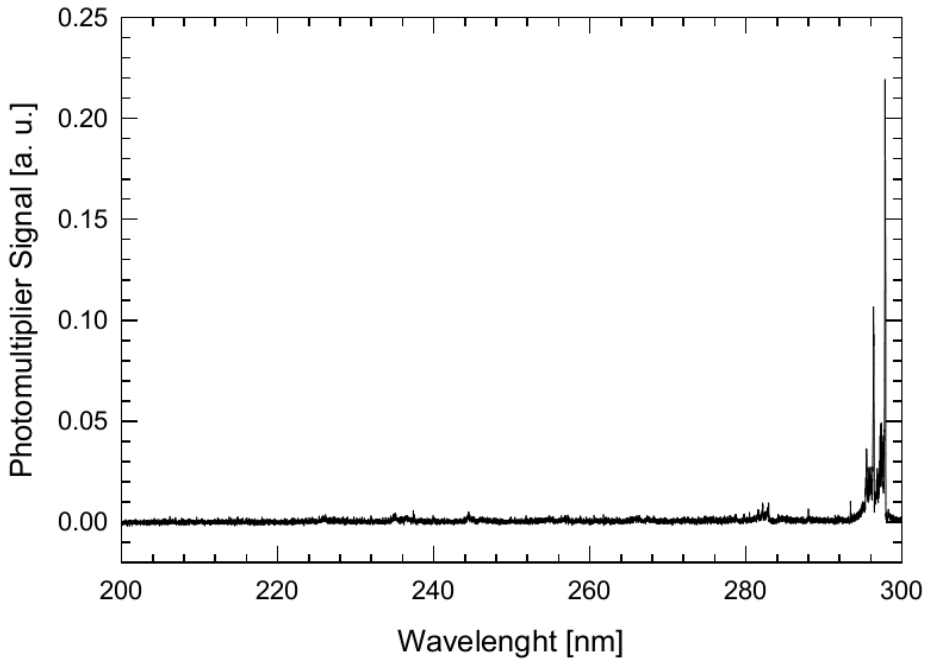

Figure 1-11. UV spectrum of a DBD in air in the 200-300 nm wavelength range [68]

Dobrynin [63] reached a similar conclusion after conducting experiments examining the effect of plasma on inoculated slides, protected from direct discharge by a MgF_2 slide (which is transparent to VUV photons >140 nm).

Thus far, based on all the literature published on this subject, it seems that the only clear consensus on the role of UV radiation in plasma sterilization is that different pressure regimes lead to the emission of different ranges of UV radiation, which in turn might influence the process of plasma sterilization.

Reactive Chemical Species: Among the primary products of electron collision are atomic and metastable oxygen and nitrogen, with subsequent reactive collisions producing a cocktail of neutral and ionic species. Atmospheric pressure discharges differ from low-pressure plasma in that their chemistry is dominated by reactive neutral species such as oxygen atoms, singlet oxygen and ozone rather than ions. In corona and DBD, ozone is the main reaction product. In other plasma sources, oxygen atoms

represent a larger proportion of the reactive species. Ozone was found to be the dominant species with single oxygen and atomic oxygen being at a concentration five to six order lower than that of ozone [25]. Other reactive species produced by plasma (N_2*(A^3 `O_u), N_2*(B^3g), O_2*($a^1\Delta_g$), O(^{1}D), O(^{3}P), H, OH, N) react and break down hydrocarbons, chlorocarbons and CFCs[24].

As discussed in Section 1.4.1, Dobrynin et al. [63] evaluated the difference between direct plasma (bacterial sample directly exposed to discharge) and indirect plasma (grounded mesh inserted in between the discharge and the bacterial sample, thus blocking the flow of charged species). In doing so, they concluded that the blocking of charged species led to a reduction in inactivation effect of the discharge. Charged particles are hypothesized to play a role in plasma sterilization by way of creating electrostatic tension on the outer surface of the bacterial cell membrane causing the rupture of the cell membrane and killing the bacteria [69]. However a detailed study of the interaction of charged particles with cells and tissues concluded that the experimental difficulties in detecting and characterizing charged species form an obstacle to obtaining direct evidence [70].

On the other hand, neutral species (O_3, NO_2, OH) have also been known to play a role in plasma sterilization. The efficacy of the plasma afterglow in sterilizing bacteria is mainly due to role of neutral species. Often times, charged particles are too short-lived to be able to reach the bacterial sample in the afterglow region. Laroussi and Leipold [68] stated that cell membranes, made up of lipid bilayers, whose important component is unsaturated fatty acids, may also be attacked by OH radicals, causing

them to break down. It has also been speculated that oxygen-based and nitrogen-based reactive species may have strong oxidative effects on the outer structures of cells [71].

The germicidal action of ozone has been well-documented [72]-[73]. However the role of ozone in plasma sterilization has not been discussed in great detail. Efremov et al. [74] discussed reaction rate constants for production and destruction of ozone formed during plasma generation. They concluded that under a small specific energy input, in dry air, there are insufficient fast processes for O_3 molecule destruction with rates comparable to the rate of its formation. This led them to also conjecture that the antiseptic property of the excited dry air flowing out of a discharge chamber is determined by its ozone concentration. They followed up this conclusion by demonstrating in their paper that exposing micro-organism concentrations to discharge-excited air, even for a short while, substantially reduced their amount. However in doing so, the composition of the discharge excited air is not discussed.

Dobrynin et.al.[63] pursued a different approach in isolating the role of ozone in plasma sterilization. They measured the ozone concentration produced by a DBD discharge in room air at ~60% relative humidity as 28 ppm. Consequently they used a commercial ozone generator (~500 ppm max output, Quinta Inc.) to produce the same concentration of ozone and examined the inactivation effect of this ozone concentration on *E. coli* and skin flora. They noted that no inactivation effect occured. However in this case, it is to be noted that the levels of ozone noted were ~28 ppm, which might be too low a concentration to have an inactivation effect on bacterial concentrations.

Temperature: Although glow discharge and DBD plasma at atmospheric pressure are primarily low-temperature plasmas, the role of temperature or heat in plasma

sterilization still needs to be discussed. As already mentioned in Section 1.4.1, increased power can cause increased heating of the substrate, which in turn could contribute to killing.

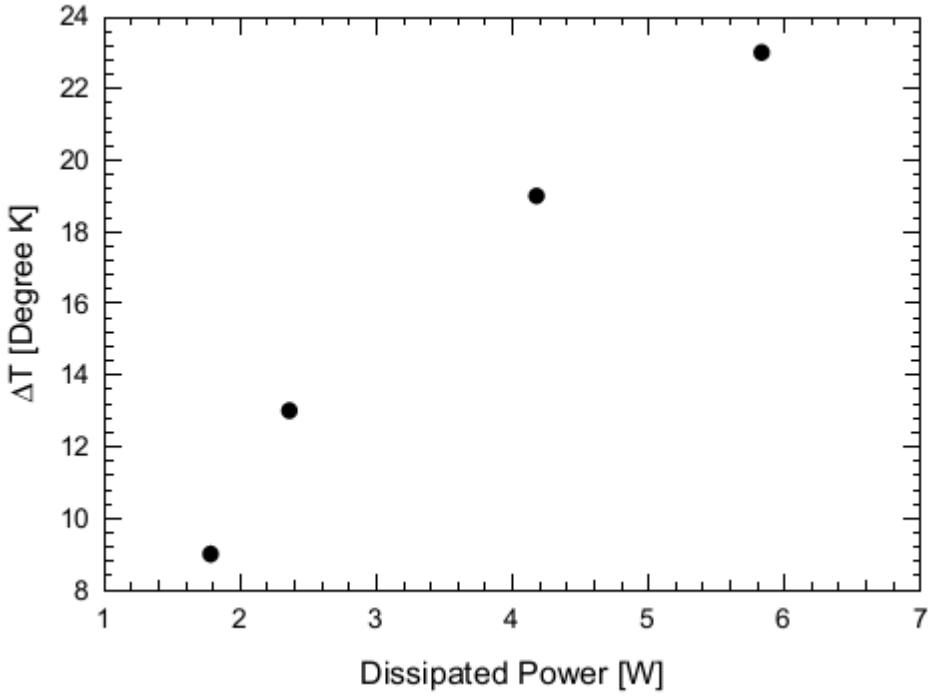

Figure 1-12. Increase of sample temperature vs. plasma dissipated power for a DBD volume plasma in air at atmospheric pressure [68]. At typical running power levels, a maximum increase of 21°C was observed, which led authors to conclude that no substantial thermal effects on bacterial cells occur.

The effect of temperature was evaluated by exposing *B. subtilis* spores to CO_2 plasma and evaluating the effect of temperature in this case [53]. It was concluded that the lower temperature of 15°C led to a lower destruction efficiency while a higher temperature of 60°C led to the highest destruction efficiency. However, Laroussi et al. [68] measured the gas temperature as well as the temperature in a sample placed 2 cm away from an atmospheric pressure DBD discharge in air. They observed that gas temperature remained close to room temperature and that a variation in power from 1-7

W showed negligible change in temperature (Figure 1-12). This led them to conclude that heat does not play a major role in killing bacterial cells.

Ohkawa et al. [75] reported that using a pulse-modulated high frequency plasma sterilization source caused a decrease in sterilization time with increase in neutral gas temperature. Thus,once again, contrary results were presented.

Thus, in conclusion, the main agents involved in the process of plasma sterilization are UV photons, reactive chemical species (charged and neutral) and temperature. Literature presents several cases that argue for and against each of these agents. The common hypothesis about plasma sterilization that was initially propounded, came as a result of the phasic behaviour seen in plasma sterilization. A survival curve is one that plots the reduction in number of micro-organisms over time.

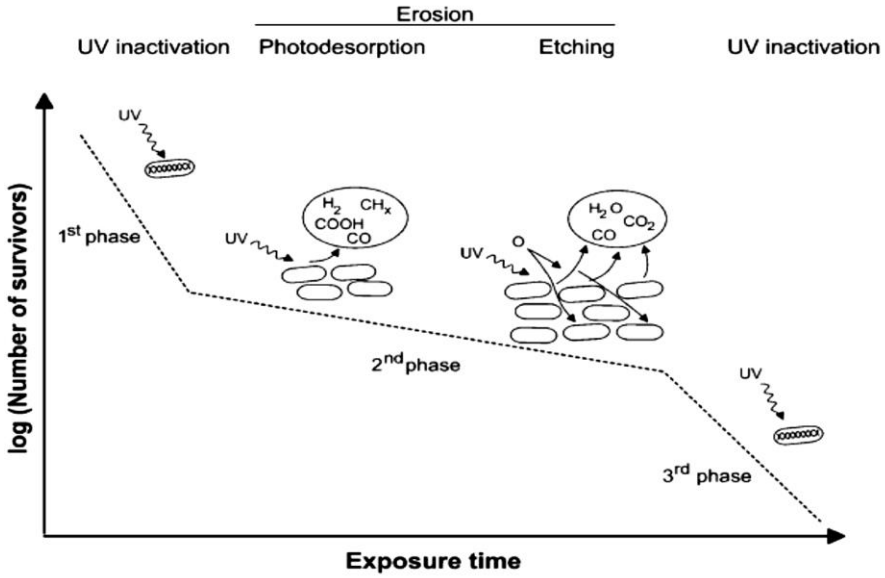

Figure 1-13. Schematic illustration of the different phases in a plasma sterilization survival curve [67]

While all other conventional sterilization methods seemed to produce linear, mono-phasic survival curves, plasma sterilization produced bi-phasic and tri-phasic

survival curves [67], [76] . A schematic illustrationof this phasic behavior is shown above in Figure 1-13.

Tri-phasic and bi-phasic survival curves led authors to initally believe that plasma sterilization followed a phasic behaviour in which UV photons inactivated the top-layer of spores rapidly and any remaining debris was then etched away by a combination of UV photons and ROS [16]. This hypothesis might still hold true, though it has not been proved conclusively. What needs to be determined is a clear mechanism of interaction of these killing agents with biological pathogen, and the order of events that causes cell destruction.

1.3.3 Plasma interaction with biofilms

A major volume of work done in plasma sterilization focuses on the effect of plasma on individual microbe concentrations. However, recent research has also focused on the fact that most microbes prefer to live as part of communities where interactions take place [77]. Biofilms are microbial communities attached to a surface and embedded in a matrix composed of exopolysaccharides together with proteins and excreted nucleic acids. Work involving the use of plasma in eradicating biofilms increases in frequency from 2007 onwards. Sladek et al. [78] reported experiments with *Streptococcus mutans* biofilms using a plasma needle (13.56 MHz, 100 mW, t=60s) and reported incomplete inactivation. This could be because of the low exposure time. The interaction of plasma (atmospheric pressure, He/N_2 gas mixture, with an input power of 4.8W) with bacterial biofilms was visualized through AFM [79]. AFM images show minor morphological changes to cells in 5 minutes, but major cell damage in 60 minutes. Lee et al. [80] used a 2.45 GHz, 1 kW MW-induced Argon plasma source to completely inactivate different bacterial biofilms (*E. coli, methicillin-resistant*

Staphylococcus aureus (MRSA)) in 20s. SEM micrographs show damaged morphologies of cells, as compared to untreated cells.

The use of plasma in biofilm inactivation holds major potential in dental health and food-processing industries. For the purpose of this study, the interaction of plasma with biofilms has been studied because (a) Biofilms are more robust in structure, which enables their exposure to plasma and consequently, microscopic analysis (b) A single-species biofilm encourages the organization of bacteria into colonies, with each colony being capable of one specific function. Some might be responsible for the exo-polysaccharide matrix formation while others might be more motile. Studying the plasma interaction with biofilms microscopically helps determine which cellular function is affected the most by plasma.

1.3.4 Numerical modeling of Plasma Sterilization

One aspect of research that has been minimally researched is the possibility of constructing a numerical model to simulate plasma sterilization. Some researchers have modeled the destruction of cells via innovative methods. Kumar et al. [81] reported an experimental as well as numerical study performed by exposing spores to elevated temperatures. They simulated the flow field inside the thermal exposure system using a turbulence model and built another model to simulate the thermal response of the spores in a high temperature gas environment. The two models were clubbed to investigate further experimental parameters such as the dependence of this thermal response on water content in spores and thermal property uncertainties.

Gallagher et al. [82] provided a numerical characterization to help predict and understand the inactivation mechanism of DBD plasma. Their simple exponential model used rate constants (chemical kinetics) to solve for species concentration. Akishev et al.

[83] used an empirical mathematical approach to predict bacterial inactivation, using not only cell-inactivation data, but also cell reparation data. A new venue of numerical modeling in plasma sterilization was opened up by solving for different species concentrations using a hydrodynamic model of equations [84]-[85].

The most exciting research in this area was reported by Babaeva and Kushner [86]. They conducted computational studies on the interaction of plasma streamers in atmospheric pressure DBDs with human skin tissue.

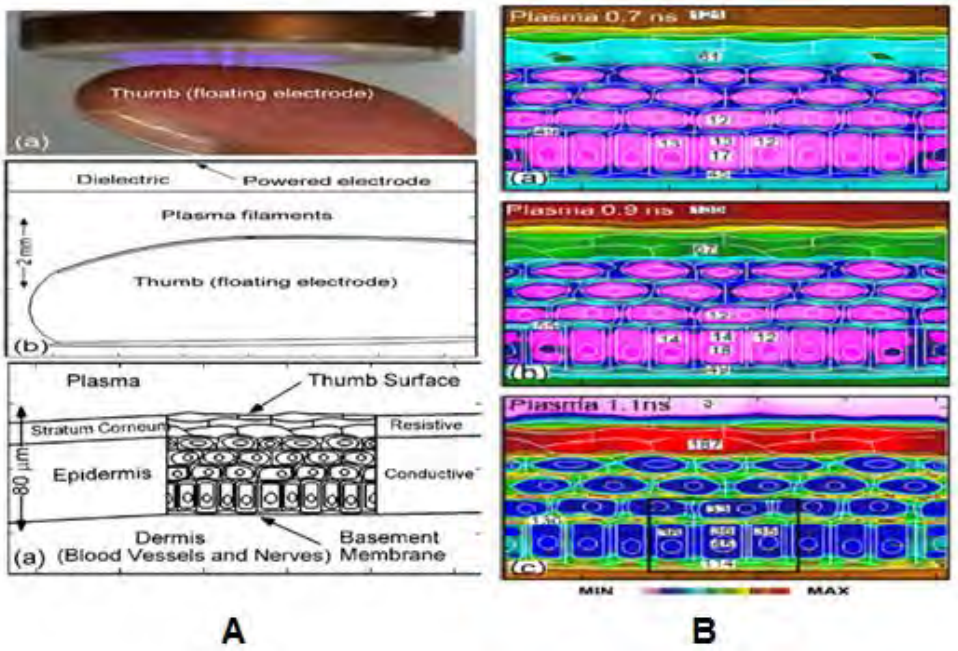

Figure 1-14. A) Computational Model used, depicting the breakup of the skin into different layers as well as the plasma source placement B) Electric field inside the epidermal layer, at different simulation time-points [86]

In Figure 1-14 (A) above, the skin was assumed as consisting of four layers: outer membrane, epidermis, inner membrane and dermis. Each layer was assigned a different ε, such that there were four different conducting layers.

The plasma source was modeled along the lines of the floating electrode DBD (developed by Fridman et al. [31]) wherein plasma (source of electrons) was positioned

above the surface of the skin. The propagation of a plasma filament towards the surface of the skin, penetrating the surface of the skin and its propagations inside was modeled. Plasma was modeled by solving for the complete set of plasma air-chemistry equations. Poisson's equation was modeled throughout the domain.

The plasma filament propagated from the source and hit the surface of the skin at 1.1 ns. In Figure 1-14(B), it was observed that at 0.7 and 0.9 ns, before the filament hit the skin surface, the electric field was fairly low. It skyrocketed at 1.1. ns (when the plasma filament hit the skin surface) with the topmost layer of the skin showing the highest electric field distribution. This study was especially useful in that it laid out a graphical visualization of what happened when a plasma filament interfered with the skin and promoted the hypothesis that the induced electrical field inside the cells caused cell-electroporation.

The objective of Section 1.3 was to provide a summary of the research in plasma sterilization. From 2000 onwards, a huge amount of research has been done in understanding plasma sterilization. However the fundamental questions still remain the same (a) What is the best combination of experimental factors to achieve efficient and effective plasma sterilization (b) What is the mechanism of plasma sterilization? Which plasma agents are responsible for killing? What happens to the cells when they are exposed to plasma? The goal of this study is to provide reasonable answers to both questions.

CHAPTER 2
RESEARCH MOTIVATION

Chapter 1 gave a detailed overview of conventional sterilization methods, the characteristics of DBD plasma and more importantly, a voluminous introduction to plasma sterilization. The pros and cons of different methods of plasma sterilization have been abundantly outlined in Section 1.3. The fundamental questions highlighted at the end of Chapter 1 were:

- What is the best combination of experimental factors to achieve fast and effective plasma sterilization (i.e. complete bacterial inactivation on plasma exposure in the shortest time)?
- What is the mechanism of plasma sterilization? Which plasma agents are responsible for killing of microorganisms?

The key to answering the first question is to design a set of experiments aimed at isolating each parameter and studying its significance on the time taken for plasma sterilization. As has been mentioned in Chapter 1, there is no one set of optimal parameters for safe, efficient and effective plasma sterilization. The best conclusion to be drawn is that every experimental parameter requires a trade-off. For instance, too high a temperature is good for effective sterilization, but bad in terms of dielectric surface heating and damage to the substrate materials. The goal in such a scenario would be to find a suitable dielectric material that can stand high temperatures, but at the same time be usable for effective sterilization. Similarly other experimental parameters to be investigated for determining an optimum set of experimental parameters for the case of DBD Plasma Sterilization would be a) Type of Micro-organism b) Input Power c) Input Frequency d) Nature of Dielectric Material.

The key to answering the second question above is to use diagnostic equipment or chemical reagents to analyze the role of a single plasma component in the process of

plasma sterilization process. As regards the mechanism of plasma sterilization, three responsible plasma components can be identified: UV photons, reactive chemical species and temperature (to a lesser extent). In order to figure out whether these three work synergistically to kill bacteria or whether one component plays a dominant role in sterilization, diagnostic equipment such as spectrometers (to study the emission patterns of the UV photons), fluorescent and electron microscopic analysis (to study the damage to the biological cells after plasma exposure) or chemical reagents (reacting specifically with different plasma chemical species or by-products) can be used. The goal is to figure out a mechanism that explains the systematic breakdown of the microorganism.

Thus plasma sterilization provides for an intriguing field of research, with its fair share of challenges. These challenges need to be overcome so that plasma sterilization may be implemented as a safe, efficient and effective alternative to conventional methods of sterilization.

Chapter 3 discusses the experimental setup and methodologies used for the DBD surface plasma experiments. Chapter 4 focuses on outlining the parametric studies conducted in an effort to characterize the sterilization efficiency of the DBD surface plasma setup used in this thesis. This sterilization efficiency is dependent on the plasma generation, which in turn is dependent on a number of input parameters, described further in Chapter 4. Chapter 5 outlines the experiments conducted in understanding the mechanism of DBD surface plasma sterilization. Finally, Chapter 6 summarizes all the results obtained in Chapter 4 & 5 and outlines areas of future work.

CHAPTER 3
METHODS & MATERIALS

3.1 Experimental setup used for plasma sterilization experiments

Figure 3-1 shows the schematic of the experimental setup used in plasma generation. It is to be noted that this experimental setup is very rudimentary and was used in the initial stages of this project. This experimental setup has subsequently been built into a more compact form, that uses the same electrical components, but in a much more power-efficient way.

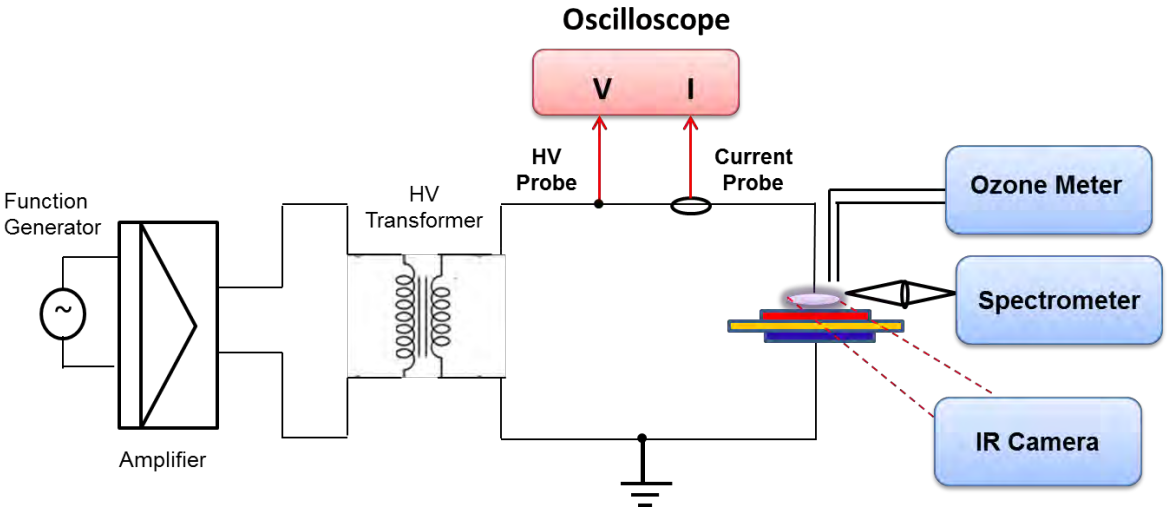

Figure 3-1. Schematic of the experimental setup used

In Figure 3-1, a function generator (HP 33120A) is used to generate an RF sine wave of frequency 14 kHz. The power of this signal is then amplified by using an amplifier (model Crown CDi4000). This amplified signal is then passed through a step-up transformer (Corona Magnetics, Inc.) which steps up the voltage. The input power from the transformer is fed to the powered electrode (red) of the device via a metal connector. The final signal being fed into the plasma device has an input voltage of 12 kV peak-peak (p-p). The other electrode (blue) of the device is grounded via a grounded

electrical bench, atop which the device sits. The powered and grounded electrodes are separated by a sheet of dielectric material, about 1.6 mm thick. The design of the plasma device is described in Section 3.2.

The spectroscopic signature of the generated DBD plasma is determined using the Ocean Optics® USB 2000+ spectrometer. This spectrometer has a detector range of 200-1100 nm, an optical resolution of ~0.3-10 nm (FWHM), a dynamic range of 1300:1 for a single scan and is fitted with a custom-made grating designed to be sensitive to wavelengths between 200-650 nm. An uncoated UV Fused Silica Plano-Convex Lens (Φ2", f= 75 mm, Thor Labs, Inc.) is used to collect and focus the incident plasma glow from the plasma device, which is then detected by the spectrometer via a fiber-optic probe. Baseline spectroscopic data for each device was collected with the device powered for 2 minutes at a sampling rate of 10s. Readings were also taken during sterilization experiments.

A 2B Tech® Ozone meter is used to measure the emitted ozone at fixed time intervals. This ozone meter operates on the principle that the maximum absorption of ozone takes place at 254 nm. Air is drawn into the ozone meter at a flow rate of about 1L/min and passed to an absorption cell via two methods: (i) directly and (ii) after passing through an ozone scrubber. The intensity of light passing through the absorption chamber in case (i) and (ii) is measured and used to determine the level of ozone in absorbed air. Air is sampled every 10s and the ozone meter has an accuracy of about 2%. The sampled ozone levels are saved to a computer via a LabView ® Interface.

An FLIR ® A320 Infrared camera is used to record a thermo graphic mapping of the electrode surface area, while it is being powered. This helps provide a visualization of the temperature fields during plasma generation, which would further assist in understanding the role of temperature in plasma sterilization. The A320 operates at a spectral range of 7.5-13 μm and has a pixel resolution of 320x240 pixels. The distance between the plasma device and infrared camera, ambient temperature and humidity and the emissivity of the FR4, SC dielectric were measured to be 0.2667 $\pm$ 0.0127 m, 24.4$\pm$2.3^{o}C, 59$\pm$ 3% RH and 0.9097$\pm$0.03, 0.929$\pm$0.03 respectively.

3.2 Design of the Plasma Device

The devices themselves have two important components: the dielectric surface and the electrodes. The two dielectrics used are Flame Retardant-4 (FR4) and semi-ceramic (SC). FR4 is a composite material composed of woven fiberglass cloth with an epoxy resin binder that is flame resistant. FR4 is used as the primary insulating backbone in a vast majority of printed circuit boards (PCBs). For the purpose of this thesis, commercial copper-clad FR4 sheets (Advanced Circuits ®) were used to manufacture the FR4 devices. 2-layer, 1.6 mm thick FR4 sheets, overlaid 1 Oz copper (Cu) are milled in the requisite electrode pattern. The Cu layer was coated with a tin (Sn) finish. The FR4 used for the manufacture of the boards has a dielectric constant (ε) of 4.29.

The other dielectric material, that has been used for testing is Rogers® 3003C semi-ceramic (SC) dielectric with ε of 3.00$\pm$0.04. For the manufacture of the SC devices, SC boards (of the same thickness as FR4), copper-clad with 1 oz thick copper foil, were etched (via immersion into ferric chloride ($FeCl_3$ solution) into the requisite electrode pattern.

For experiments in this study, bacterial samples were deposited on the plasma device and subjected to the effect of plasma. The device has a surface plasma configuration, as shown in Figure 1-4(B) in Chapter 1. It consists of a sheet of dielectric, both sides of which are embedded with electrodes. The grounded electrode is a square sheet of metal. Various designs were tested out for the top electrode, as shown in Figure 3-2 before deciding on the comb like design in Figure 3-2(c). The top electrode is typically powered (i.e. input voltage is supplied to this electrode and plasma is visible on this electrode surface) during sterilization experiments.

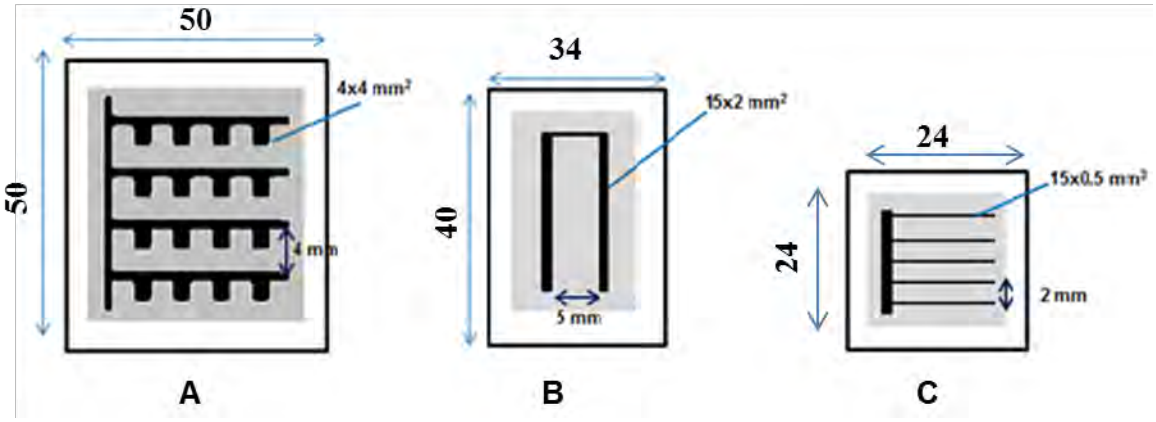

Figure 3-2. Three 'powered' electrode configurations considered (All dimensions in'mm'). 'Black' denotes powered while 'grey' denotes grounded (*on the opposite side of the dielectric surface*).

Figure 3-2(A) shows a sawtooth-like electrode design for the powered electrode. Figure 3-2 (B) shows a π- shaped electrode design. Figure 3-2 (C) shows a comb-like electrode, which is the current electrode design used. In all three design configurations shown in Figure 3-2, the light-grey colored square outlining the electrode represents the sheet of copper (grounded electrode) embedded on the *opposite side of the dielectric surface.* Figure 3-3 below illustrates the powered devices. In all three images, a red arrow denotes the point at which a metal connector is attached to the electrode surface.

This is the point through which input voltage from the transformer is supplied to the electrode.

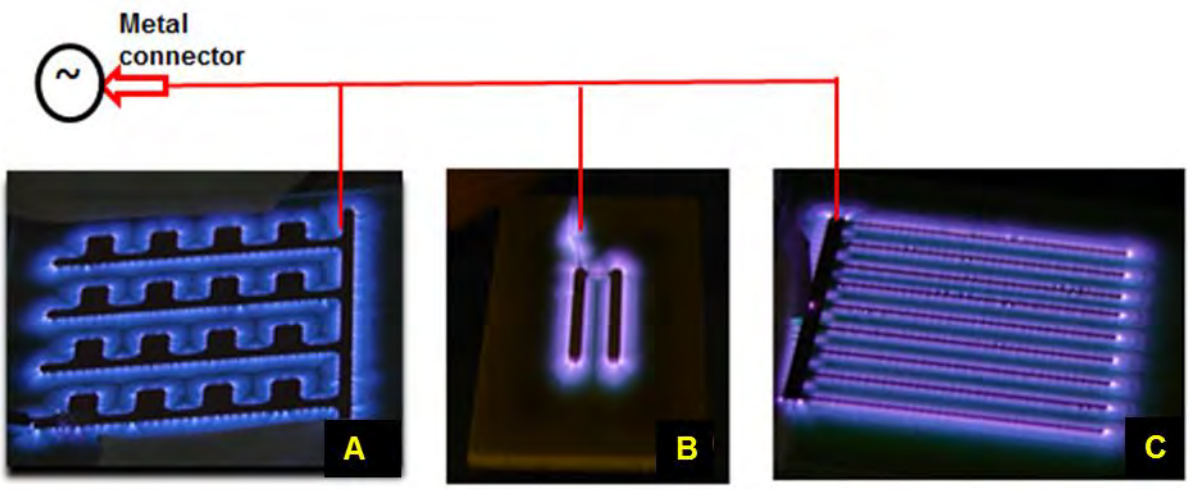

Figure 3-3. The three electrode configurations, shown in Figure 3-2, when powered

Initial feasibility tests with *Saccharomyces cerevisiae* (bakers' yeast) were conducted using the ‘'sawtooth' electrode design, shown in Figure 3-3(A). However, over time, it was observed that experimental results with this design were beginning to show inconsistency. The reason became apparent after a couple of stamp tests. A stamp test comprises a device being inoculated with a bacterial sample (i.e. the sample is deposited on top of the powered electrode and spread uniformly over the electrode surface), powered for a required time interval and then stamped face-down onto an agar plate. This agar plate is then incubated for 24-48 hours. For a device that has been completely sterilized, there should be no visible CFU (colony forming units) on the agar plate for 20 minutes. All three electrode designs were subjected to the stamp test. The results are shown in Figure 3-4, given below.

In Figure 3-3(A), it is evident that when the device is powered, plasma completely covers the dielectric surface in between the electrodes, but the actual electrode surface

area is not enveloped by plasma. This observation is supported by the results from the stamp tests, as shown in Figure 3-4(A) below. In this figure, it is observed that the surface area on the agar plate, covered by the sawtooth electrode itself, is dotted with a number of colonies while the rest of the plate is clean. Thus the wide electrode provides a haven where the test organism survives. This was not seen with narrower electrode configurations.

Figure 3-4. Stamp Test (at 60s) for three different electrode designs A) Sawtooth B) π-electrode C) comb-like electrode design

The π-electrode design, shown in Figure 3-4(B) was initially devised to combat the problem with the sawtooth electrode. However, as the stamp test from Figure 3-4 (B) indicates, while the overall vulnerability to incomplete sterilization is reduced due to a simpler design, the thickness of the two main electrodes is still too large for plasma sterilization to be effective. This conclusion is corroborated by the image of the powered π-electrode device, shown in Figure 3-3(B), wherein it is evident that plasma encompasses the entire inoculated area, except the thick electrode surface.

These observations led to the current comb-like electrode design, shown in Figure 3-2 (C) and 3-3(C). The entire electrode surface area is covered with uniform plasma, as is evident from Figure 3-3(C). Although the connector electrode for this design is 1-2 mm thicker than the individual electrodes, the plasma coverage seems to

compensate for this vulnerability, as is evident from the stamp test in Figure 3-4(C). Therefore, this electrode design was chosen for all subsequent experiments. This set of experiments also emphasized the significance of electrode surface area as a factor in plasma sterilization. Lesser the width of the electrodes, more efficient the sterilization.

3.3 The portable sterilization setup

The APRG lab, wherein most of the experimental work has been done has been set up as a BSL-I (Bio-safety level-I) facility. For experiments with BSL-II pathogens (i.e. the extremely “bad” bugs), experiments had to be conducted at the Emerging Pathogens Institute (EPI), UF, which is a BSL-II Facility. However this posed a problem, since the experimental setup shown in Figure 3-1 is quite cumbersome and non-portable. Hence a new ‘portable’ experimental setup was desirable.[1] Such a portable experimental setup has important real-world applications with battery-operated, portable sterilizers desirable for scenarios such as triage situations in third-world countries or disaster-relief situations.

A portable experimental setup, shown in Figure 3-5 below, (shown in Figure 3-1) was developed by Raul Chinga, using appropriate electrical components. The power supply for this setup achieves an output voltage of 10 kV p-p at 47kHz. The whole setup measures ~10.16 x 6.35 cm^2. The previous setup utilized a crown CDI4000 audio amplifier, which is great for audio amplification purposes, but very inefficient for amplification of single sinusoidal signal coming from the function generator.

[1] The author profusely thanks Raul A.Chinga, of the Department of Electrical Engineering ,UF for his invaluable work in building the portable experimental setup. Tests with BSL-II pathogens would have been infinitely more difficult to setup and organize, if not for the portable setup.

Compared with the previous set up used, this design operates at a single frequency band, which greatly reduces the size of the system due to the need for fewer and simpler components.

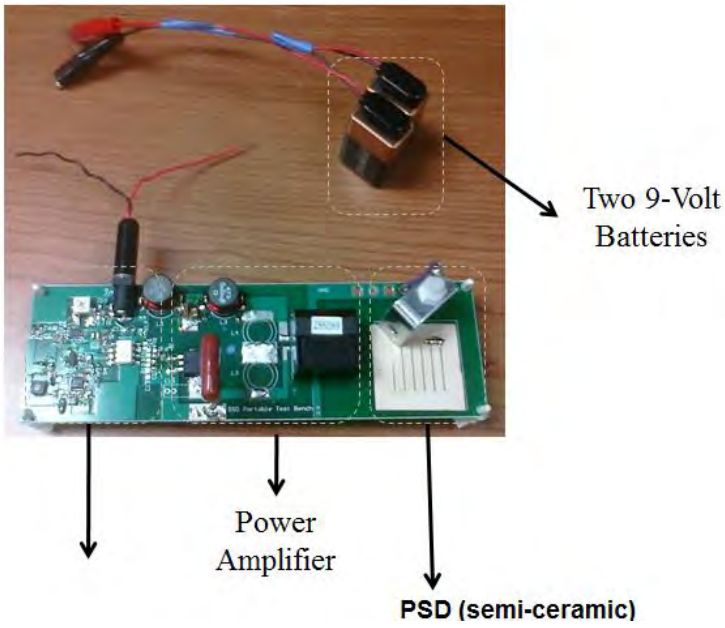

Figure 3-5. Portable experimental setup, using devices made of Rogers® 3003C semi-ceramic dielectric

The system is operated at the frequency band at which the transformer resonates with the electrode. This frequency band can be shifted depending on the physical characteristics of the transformer, which is set by the user. However, the intense heat produced at this higher operational frequency was too much for the FR4 to handle, which is why this setup was operated with the SC devices only

3.4 Description of Biological Pathogens Tested

A wide variety of microorganisms were tested for sterilization. These are summarized in the Table 3-1 given below. Owing to the BSL-I nature of the testing facility, most of the parametric studies as well as other diagnostic tests were conducted using the BSL-I organisms listed in Table 3-1. The sterilization tests with the BSL-II

pathogens were conducted to demonstrate the sterilization efficiency of the DBD plasma.

Table 3-1. Listing of all the microorganisms tested

MICROORGANISM	STRAIN TYPE	TYPE OF PATHOGEN	BSL	GRAM- / GRAM+
Saccharomyces cerevisiae	N/A	Fungus	I	G+
Escherichia coli (non-pathogenic)	C600	Bacterium	I	G-
Mycobacterium smegmatis(non-pathogenic)	ATCC 19420	Bacterium	I	G+
Pseudomonas aeruginosa	*6003-7*	Bacterium	II	G-
Yersinia enterocolitica	*SSUD 4037*	Bacterium	II	G-
Salmonella.enterica	*EPI 6031*	Bacterium	II	G-
Listeria monocytogenes	EPI 1132	Bacterium	II	G+
Vancomycin Resistant Enterococcus(VRE) faecium	VRE 82	Bacterium	II	G+
Escherichia coli(pathogenic)	EPI 562	Bacterium	II	G-
Vibrio cholera	N16961	Bacterium	II	G-
Acinetobacter baumannii	MD112	Bacterium	II	G-
Methicillin Resistant Staphylococcus Aureus (MRSA)	*WCH132*	Bacterium	II	G+
Geobacillus stearothermophilus	ND	Bacterial Spore	I	G+
Bacillus subtilis	*NCIB3610*	Bacterial Spore	I	G+

Most bacteria are either gram-positive (G+) or gram-negative (G-) and stain purple or red when subjected to a Gram-stain test. The differences in staining are due to fundamental differences in the structure of their cell walls, as shown in Figure 3-6 below.

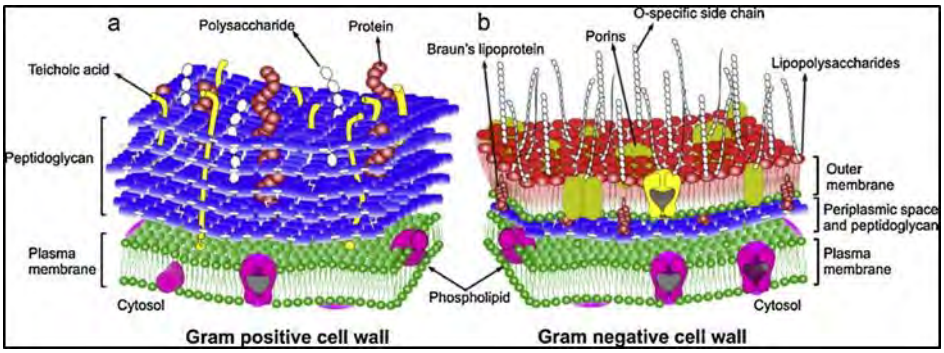

Figure 3-6. The bacterial cell wall (a) The Gram-positive envelope (b) The Gram-negative envelope

In G+ bacteria, the lipidic plasma membrane with embedded proteins is covered by a multi-layered peptidoglycan shell decorated with polysaccharides, teichoic acids and proteins. In G- bacteria, a thin peptidoglycan layer surrounds the plasma membrane and is covered by an asymmetrical outer membrane containing lipopolysaccharides, which lies on the peptidoglycan layer. Thus G-ve bacteria are more easily killed by species that damage membranes. [87]

Yeasts which stain G+, are eukaryotic organisms with a polysaccharide cell wall consisting of a moderately branched 1,3-β- glucan backbone cross-linked with 1,6-β-glucan, chitin and proteins. The structure of the yeast cell wall is shown below in Figure 3-7.

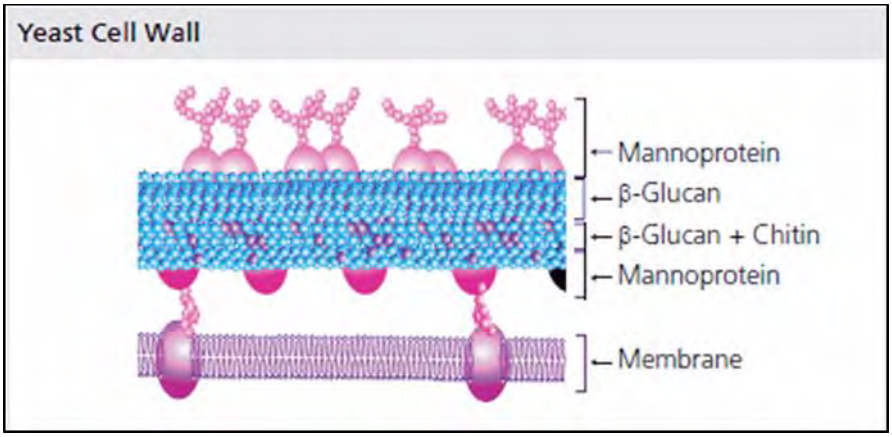

Figure 3-7. Structure of the yeast cell wall. The wall is primarily composed of mannoproteins and β-glucan that is linked (1->3) and (1->6). Ergosterol is the major lipid component of the underlying plasma structure. [88]

In order to understand the interaction of plasma with the structure of a microorganism, it is necessary to understand the structure of the micro-organism i.e. the primary cell structures protecting a micro-organism (cell envelope), the proteins essential to its survival and the organelles needed for it to breathe, grow and reproduce.

Given below is a brief description of the cell structure for each of the types of pathogens discussed.

Table 3-2. Description of organelles and essential proteins in different types of microorganisms

Type of Pathogen	*Cell Envelope*	*Important cell organelles*	*Necessary proteins/compounds*
Yeast (Fungi)	Cell wall, Periplasm, Plasma Membrane	Mitochondria (respiration), Nucleus (DNA replication and repair), Golgi apparatus and vacuoles (protein breakdown)	Proteins, Glycoproteins, Polysaccharides, Polyphosphates, lipids, nucleic acids
G+ bacteria	Cytoplasmic lipid membrane, thick peptidoglycan layer	Capsule polysaccharides, flagella (only in some species), ribosomes, nucleus	Teichoic acid, peptidoglycan, polysaccharides, lipoproteins
G- bacteria	Outer membrane containing lipopolysaccharide, Cytoplasmic membrane, thin peptidoglycan layer,	Flagella (only in some species), ribosomes, nucleus	Peptidoglycan, polysaccharides, lipoproteins.

Table 3-2 continued

Spores	Encased in a protein-rich coat, sometime surrounded by an exosporium	Depends on the host-organism, forming the endospore. Usually consists of the DNA and a portion of the cytoplasma of the host.

3.5 Experimental Protocols Followed

Before any sterilization experiment, both the bench and the metal connector are swabbed with alcohol to disinfect the experimental setup.

Additionally, before each experiment, the optical density (OD) of the microbial sample is measured using a spectrophotometer. The optical density is an important indicator of the viability of a bacterial sample.

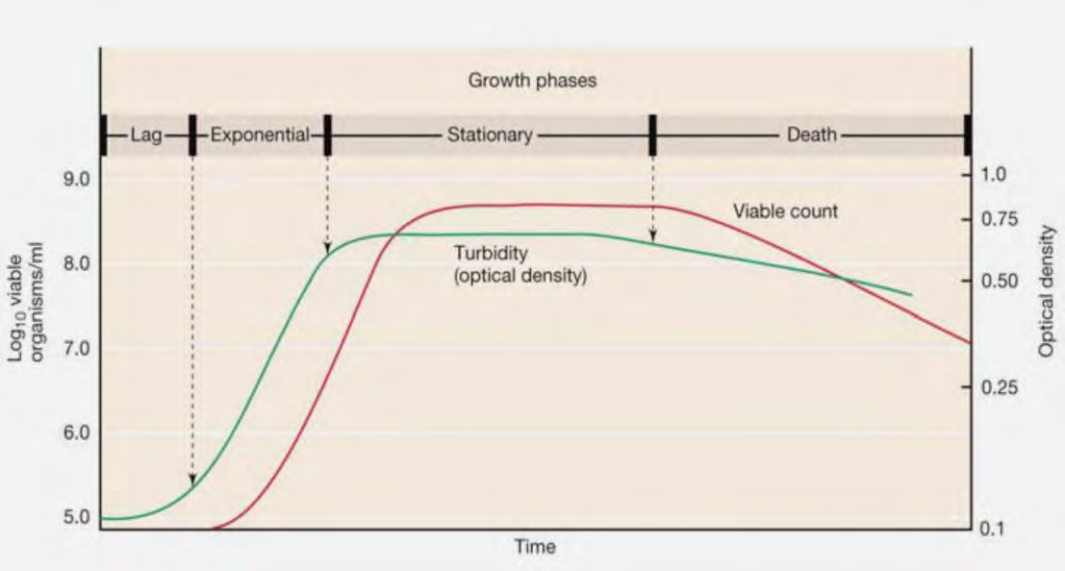

Figure 3-8. Typical growth curve for a bacterial population in a batch culture [89]

Figure 3-8 above gives a plot of the OD versus time, during the lifetime of a bacterial cell concentration. As is seen in Figure 3-8, any bacterial culture starts off with a lag phase (wherein a few bacterial colonies have grown), an exponential or

logarithmic phase (wherein growth is linear and cells are actively reproducing), a stationary phase (when maximum growth has been reached and a 'plateau-ing' effect is seen) and a death phase wherein cells begin breaking down. With the test organisms used in this study, an OD of 0.5-1 corresponds to the late logarithmic phase (which is the actively growing phase) and a high concentration of cells (~10^{6-8} CFU/ml) in the culture.

3.5.1 Preparation of bacterial biological test samples for experiments:

Saccharomyces cerevisiae (baker's yeast) was obtained from the grocery store, mixed in hot water and held at room temperature for 1 hour. A sterile loop was dipped into this solution and streaked onto a Sabouroud's (SAB) agar plate, which was then incubated at 30°C overnight. A single colony was re-streaked on SAB agar and incubated at 30° overnight. *Mycobacterium smegmatis* ATCC 19420 was grown on Middlebrook 7H10 agar plates or in Middlebrook 7H9 liquid medium at 37°C.

G. stearothermophilus was grown on trypticase soy agar or broth at 50°C. *E. coli* C600 was grown on Luria-Bertani (LB) agar or broth at 37^{o}C. All cultures were frozen at -80^{o}C in the appropriate broth with 25% glycerol and inoculated onto fresh plates before use. For each sterilization experiment, one to three colonies were inoculated into the appropriate broth and incubated at the appropriate temperature, with shaking, until the optical density (OD) of the microbial sample was between 0.5-1.

Samples of *B. subtilis* were grown via two different methods (a) In LB medium (commonly used to culture *E. coli* and other related species) (b) In minimal salts glutamate glycerol (MSgg) medium(a bio-film promoting medium). A sterile inoculating loop was swabbed with frozen cultures of *B. subtilis* and streaked onto an LB plate. This plate is incubated at 37^{o}C for 12 hours. Another inoculating loop was then used to pick

up a single colony from the incubated plate. This loop was then swirled in a glass test-tube filled with 3 ml of LB broth. This test-tube was then vortexed in a shaker, maintained at 37^{o}C for 3 hours. After 3 hours, the optical density (OD) of the sample was checked to ensure viability. This made up the LB broth culture. Subsequently, 0.3 ml of this culture was mixed with 2.7 ml of MSGG broth and vortexed for an additional half hour. After half an hour, this sample was also checked for viability by checking OD.

For each plasma sterilization experiment, the plasma device was inoculated with the requisite volume of bacterial sample. This requisite volume is known as the *inoculation volume***.** This inoculation volume is 20 µl in most cases, unless otherwise mentioned. This bacterial sample is then spread uniformly over the entire electrode surface area, using a sterile inoculating loop.

3.5.2 Post-processing of bacterial samples after experiments

- Once the experiment is completed, this device is taken and deposited in a sterile bag filled with 5 ml of culture broth (relevant to the bacterial sample being tested). The bag is sealed and agitated thoroughly using a Fisher Scientific ® Mini Vortexer Lab Mixer to wash off any micro-organisms clinging to the device.
- 0.1 ml of this broth is pipetted out into a clean dilution blank filled with 0.9 ml of Phosphate Buffered Saline (PBS) Solution and the dilution blank is vortexed for 10s. This dilutes the number of colony forming units (CFU)/ml in the bag by a tenth.
- This process is repeated, using a new dilution blank each time, until the fourth dilution is reached. Thus, a dilution series is made for each device used in the experiment.
- 0.1 ml from each dilution blank in the dilution series is then pipetted out onto a fresh agar plate (relevant to the type of inoculating pathogen) and spread uniformly.
- These plates are then incubated at the required temperature for 24-48 hours. Colony-count methods are used to estimate the number of CFU/ml on the 0th dilution.
- This process is repeated for each device being tested in the experiment.

- A survival curve (plot of logarithm of number of CFU (colony forming units)/ml versus testing parameter) is then plotted. Testing parameter can be sterilization time, input voltage etc.
- Experiments are performed in triplicate (unless otherwise mentioned) to ensure repeatability.

3.5.3 Ozone Safety Protocol[2]

The DBD plasma devices also produce ozone as a byproduct. This concentration of ozone is greatest at the locations nearest to the device. To ensure that laboratory personnel are not exposed to unsafe levels of ozone, an ozone monitor is used to determine safe operating conditions. Occupational Health and Safety Hazard (OSHA) standards regulate employee exposure to ozone gas through its Air Contaminants Standard, 29 CFR 1910.1000. The permissible exposure limit (PEL) is listed as an 8-hour, time-weighted average value of 0.1 part of ozone per million parts of air (ppm) and the short term exposure limit (15 minutes) is 0.3 ppm. All experiments must be done under conditions that stay below these exposure limits.

This protocol is an internal safety document recommended for the plasma generation device with chamber door open or closed. Based on the test results it was established that for this particular set-up at any instant ozone is within allowable levels according to OSHA regulations.

Step 1: Switch on the 2B Tech® 202 Ozone monitor (1ppb resolution) 10-15 minutes before the experiment. It should read room ozone concentration as ~0.02ppm.

Step 2: Connect circuit according to Figure 3-1. Double check all connections. Make sure the LabVIEW interface is able to read the ozone-meter.

[2] The author thanks Poulomi Banerjee for her rigorous work in setting up an ozone safety protocol

Step 3: Set-up the experiment. Usually, experiments are conducted within an acrylic chamber (48”x24”x23”) , which is always kept closed while the device is running. Additionally, as a precaution, the chamber is kept closed for another 10 minutes after switching off the device. Cover the device with a pre-designed charcoal mesh (to be explained, in Chapter 4) with particle size between 1.4 mm to 4.75 mm. The charcoal adsorbs the ozone

Step 4: User should always be in the safe zone from the device, which is at least 36 inches away from the outer acrylic wall of the chamber. It was observed that ozone does not exceed maximum allowable limit at this distance even when the chamber door is open.

Step 5: During an experiment, do not keep the device running for more than 20 minutes at a time. No more than 15 experiments should be run in one day. The charcoal mesh should not be removed at any point of the experiment.

Step 6: When removing the concerned device from the acrylic chamber (for further post-processing), check the ozone levels inside the chamber. A 3M® 8514 respirator mask is available for ozone protection up to 10 times OSHA PELs (Permissible exposure limits) and may be worn while shutting down the device or for all subsequent protocols.

If there is excess ozone at any stage of the experiment, power down the setup immediately. Open the doors and windows of the room. Step away from the device.

Thus far, Chapter 3 outlined the experimental setup used, the diagnostic measures employed to evaluate different experimental parameters, the different types of pathogens tested and the experimental protocols employed before and after all

plasma sterilization experiments completed during the course of this study. Chapter 4 and 5 describe the bulk of the research completed in understanding DBD plasma sterilization.

CHAPTER 4
PARAMETRIC STUDIES IN DBD SURFACE PLASMA STERILIZATION

In trying to understand DBD surface plasma sterilization, my research followed two paths (1) The bulk of research in plasma sterilization uses mostly volume plasma configurations. The DBD *surface* plasma setup used in this paper required a different set of experimental protocols to be developed, in order to facilitate the testing of microorganisms exposed to plasma. Before understanding the mechanism of plasma sterilization, it was necessary to conduct a parametric study in order to understand the sterilization capabilities of such a setup. The variation of the different input parameters involved in plasma generation help understand what enhances and what inhibits DBD surface plasma sterilization (2) Studying the mechanism of surface plasma sterilization involves understanding how each component of plasma (UV photons, reactive chemical species and temperature) affects the process of plasma sterilization. This has been further explained in Chapter 5.

This chapter describes the parametric studies conducted in understanding DBD surface plasma sterilization. The plasma sourced used in this study is an AC, RF-plasma operating at an input frequency of 14 kHz and an input voltage of 12 kV p-p (unless otherwise mentioned). The different parameters tested were 1) Type of Pathogen 2) Inoculation Volume 3) Nature of dielectric substrate 4) Input power/frequency 5) Operating Pressure

4.1 Type of Microorganism

The protocol for each of the sterilization experiments is the same: take a clean plasma device, inoculate it with the requisite volume of microorganism sample (this volume is defined as inoculation volume), power the device for a fixed time interval (Δt),

thus generating plasma, turn off the plasma at the end of Δt, remove the device carefully from the electrical bench and then subject it to the post-processing protocol described in Section 3.5.2. Plates recovered from each device tested are incubated as previously described and colony counts are obtained in order to recover the number of microbial survivors (N) in each case. 'N' is expressed in terms of colony forming units (CFU).

A survival curve is the plot of $\log_{10}N$ versus the plasma exposure time (Δt). In this study, survival curves were obtained using *S. cerevisiae (Yeast), Escherichia coli, B. subtilis, G. stearothermophilus* spores and a wide range of BSL-II microorganisms, further described below.

In the case of plasma sterilization, the norm is to triplicate each experiment in order to ensure repeatability. Hence each sterilization experiment described in this study has been triplicated whenever possible. However it is prudent to analyze the source of error in these experiments. Error analysis for the purpose of experiments discussed herein can be classified into two types:

Analysis of the error associated with the microbiological technique used during post-processing: The post-processing protocol that each device is subject to after plasma exposure is explained in detail in Section 3.5.2. Most of the error analysis methods used here are obtained from Niemela et al. [90]. Assuming that there is no significant change in the volume of bacterial sample deposited on the device, due to the inoculating loop, the other experimental uncertainties introduced are given below:

(a)Variation of particle numbers due to uncertainties in counting: This is expressed by a term known as Poisson scatter ($w_z^2 = \frac{1}{z}$, where 'z' is the average number of colonies observed).

(b)Uncertainty of the test-portion volume (w_v): This itself is the result of three main influences: a) repeatability of filling and emptying the measuring device (pipette) b) specification of glassware manufacturer c) temperature effect when calibration and measurement takes place at different temperatures. For our purpose, (a) and (c) are assumed to remain insignificant (i.e. no systematic errors).

(c)Uncertainty of the dilution factor: The uncertainty variance of a dilution step is obtained from the below formula:

$$w_f^2 = \frac{(u_b^2 + b^2 w_a^2)}{a + b^2} \quad (4\text{-}1)$$

where a= suspension transfer volume (0.1 ml), b= dilution blank volume (0.9 ml), u_a= standard uncertainty of 'a' (0.3 µl, from manufacturer), u_b= standard uncertainty of 'b' (1.5 µl, from manufacturer), w_a= relative standard uncertainty of 'a' (0.003). If the total dilution consists of 'k' similar steps, combined RSD^2 of the dilution factor = $w_F^2 = k w_f^2$. For instance, if a sample has been diluted to 10^{-4}, k= 4.

Hence total uncertainty of the result = $w_y = \sqrt{w_F^2 + w_v^2 + w_z^2}$, where w_F^2 and $\frac{1}{z}$ are already defined and w_v^2 is the uncertainty associated with the 0.1 ml that is transferred from the dilution blank to the agar plate (Since the same pipette is used for transferring volume 'a' and 'v', $w_v = w_a$)

Each sterilization experiment typically has 4-5 data points at which to test sterilization. For each of these points, a different plasma device is used. Although each device is manufactured using the exact same specifications, there is always an element of uncertainty involved. Moreover, once the inoculated device is placed on the electrical

bench and the device powered, there is a short lag time, during which the input voltage is manually increased to 12 kV p-p. This also introduces a factor of uncertainty. Since DBD plasma sterilization occurs on very short time scales, these uncertainties affect 'z', which in turn affects the total uncertainty calculated. Thus, for the purpose of the experiments discussed herein, experimental error is difficult to estimate via this method

Analysis of the variation of plate counts obtained in each sterilization experiment : Most commonly, the Analysis of Variance (ANOVA) is used to compare groups of measurement data. For instance, if a group of five random students in four different laboratories were to conduct the same experiment and record their observations, the ANOVA could be used to compare the variance of the mean of the observations within each group of students as well as the average variance within each laboratory.

In a one-way ANOVA, there is one measurement variable (values that are measured or recorded) and one nominal variable (categorical variables which are not measured, but rather defined at the beginning of the experiment). However for each sterilization experiment, there are usually two nominal variables (the type of device used and the sterilization parameter being tested). Experimental protocols designed for this setup do not permit the usage of the same device for each data point in a single sterilization experiment. The application of the one-way ANOVA assumes homoscedasticity (data obtained in all three trials have the same standard deviation), which does not hold true for the plasma sterilization experiments. For instance, a plasma exposure of 60s, using a SC device, might lead to a 4-$\log_{10}$ reduction in one

trial, but a 3-$\log_{10}$ reduction in another and a single $\log_{10}$ reduction in the 3rd trial. Hence it is unsuitable to use ANOVA for the sterilization tests described in this study.

Thus, for the purpose of this study, sterilization data in different cases is presented in one of two ways. For experiments with three trials or more, the mean of data, over all the trials, at each data point has been calculated and plotted on a $\log_{10}$ scale (For instance, Figure 4-1 below). The variation in plate counts between trials at each time point is shown in terms of the standard deviation. However, for some other experiments with two trials or more, data for all the trials has been presented in one plot, simply because the variation in data is better presented this way (For instance, Figure 4-2, 4-3).

BSL-I Microorganisms- Microorganisms tested in this case were *S. cerevisiae, E. coli* C600 *and Mycobacterium* smegmatis (Table 3-1). Even though it is a fungus, *S. cerevisiae* stains similar to gram-positive (G+) bacteria. The latter two are classified as gram-negative (G-) and G+ bacteria respectively. A detailed description of gram-positive and gram-negative bacteria is given in Chapter 3. All BSL-I microorganisms have been tested on both FR4 and SC devices. Survival curves obtained using SC devices are described in Section 4.3. While sterilization tests were repeated in triplicate using *E. coli* and *S. cerevisiae,* the sterilization tests with *M. smegmatis* were not repeated.

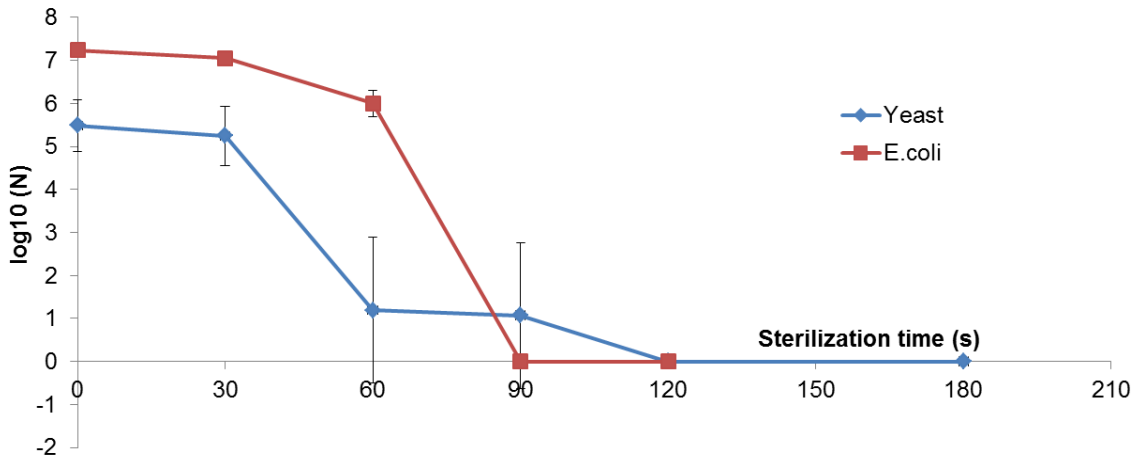

Figure 4-1. Survival curves obtained using FR4 plasma devices and *S. cerevisiae* (Yeast) and *E. coli* as test pathogens. Complete sterilization is obtained within 90-120s.

Figure 4-1 above shows the survival curves for two test pathogens, *S. cerevisiae* and *E. coli* respectively. Plasma exposure times of Δt= 30,60,90,120s were tested using FR4 devices. The sterilization plots in Figure 4-1 have been plotted by obtaining the average of $\log_{10}$ (N) over a number of trials versus sterilization time (t). As explained in Section 4.1.1, the error bars, plotted as the standard deviation of this data, do not indicate error associated with the experiments, but rather the variation observed in the number of survivors at that particular time point.

Figure 4-1 demonstrates that, using FR4 devices, complete inactivation of *Yeast* and *E. coli* is obtained in 90s and 120s respectively. Complete inactivation implies the reduction of a pathogen concentration from N_o CFU (at t= 0s) to zero CFU. For yeast, an additional sterilization time point of 180s was also tested, wherein also complete inactivation is observed. From Figure 4-1, it is also evident that a greater variation in plate counts is seen in the case of yeast as compared to the case of *E. coli*. This variation is especially noted at t=60s and 90s. Due to the noted variation, sterilization experiments using yeast were repeated over 6 trials instead of the standard 3. During

these trials, it was observed that in 4 out of 6 trials, complete inactivation of yeast occurred after t= 60 and 90s. The incomplete inactivation in the remaining 2 trials at t= 60s and 90s is what contributes to the large variation observed for yeast in Figure 4-1.

Ying et al. [55] used a 10 kV, 6.5 kHz volume plasma configuration to report a 5-$\log_{10}$ reduction in yeast concentration after 5 minutes of plasma exposure time. 100% reduction was not obtained within this time. Sohbatzadeh et al. [61] reported a 100% reduction in E. coli concentration after exposing bacterial samples for 15 minutes to a 50 Hz, 5.4 kV DBD plasma (volume-discharge configuration). On the other hand, Lee et al. [45] reported complete sterilization of *E. coli* on exposure to a 2.45 GHz, microwave plasma. Compared with these results, our reported sterilization time is considerably reduced.

Since only a single sterilization test for *M. smegmatis* was done, using both FR4 and SC devices, the data is not reported here. Incomplete inactivation was noted for both FR4 and SC devices in the case of *M. smegmatis*. Starting from an intial bacterial concentration of 10^6 CFU, a plasma exposure time of 2 minutes resulted only in a 2-3 $\log_{10}$ reduction.

B. subtilis cells were also exposed to plasma at the same input parameters of 14 kHZ frequency and 12 kV p-p. *B. subtilis* is a Gram-positive, rod-shaped spore-forming bacterium, commonly present in soil and the human gut. They have become widely adopted as a model organism for laboratory studies. As described in Section 3.5.1., the *B. subtilis* samples were prepared in two different media: LB and MSgg media. For the sake of discussion, *B. subtilis* cells grown in LB and MSgg medium will be referred to as *B. subtilis-I* and *B. subtilis-II* respectively. While LB medium enables the *B. subtilis* cells

to express the wild-type single cell phenotype, MSgg medium enables them to express a phenotype that promotes biofilm growth [91]. A biofilm is an assemblage of one or more bacterial species that forms on a surface. The bacteria are embedded in an exo-polysachharide matrix. Biofilms tends to be more resistant to biocides than the wild-type. Figure 4-2 shows the survival curves for both types of *B. subtilis* cells. While *B. subtilis-II* were completely inactivated within 4 minutes, it is interesting to note that *B. subtilis-I* concentration plateas at about 10^4 CFU after 6 minutes of plasma treatment. We do not know the number of spores formed under these two growth conditions and the plateau may represent spore survival.

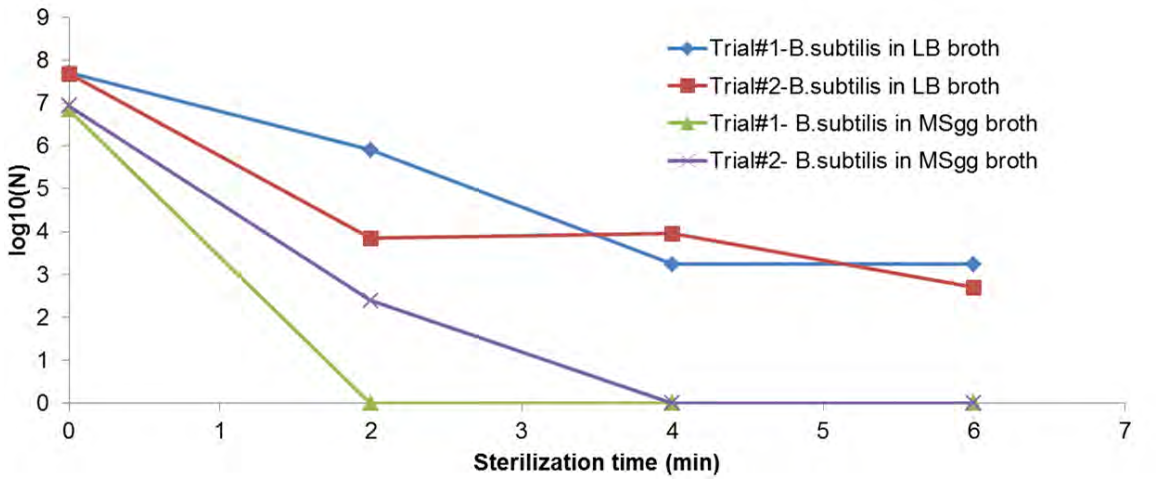

Figure 4-2. Survival curves, using FR4 devices for *B. subtilis* cells grown in LB and MSgg medium

Sterilization tests with *B. subtilis* were conducted in duplicate. Hence data for both trials are shown in Figure 4-2 above. Complete inactivation is obtained in 4 minutes in the case of *B. subtilis-II* while even after 6 minutes, incomplete inactivation is observed in the case of *B. subtilis-I.* As already stated, *B. subtilis-I* and *B. subtilis-II* differ in the type of phenotypes expressed. Simply put, the cells in *B. subtilis-I* tend to have a higher degree of locomotion [92] while the cells in *B. subtilis-II* are more likely to

form exo-polysaccharide matrices [93]-[94]. Thus Figure 4-2 seems to indicate that matrix-forming *B. subtilis* cells are more susceptible to plasma than motile *B. subtilis* cells. The percentage of spores formed under each condition is not known at this time.

Akishev et al. [83] reported similar experiments wherein they use a plasma jet (operating at a power of 60 W) to inactivate both vegetative cells and spores of *B. subtilis*. Their experiments reported incomplete inactivation of both types (~4 $\log_{10}$ reduction) in CFU, even after 10 minutes of plasma exposure. However they reported complete inactivation in one particular type of vegetative cells (*B. subtilis*) cultured on a less nourishing medium. Hence they concluded that the type of medium in which cells are cultured also affects their inactivation time. This susceptibility of a particular cell type to plasma will be discussed in greater detail in Chapter 5.

The last kind of BSL-I microorganism to be tested was a purified suspension of *Geobacillus stearothermophilus* spores. *G.* stearothermophilus spores are rod-shaped, Gram-positive bacteria, widely distributed in soil and are usually a cause of spoilage in food products [95]. *G. stearothermophilus* spores are commonly used as biological indicators for periodic checks of sterilization cycles as they are highly heat resistant. *G. stearothermophilus* purified spores were used for sterilization tests to examine the resistance of spores themselves without any contaminating vegetative cells.

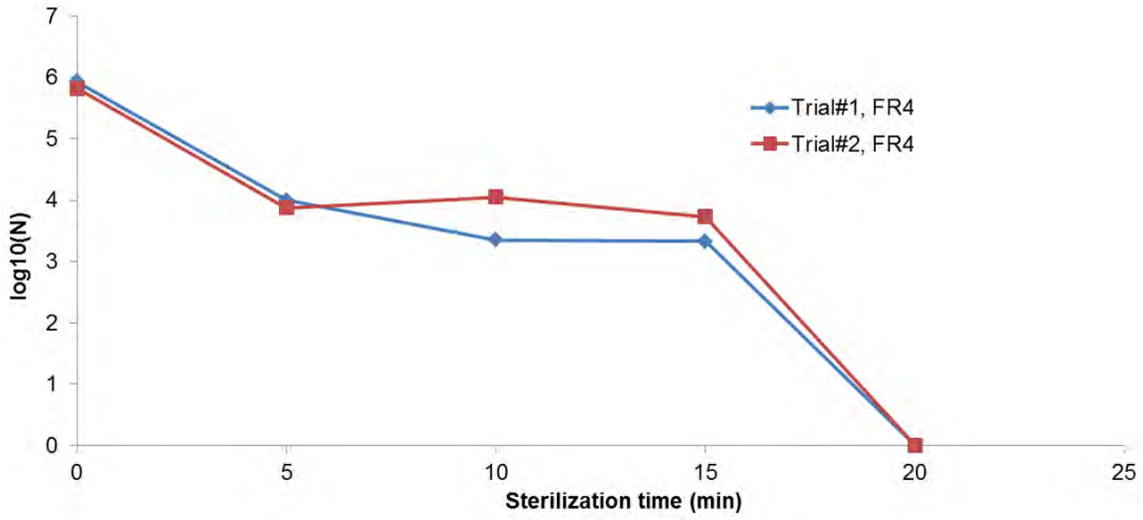

Figure 4-3. Survival curves, using FR4 devices for G*. stearothermophilus* spores

Figure 4-3 above shows the survival curves for *G. stearothermophilus* spores (with an inoculation volume of 40 µl). Here also, only FR4 devices were used and sterilization tests were conducted in duplicate. Data for both trials is shown in Figure 4-3. Complete inactivation of *G. stearothermophilus* spores is obtained within 20 minutes. Figure 4-3 shows a triphasic behavior, with an initial drop in spore concentration, followed by a lag phase and finally, a rapid tail phase.

In order to compare sterilization efficiency, the D-value is often used as a comparison parameter. 'D' value for any survival curve is defined as the time taken for a reduction of 90% in the CFU i.e. the time taken for a single $\log_{10}$ reduction. The D-value can be calculated using the formula [71]

$$D = \frac{t}{\log_{10} N_0 - \log_{10} N} \tag{4-2}$$

From Figure 4-1, a phasic behavior is noted (bi-phasic for *E. coli* and tri-phasic for yeast). Typically a D-value can be calculated for each of these phases.However owing to the experimental protocols designed for each of these tests, select time points

(30s-120s) can only be tested. From survival curves shown in Figure 4-1, a slow inactivation phase followed by a steep drop in pathogen concentration is observed. Since experimental protocols allow only a limited number of time-points, D-value for each phase cannot be calculated. However, the D-value for the initial linear portion of the survival curve has been calculated and shown below in Figure 4-4.

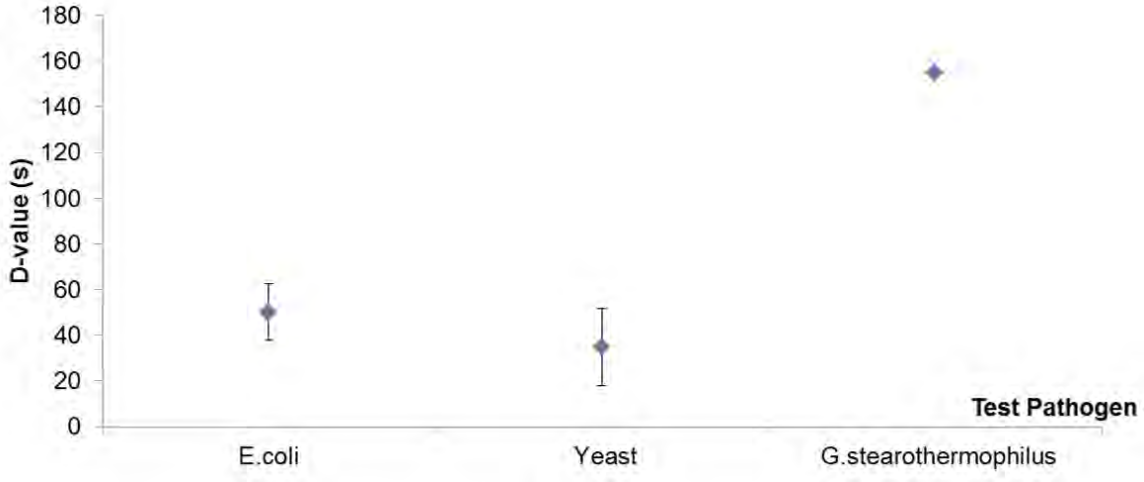

Figure 4-4. Comparison of D-values for the different test microorganisms, using FR4 devices

In Figure 4-4 above, D-value is calculated as an average of the D-values from individual sterilization trials for each test organisms. Thus, for *E. coli*, *yeast* and *G. stearothermophilus,* the D-values are calculated as 50s, 35s and 155s (2.5 minutes) respectively. The larger variation in D-value in the case of yeast is mirrored in Figure 4-1. For the purpose of sterilization experiments, yeast seemed a little less dependable as a test organism. Hence for all successive sterilization tests, *E. coli* was used as the test organism.

BSL-II Pathogens: Sterilization experiments were also carried out with a host of BSL-II pathogens, using the portable experimental setup (Section 3.3) and hence, using only SC devices. Plasma generation parameters used were an input voltage and

frequency of 10 kV p-p and 47 kHz respectively. Table 4-1 below shows the results of these tests.

Table 4-1. Results obtained from Plasma Sterilization Experiments with BSL-II pathogens

Type of pathogen	Sterilization time (min)	Observed reduction in bacterial concentration	Complete inactivation	G-ve or G+ve
P.aeruginosa 6003-7	2	8 $\log_{10}$	YES	G-
Y.enterocolitica SSUD 4037	2	8 $\log_{10}$	YES	G-
S.enterica EPI 6031	3	7 $\log_{10}$	YES	G-
Listeria monocytogenes	3	8 $\log_{10}$	YES	G+
Vancomycin Resistant Enterococci (VRE)	3	8 $\log_{10}$	YES	G+
Escherichia coli	3	8 $\log_{10}$	YES	G-
Vibrio cholera	3	8 $\log_{10}$	YES	G-
Acinetobacter baumannii	3	4 $\log_{10}$	NO	G-
MRSA WCH132	2	3 $\log_{10}$	NO	G+

While a detailed survival curve was plotted for BSL-I pathogens, using equally plasma exposure time intervals (30s, 60s, 90s and 120s), the same was not done for BSL-II pathogens. Owing to the caution needed in a BSL-II environment and the availability of a single portable experimental setup during this time, only a single sterilization time point was tested for most of the BSL-II pathogens. However, a complete survival curve was plotted for MRSA WCH132 **(**initial concentration= 10^8 CFU)**,** wherein different inoculated devices were exposed to plasma for 30s, 60s, 90s, 120s. Only a 3 $\log_{10}$ reduction was observed in 2 minutes. Even when the sterilization time was extended to 3 minutes, only a 4 $\log_{10}$ reduction in bacterial concentration was observed, but complete inactivation proved elusive, suggesting that this strain of MRSA is more plasma-resistant than other vegetative cells.

The main purpose of the BSL-II tests was to characterize the effectiveness of the generated DBD plasma in sterilizing BSL-II pathogens. In doing so, it is obvious that the DBD plasma used in this study is capable of completely inactivating a wide variety of resistant pathogens within 2-3 minutes. Table 4-1 also points to the fact that inactivation due to the generated plasma exposure seems to be independent of whether the pathogen is gram-negative (G-ve) or gram-positive (G+ve), since similar sterilization times have been noted for both types of pathogens.

Thus Section 4.1 provided a summary of the sterilization effectiveness of DBD surface plasma against a wide range of vegetative and spore-producing pathogens. Another factor that also determines sterilization effectiveness is the inoculation volume used for sterilization tests i.e. the amount of pathogen sample deposited on the surface of the plasma device. This is further discussed in Section 4.2.

4.2 Inoculation Volume

For the purpose of this study, the volume of pathogen sample deposited on the electrode surface of the plasma device is defined as the *inoculation volume.* This sample is then spread uniformly over the entire surface area of the electrode, using a sterile inoculation loop. This experimental parameter is important, owing to the relationship between pathogen density and sterilization time and due to the presence of water, proteins and salts in the inoculum. The purpose of testing a higher inoculation volume was to understand the dependence of sterilization time on the volume of liquid bacterial sample deposited on the dielectric surface i.e. whether a higher volume of liquid sample led to a longer sterilization time. To that end, survival curves were obtained using a higher inoculation volume (40 μl).

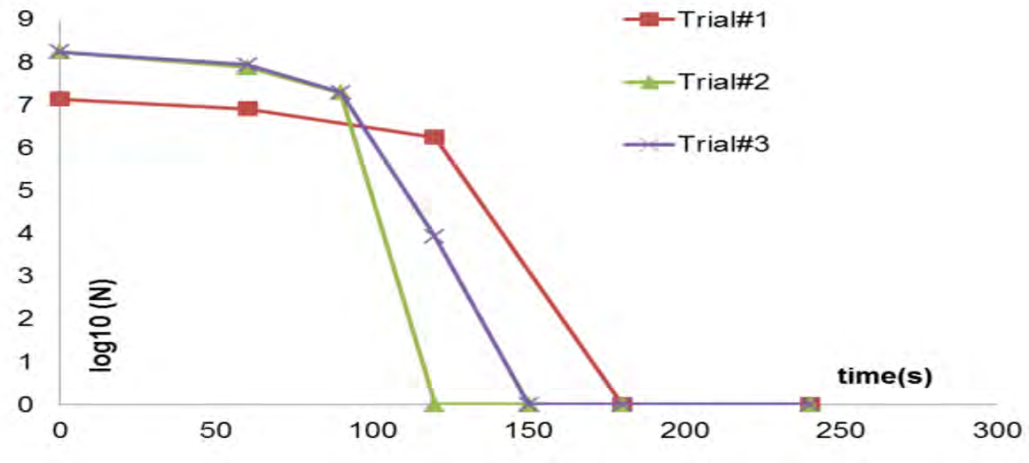

Figure 4-5. Survival curves for inoculation volume= 40 µl of E. coli

Figure 4-5 above shows the survival curve for all three trials, using 40 µl of *E. coli*. The sample of *E. coli* used for these experiments had an OD in the range of 0.5-1, which correlates to 10^8 CFU/ml. Hence 20 µl and 40 µl of this sample should correlate to $2x10^6$ CFU and $4x10^6$ CFU respectively. However, this difference in CFU is not significant enough i.e. essentially, the same number of *E. coli* cells are being deposited in different sample volumes.

As is evident, while 20 µl of *E. coli* requires a complete sterilization time of 90-120s, 40 µl requires a complete sterilization time of 150-180s. Furthermore, the "passive phase" wherein there is little or no loss of viability, that was noted in Figure 4-1, is extended by about 30s here i.e. the rapid drop in *E. coli* concentration occurs after t>90s, as opposed to after 60s in the case of the lower inoculation volume (20 µl). Thus a higher inoculation volumes leads to a longer sterilization time. However this extension in sterilization time seems to be more dependent on the volume of sample deposited than the number of CFU in the sample.

Thus far, in the sterilization tests discussed in Section 4.1 and 4.2, only FR4 devices have been used. However a different dielectric material was also used for sterilization tests, the results of which are discussed in Section 4.3.

4.3 Nature of Dielectric Material

The nature of the dielectric material/substrate is a very significant factor in plasma sterilization. The ability of the dielectric material to withstand larger number of plasma cycles determines the lifetime of a plasma sterilization device. This ability could be dependent on sterilization time, type of organic residue/material usually remnant on the substrate material and input plasma power density.

Kelly-Wintenberg et al. [19] commented on the nature of the substrate material and its influence on the 'D'-value. They used a volume-DBD plasma setup, using *E. coli* as the test organism and conducted sterilization tests using polypropylene, glass and agar as possible substrates. They found that sterilization on polypropylene surface took the least 'D' time, followed by glass and then agar. They speculated that the cells drying out on glass slides require a larger concentration of active species for effective sterilization, as opposed to cells which do not penetrate the fibers of poly-propylene surfaces and hence require lesser concentration of active species.

Lerouge et al. [14] speculated on the relationship between substrate material and 'D' value, proposing four explanations:

- dielectric heating of the substrate material according to relationship

  $$P = \pi f \tan\delta \varepsilon' E^2 \qquad (4\text{-}3)$$

  Here P= RF power absorbed, E is electric field value, ε' is relative permittivity, *f* is the excitation frequency and tanδ is the loss tangent.

- Different pathogens cling to different surfaces differently, depending on degree of adhesion.

- Substrate interference with the process: This can happen, if during the course of plasma exposure, substrate itself gets pitted or etched, thus increasing its adsorption capacity and hence enabling it to adsorb a larger concentration of chemical species available, thus hampering sterilization.
- A possible “catalytic” effect of the substrate, in which the substrate itself sets off the ionization process.

Sterilization experiments with FR4 devices have been discussed in great detail in Section 4.1 and 4.2. Figure 4-6 below compares sterilization effectiveness between FR4 and SC devices using (A) yeast and (B) *E. coli* as test organisms. The testing protocol with SC devices is the same as with FR4 devices. Inoculation volume used was 20 μl.

As is evident from Figure 4-6, the time taken for complete sterilization in the case of SC devices is 180s and 120s in the case of *Yeast* and *E. coli* respectively. Even for complete bacterial inactivation, FR4 devices take ~30s lesser time for complete sterilization, as compared to SC devices. The D-value (time required to sterilize 90% of the bacterial concentration) for the FR4 dielectric is lesser than the SC dielectric, both for *E. coli* and Yeast. This is shown in Figure 4-7 below.

The shortest ‘D’ value appears to be for FR4 in the case of yeast. For *E. coli*, the D-value in the case of FR4 is ~20s shorter than in the case of SC. The D-value in the case of yeast, for SC, is the highest and shows the highest standard deviation. The high standard deviation in this case implies that the sterilization of yeast using the SC dielectric was highly unreliable.

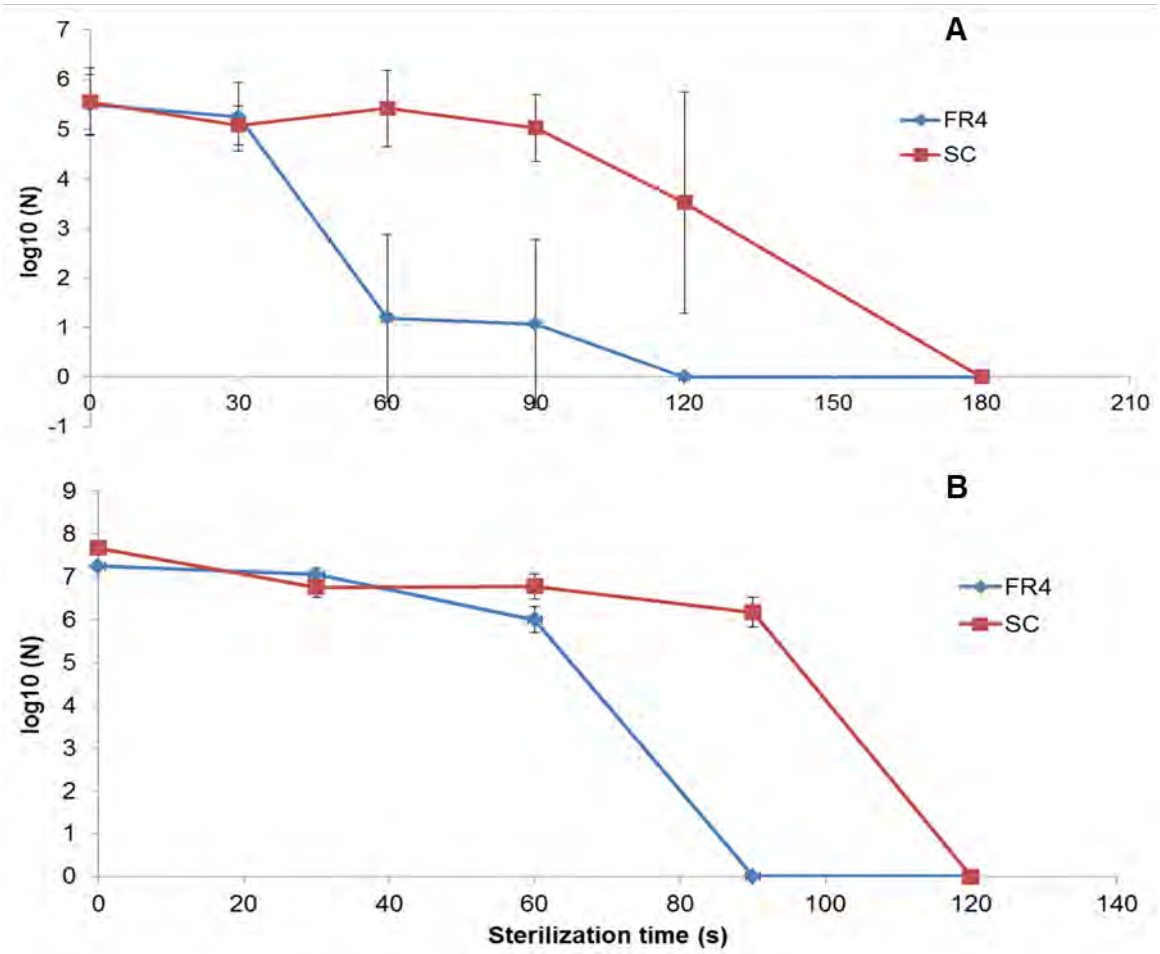

Figure 4-6. Survival curves comparing FR4 and SC plasma devices for A) *S. cerevisiae and B) E. coli*

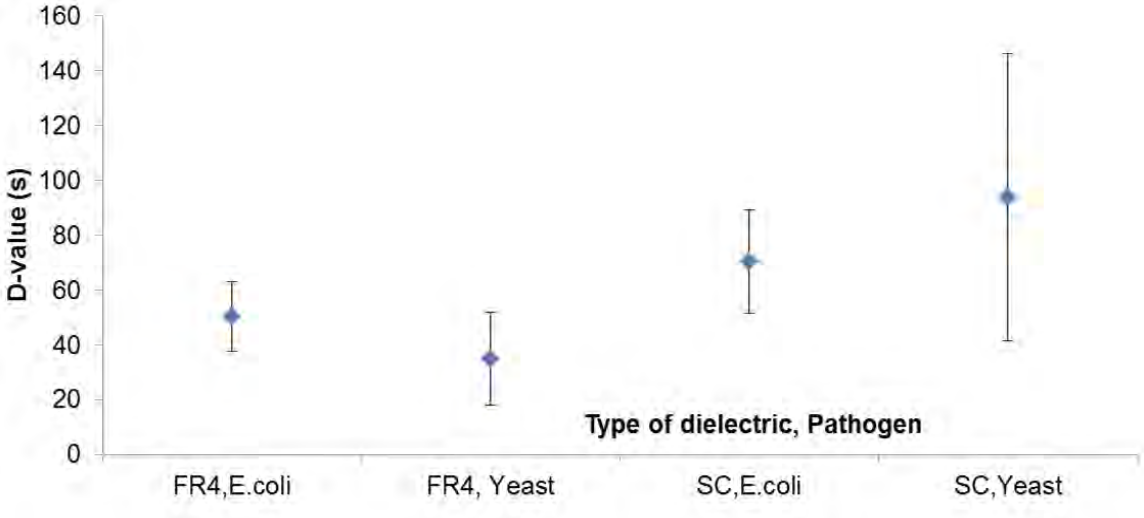

Figure 4-7. Comparison of D-values for the different (dielectric, test pathogen)

In order to get a better understanding of the difference in FR4 and SC for the purpose of plasma sterilization, clean and inoculated devices (both FR4 and SC) were powered and diagnostic data (spectroscopic, ozone, surface temperature and input power) measured. The former three and their significance are explained in further detail in Chapter 5. Section 4.4 discusses the input power data and its significance.

Scanning Electron Microscopy (SEM) and Energy Dispersive Spectroscopy (EDS) analysis was used to observe the substrate modification after several cycles of plasma sterilization. SEM imaging and EDS analysis were done in the Major Analytical Instrumentation Center (MAIC) at the University of Florida. SEM imaging of a device consists of scanning an electron beam across the surface of a sample, line by line, much like reading a book. This is a called a *raster* pattern. At each location where the electron beam strikes the sample, an electron signal is used to produce contrast in the image displayed on a cathode ray tube (CRT) viewing screen. In SEM terminology, magnification is the difference between the size of the scanned area on the sample surface and the size of the display showing the resulting image. Simply put, SEM magnification is akin to imaging a small 1 mm x1 mm square on a surface and displaying it in a 100 mm x 100 mm square, which corresponds to a 100x magnification. This is fundamental in understanding, simply because the magnification in the case of SEM is significantly different from light microscopy.

For the purposes of the SEM studies discussed herein, a JEOL SEM-6400[3] scanning electron microscope, with an accelerating voltage of 15 kV and a magnification of 10x-300000x was used. The SEM images shown herein were obtained

[3] For the SEM imaging, Thanks are due to the folks over at Major Analytical Instrumentation Center (MAIC), UF , especially Wayne.A.Acree and Dr.Mike Kesler.

at a magnification of 2000x. The scale bar, at the top left corner of the image, provides an idea of the length scale of structures in the image.

In addition to analyzing the appearance of the dielectric substrate, an idea of the elemental makeup of the individual dielectric substrate was also obtained using EDS analysis. The elemental makeup can determine the difference between the FR4 and SC dielectric and detect the deposition of additional salts or oxides during plasma sterilization. Owing to the nature of the EDS setup, a qualitative, rather than quantitative idea of the elemental makeup of the surface can be achieved i.e. for a given dielectric surface, its elemental makeup can be determined, but not the percentage of each element. When an electron beam hits the surface, atoms in the dielectric surface interact with this beam and undergo energy shell transitions, resulting in the emission of an X-ray. This emitted X-ray has an energy characteristic of its parent element, which can then be identified. This sums up the process of Energy Dispersive X-ray spectroscopy.

The primary goal of the SEM and EDS studies was to test the effect of prolonged plasma generation on the dielectric substrate. Fresh FR4 and SC devices were taken and subjected to one of the protocols described below. Once the protocol for each device was repeated for the requisite number of cycles, they were then prepped for SEM imaging and EDS analysis.

Table 4-2. Description of protocols that the different devices were subjected to, prior to SEM Testing.

Protocol#	Description of Protocol	No. of cycles
1	Clean device, no plasma, serves as control	0
2	Clean device, powered continuously for 20	1

	minutes	
3	Inoculated with 20 μl of *E. coli* and powered for 2 minutes.	5 (=10 min of plasma)
4	Inoculated with 20 μl of *E. coli* and powered for 2 minutes.	10 (=20 min of plasma)
5	Inoculated with 20 μl of *E. coli* and powered for 2 minutes.	25 (=50 min of plasma)

It should be noted that for protocol#2, a continuous plasma run time of 20 minutes was used to mimic protocol#4, minus the constant inoculation with *E. coli.* The goal of doing so was to compare the effect of prolonged plasma exposure on a clean device versus an inoculated device.

Figure 4-8 (A-E) below depicts SEM images taken of the dielectric surface of the different devices (corresponding respectively to protocols 1-5) at 2000x magnification. Figure 4-8 (F-J) depicts images of the electrodes of the same devices at 2000x magnification. Figure 4-9 represents similar images for the SC devices. The scale bar for all images, at the top left corner, is 20 μm.

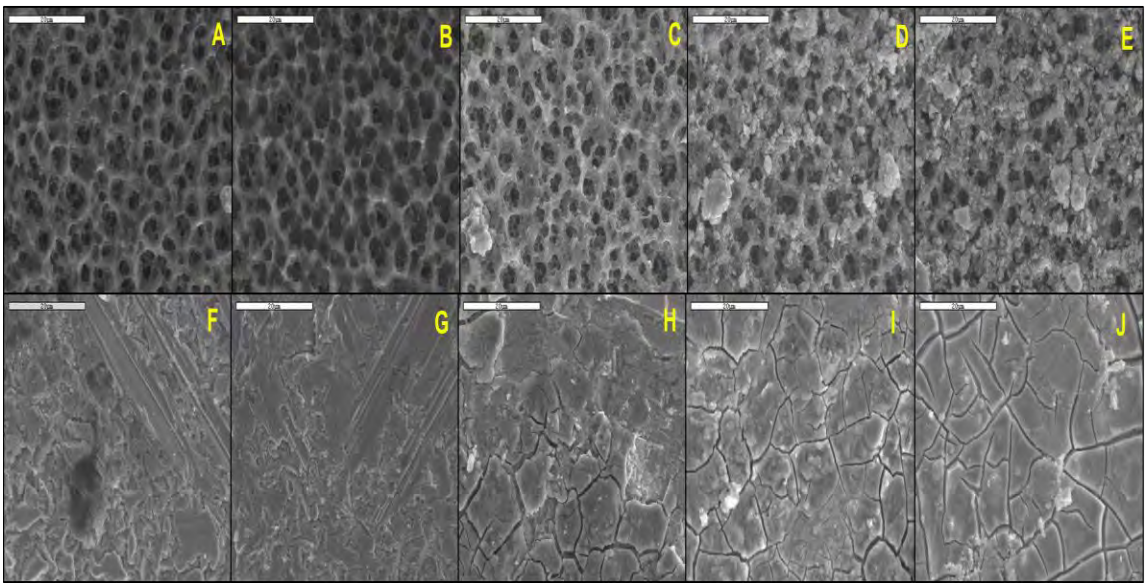

Figure 4-8. SEM images of FR4 devices at 2000x magnification. Images A-E correspond to the SEM images of the dielectric surface of the devices used for protocols #1-#5 respectively. Images F-J correspond to the SEM images of the electrode surface of the same devices. The scale bar at the top left corner, is 20 μm.

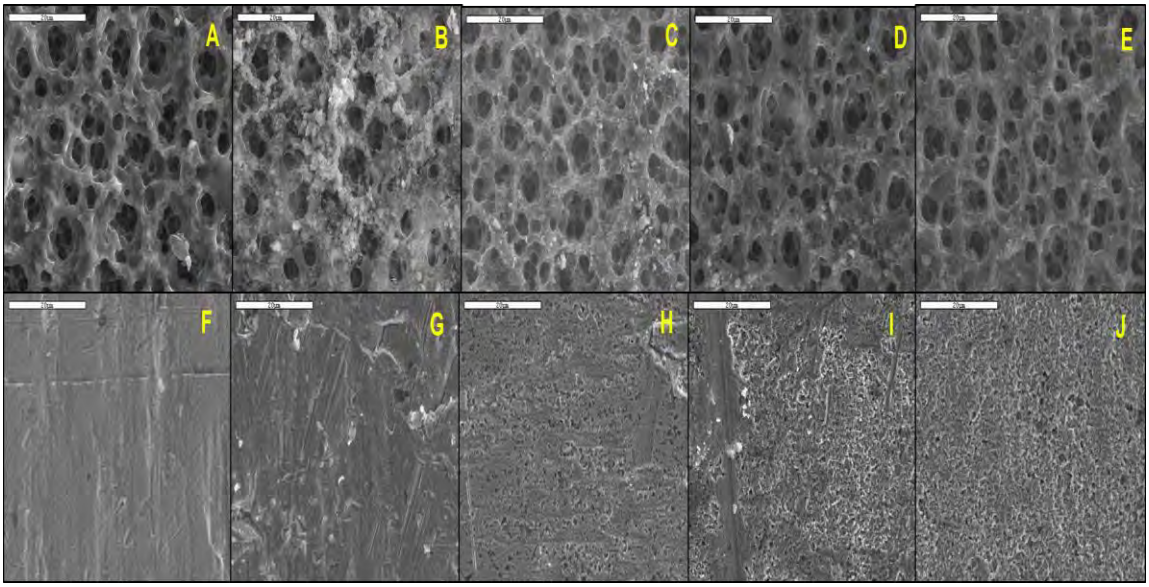

Figure 4-9. SEM images of SC devices at 2000x magnification. Images A-E correspond to the SEM images of the dielectric surface of the devices used for protocols #1-#5 respectively. Images F-J correspond to the SEM images of the electrode surface of the same devices. The scale bar at the top left corner, is 20 μm.

Comparing Figures 4-8 (A) and (B) there does not appear to be much of a modification of the dielectric substrate due to plasma generation for 20 minutes (B), as compared to the dielectric substrate of a new device (A). Comparing 4-6 (C)-(E), it is noticed that the dielectric substrate is different from (A) or (B). Primarily there seems to be a deposition of a grainy material on the dielectric surface. The grainy material can be either the accumulation of salts or molecules from cell debris from constant deposition of the *E. coli* sample or the accumulation of electrode sputter due to repeated plasma generation. Comparing Figures 4-9 (A)-(E), this same behavior is not noticed for SC devices. However, SEM imaging focuses on analyzing a single cross-section of the surface being examined. Hence the absence of the grainy material in Figures 4-9(C)-(E) could also be because the particular cross-section being analyzed is devoid of the grainy material. The important point to conclude from Figure 4-8 and Figure 4-9 (A)-(E) is that the different protocols do not seem to affect the dielectric surface, except for the deposition of a grainy material, in some of the cases.

Similarly, comparing electrode surfaces for FR4 devices (4-8 (F-J)) and SC devices (4-9 (F-J)), it is observed that electrode surfaces (F-G) appear to remain the same, while electrode surfaces (H-J) appear segmented (in the case of FR4) and sputtered (in the case of SC). Since this segmented/sputtered appearance is not noticed in the case of the FR4/SC device powered solely for 20 minutes, without *E. coli* deposition, it is likely that the constant deposition of the *E. coli* culture leads to electrode corrosion.

EDS studies were used to identify the elemental composition of the dielectric surface of the various plasma devices, after they were subjected to the different

protocols. In the EDS analysis shown below for a FR4 device (Figure 4-10) and SC device (Figure 4-11), the absence of a way of determining relative ratios of elements makes it difficult to derive any information about the elemental variation among the different electrode surfaces and the different dielectric surfaces. Figure 4-10 (A) displays a high concentration of bromine (Br) and trace concentrations of tin (Sn). Bromine is often used to enhance flame-resistant properties in in FR4 laminates, which is why it is detected in the higher concentrations on the EDS plot. The FR4 dielectric, used for making the devices, is copper clad with a copper (Cu) layer overlaid with a tin (Sn) finish. It is possible that milling of this Cu+Sn layer during device manufacture led to Sn residues on the surface, which explains the trace concentrations of Sn on the EDS plot too. Figure 4-10 (B) on the other hand displays a high concentration of Sn (due to the electrode surface) and Chlorine (Cl).

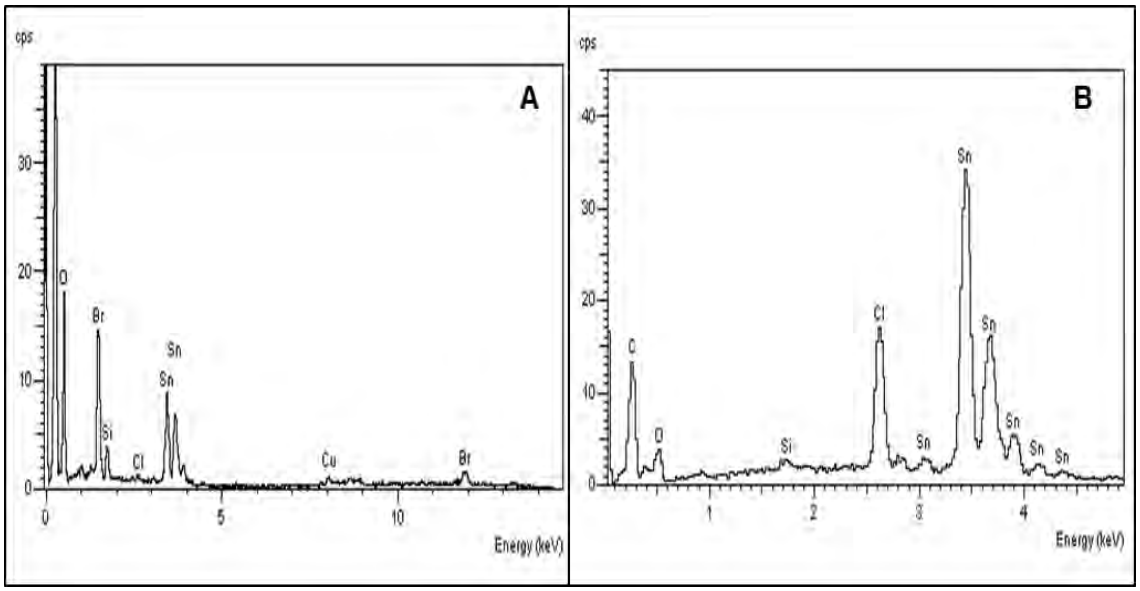

Figure 4-10. EDS analysis of the A) dielectric surface B) electrode surface for a FR4 device

Figure 4-11 (A) shows a high concentration of Silicon (Si), which is likely a component of the SC dielectric surface. Figure 4-11 (B) shows a high concentration of

copper (Cu), which is expected since the electrode is made up of copper. For the sake of simplicity, EDS plots for the other protocols have not been shown. However, from these plots, additional information such as the variation of elemental ratios from device to device or the detection of additional salts deposited on the devices due to continuous plasma generation, is not derived.

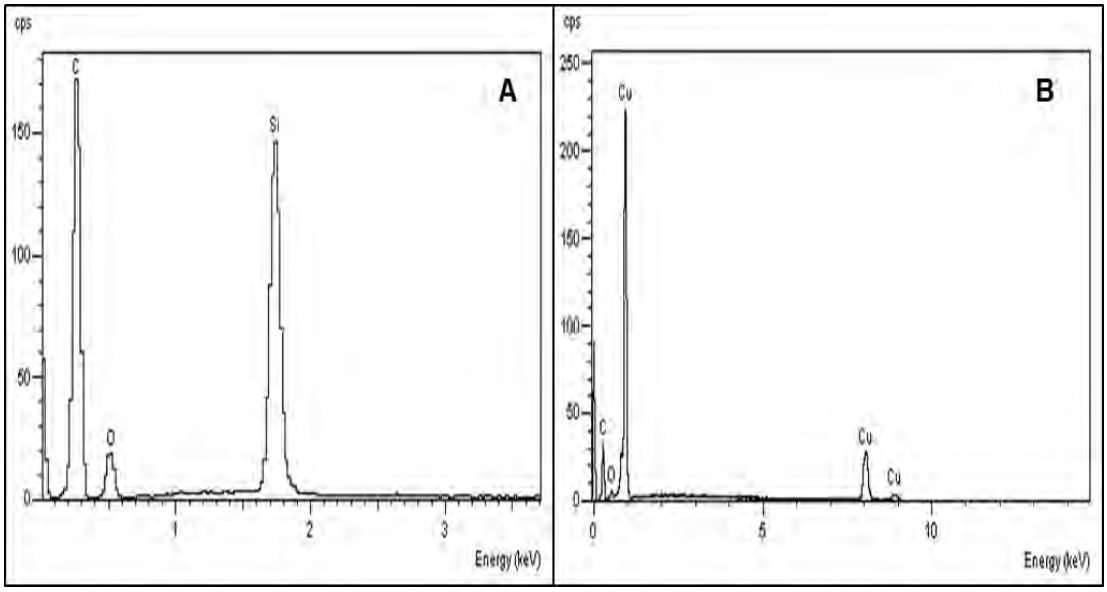

Figure 4-11 EDS analysis of the A) dielectric surface B) electrode surface for a SC device

Thus SEM and EDS analysis of a variety of FR4 and SC devices subjected to a number of protocols (Table 4-2) do not highlight clearly the substrate modifications taking place due to the different protocols. While some information is provided in terms of elemental signatures and electrode appearance, it seems that the different protocols do not produce any consistent dielectric substrate modification both in FR4 and SC.

This is very puzzling since it has been observed that prolonged sterilization experiments using SC plasma devices leads to inconsistent sterilization results. In fact, the SEM/EDS study was designed in order to identify and study the development of this

inconsistency. However, even after 25 sterilization cycles (~50 minutes of plasma exposure), the reason for this inconsistency is not apparent. This inconsistency is not noted in the case of FR4 plasma devices.

Alternative dielectrics like polymethyl methacrylate (PMMA, or more commonly, acrylic), Teflon or Kapton ® or gorilla glass are of interest, but are not available with pre-applied electrode material. A preliminary study was conducted using PMMA dielectrics. PMMA devices were fabricated using acrylic slabs and copper adhesive tape (for the electrodes). The current electrode design was fabricated using copper-adhesive tape and adhered to the PMMA slab (electrode dimension 2.4 x 2.3 cm^2). Figure 4-12 below demonstrates such a device compared with a similar FR4 device.

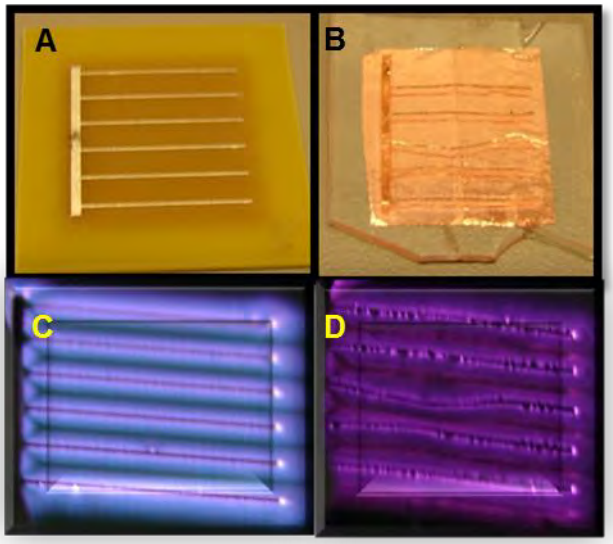

Figure 4-12. Comparison between a FR4 device and a PMMA device. A and B depict the unpowered FR4 and PMMA devices respectively. C and D depict the same device, powered.

Such PMMA devices were subjected to sterilization tests to obtain a survival curve in either case. 40 µl of yeast was used as the inoculation volume. Complete sterilization was noted in 90s with the PMMA devices. However the method of

fabrication and testing for the PMMA devices was crude. Additionally when the devices were dipped in ethanol to disinfect them before sterilization experiments, the adhesive of the copper tape dissolved, thus leading to a distorted electrode shape. This introduced an uncertainty in the experimental results. However, the aim of the tests with PMMA was to explore plasma sterilization capabilities using a different dielectric (other than FR4 and SC). This confirmation was provided by the PMMA sterilization tests.

4.4 Input power and frequency

The input power to the plasma devices was calculated via the measured input voltage and the input current. Input voltage and current are measured using a Tektronix P6015A high-voltage probe, a current probe (Corona Magnetics Inc.) and an Agilent® DSO1004 Oscilloscope. Power (P) was then calculated by the formula

$$P = \frac{1}{N}\sum_{i=1}^{N} VxI \tag{4.4}$$

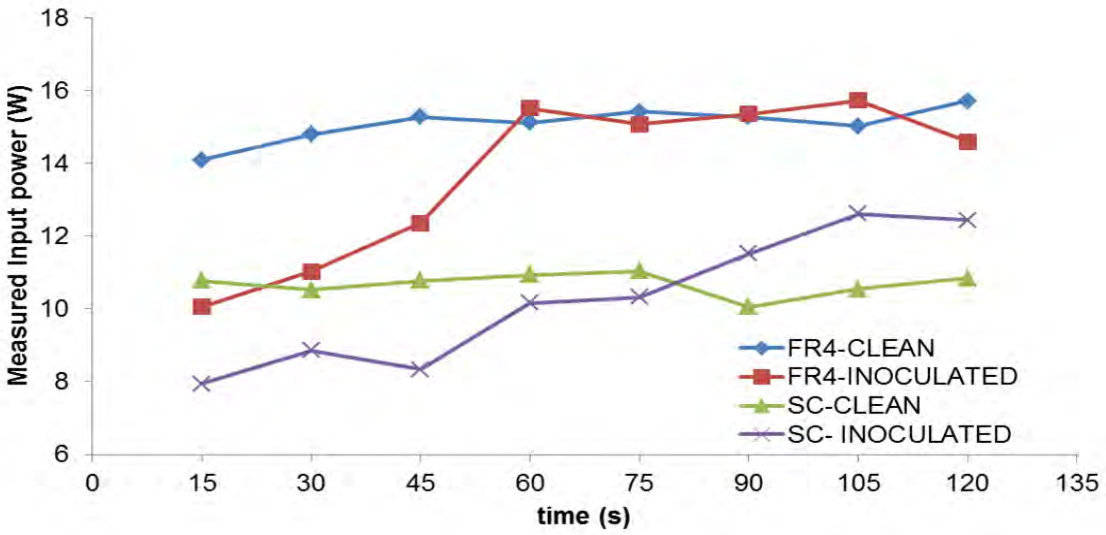

Figure 4-13. Comparison of the temporal variation of input power for clean and inoculated devices in the case of FR4 and SC dielectric.

The input power measured for a clean device versus an inoculated device, for FR4 and SC, is shown above in Figure 4-13. In order to plot this power over time, a clean/inoculated device was powered at 14 kHz, 12 kV p-p for 2 minutes, over the course of which, voltage (V) and current (I) were sampled every 15s. From Figure 4-13, the input power absorbed by the clean FR4 device was observed to be greater than that absorbed by the clean SC device. This measured power remained almost constant over the entire 2 minute interval. It was also observed that the input power absorbed by the inoculated FR4 device is greater than that absorbed by the inoculated SC device. However this measured power varies over the 2 minute interval. Initial measured input power is low, increasing over the 2 minute interval.

Also studied was the dependence of sterilization effectiveness on the input voltage. Input voltages were varied from 6 kV p-p to 14 kV p-p, in increments of 2 kV p-p. Figure 4-14 given below shows the variation of average measured input power versus each input voltage tested for a clean FR4 and SC device. .

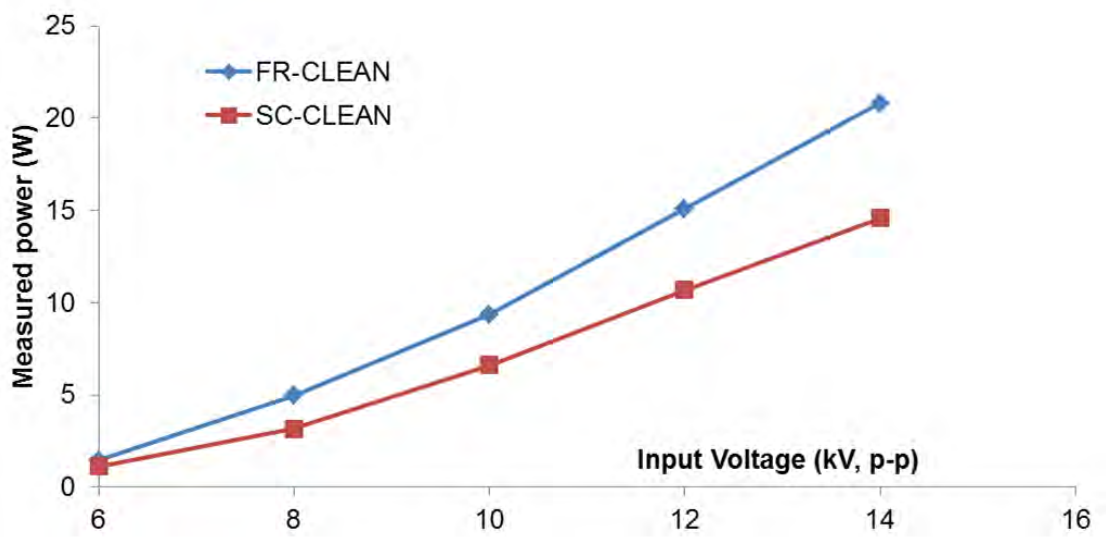

Figure 4-14. Comparison of the average measured input power (W) for each input voltage (kV p-p)

The trend noticed in Figure 4-13 holds true for Figure 4-14 also: measured input power stays more or less constant over time in the case of a clean FR4/SC device. Evaluating the trend lines of the plots in the above figure, an expected quadratic dependence is observed ($P \alpha V^2$).

For each input voltage, an inoculated device was powered for 2 minutes and then subjected to the post-processing protocol described in Section 3.5.2. Tests were performed in triplicate. The variation of input power over time, for different voltages in the case of an inoculated FR4 and SC plasma device is given below in Figure 4-15.

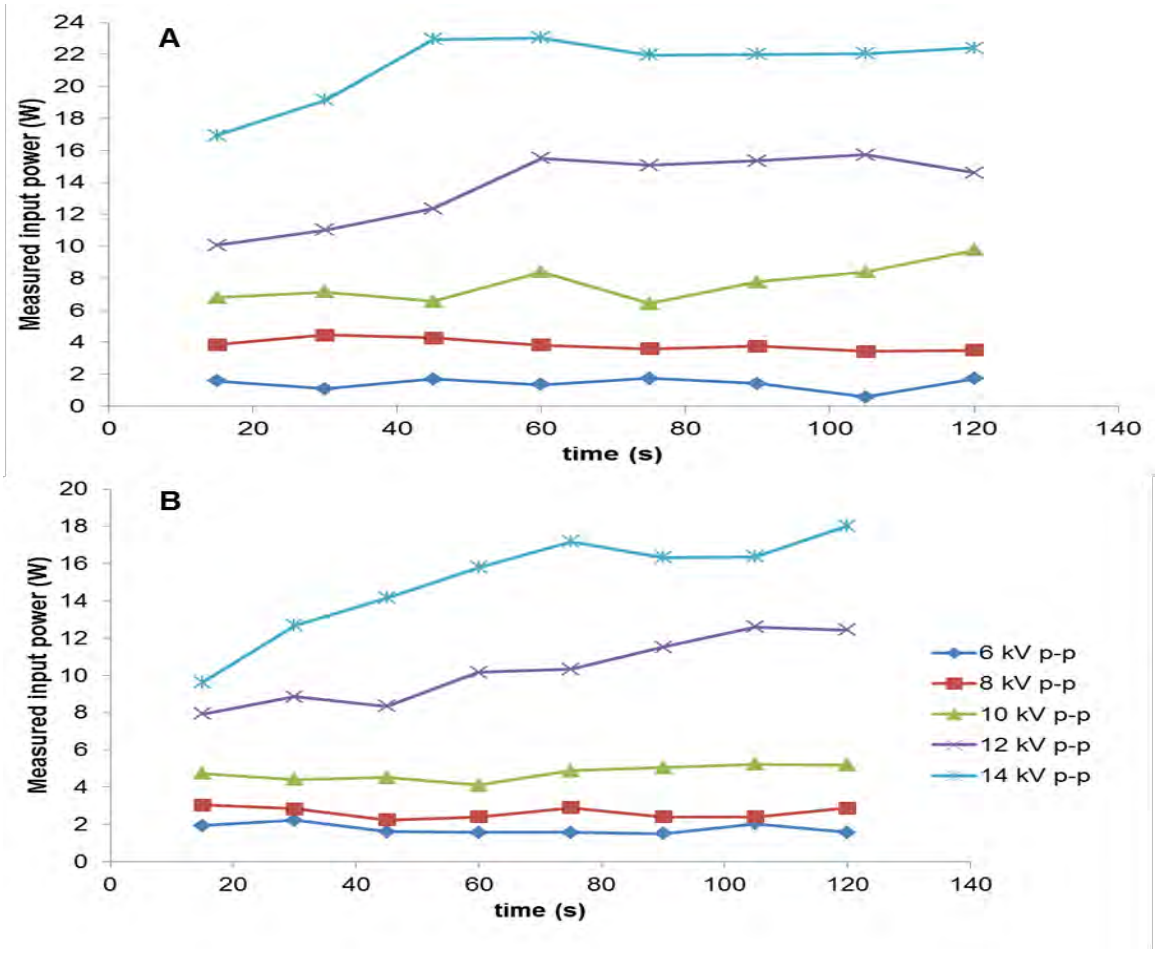

Figure 4-15. Temporal variation of input power for different input voltages using inoculated devices for A) FR4 and B) SC.

Figure 4-15 shows similar trends in the case of both FR4 and SC. At V= 6 ,8, 10 kV p-p, plasma is barely generated and the liquid bacterial sample deposited on the device does not evaporate at all, which explains the minimal variance in power observed for these voltage values. At V= 12 and 14 kV p-p, the deposited bacterial sample starts evaporating soon after 30s and is completely evaporated at 60s for FR4. Correspondingly, in Figure 4-15 (A), a rise in input power is observed until 60s, after which power remains constant. However, in Figure 4-15 (B), a continuous rise in input power is observed, since the sample is constantly evaporating in the case of SC.

Sterilization tests at each of the different input voltages were also conducted in order to understand the dependence of sterilization efficiency on input power. This is shown below in Figure 4-16.

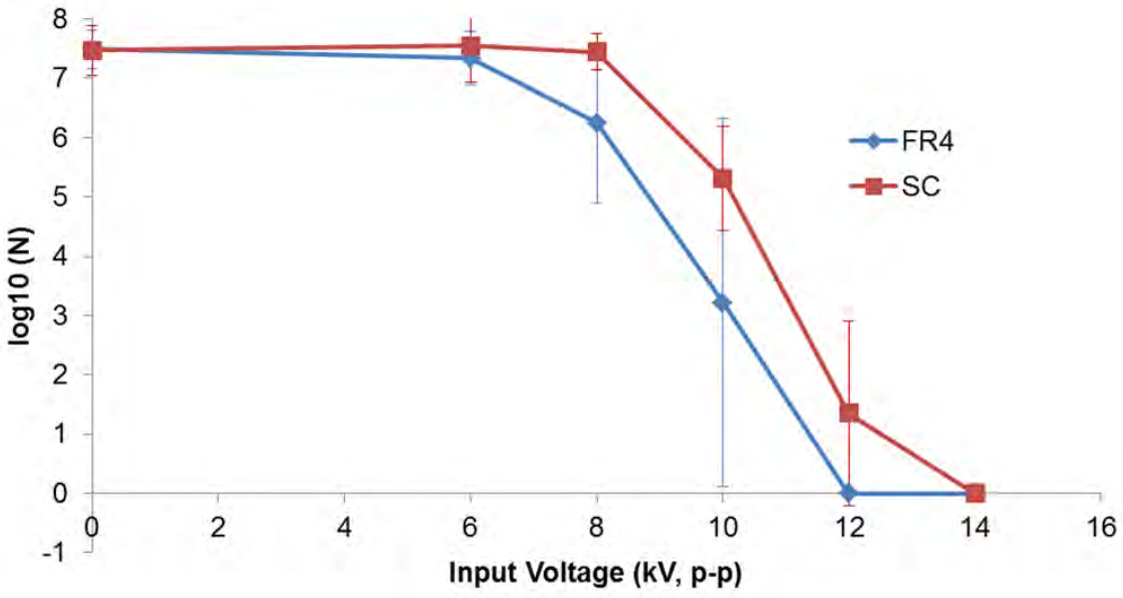

Figure 4-16. Dependence of sterilization effectiveness on input voltage (V)

Since the power varies over time for an inoculated device, Figure 4-16 has been plotted with the X-axis corresponding to input voltage and the Y-axis corresponding to number of survivors ($\log_{10}$). From Figure 4-16, it is concluded that lower voltages (6,8,10

kV p-p) are not effective both in the case of FR4 and SC. In the case of SC, 12 kV p-p seems to be inconsistently effective, but 14 kV p-p produces complete bacterial inactivation in all the trials considered.

Similarly, in order to understand the effect of varying input frequency on sterilization, tests were conducted at a higher frequency (60 kHz) using the portable plasma sterilization setup, described in Section 3.3. At such a high frequency, the setup was only capable of operating at V_{max} =10 kV p-p. Hence sterilization tests were conducted at 9 and 10 kV p-p.

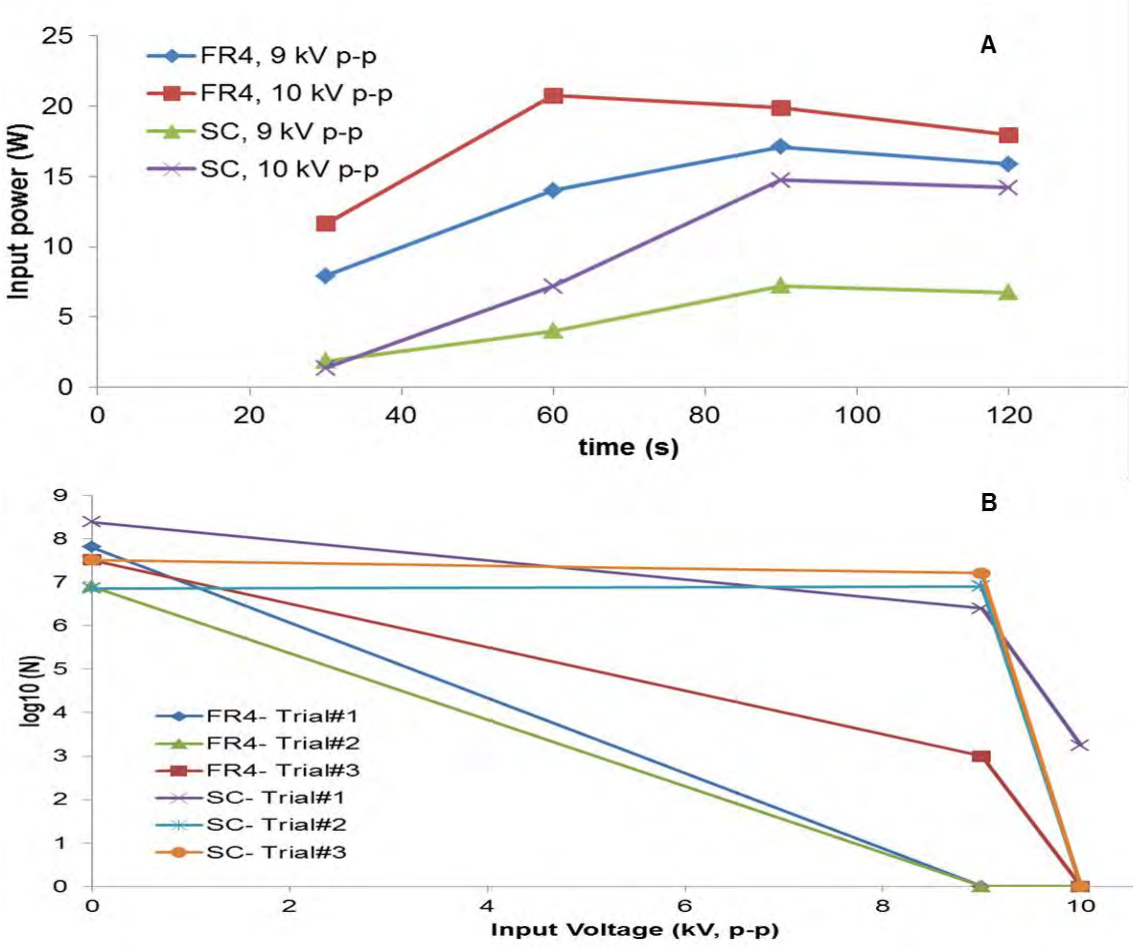

Figure 4-17. A) Temporal variation of input power for an inoculated FR4 and SC device (f= 60 kHz, V= 9-10 kV p-p) B) Dependence of sterilization on input voltage at f= 60 kHz, for FR4 and SC

Figure 4-17 (A) above shows the temporal variation of input power at 60 kHz, V= 9,10 kV p-p for both FR4 and SC devices. The input voltage and current were sampled every 30s over a 2 minute interval. The trend of increasing input power with respect to time, for an inoculated case, is noted here also. Figure 4-17 (B) shows the survival curves obtained for these tests. In the case of FR4, an input voltage of 9 kV p-p leads to complete bacterial inactivation in 2 out of 3 cases. An input voltage of 10 kV p-p leads to complete bacterial inactivation in all three cases. In the case of SC, an input voltage of 9 kV p-p does not lead to bacterial inactivation in any of the cases. However 10 kV p-p leads to complete bacterial inactivation in 2 out of 3 trials, thus implying that 10 kV p-p might be the threshold sterilization input voltage for SC plasma devices. An input voltage slightly higher than 10 kVp-p or a sterilization time slightly higher than 2 minutes might be enough to ensure repeatable, complete bacterial inactivation in the case of SC.

4.5 Operating pressure

The aim of the plasma sterilization experiments conducted at pressures lower than normal atmospheric pressure was to evaluate whether DBD surface plasma sterilization was enhanced at lower pressures.

Low pressure experiments were conducted in a vacuum chamber. The chamber was made out of acrylic and constructed such that it can be evacuated to pressures as low as 20 Torr. For each experiment, an inoculated device was placed inside the chamber, the chamber sealed and the air evacuated to the requisite pressure, using an air pump. Plasma was generated in this low-pressure environment for the requisite sterilization time, Δt. Once this was done, pressure was slowly increased back to

atmospheric pressure, chamber opened and the device removed and subjected to the post-processing protocol described in Chapter 3.

There were a number of difficulties associated with using the vacuum chamber at reduced pressures for DBD surface sterilization experiments. The total time required for placing the inoculated device into the chamber, evacuating the chamber and powering the device takes ~1.5 minutes. In this time, there is the possibility that some of the pathogens in the bacterial sample on the device may be adversely affected, due to the low-pressure environment inside the chamber. Also, due to operating constraints imposed on the ozone meter, ozone measurements were not possible.

Another operating constraint was the limitation on operating pressure, due to device design. As the pressure is lowered, the plasma glow becomes more diffuse, as shown in Figure 4-18.

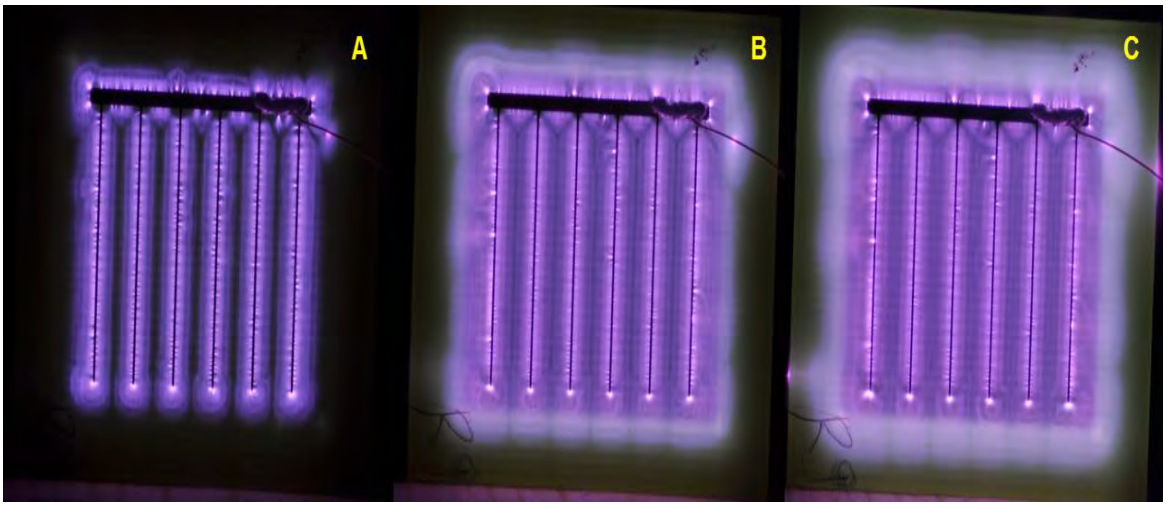

Figure 4-18. Images of the devices at A) 760 Torr B) 500 Torr C) 400 Torr

Plasma glow is confined to the electrode surface area. At 500 Torr, plasma glow extends a little beyond the electrode surface area and at 400 Torr, it has extended almost to the edge of the dielectric surface. It was noticed that for P<350 Torr, the

plasma glow extended beyond the edge of the dielectric surface, causing the formation of an electric arc This is because at P<350 Torr, the extremely high voltage is applied close to the edge of the device, in which case, electrons travelling from the cathode (grounded electrode) take the path of least resistance to the anode (powered electrode) and hence arc over the edge of the device. Thus operating pressure had to be limited to 400 Torr, in order to work with the plasma devices currently being used.

The spectroscopic signatures obtained during the operation of the plasma devices at reduced pressures was observed to be similar to the spectroscopic signature of DBD plasma at atmospheric pressure, except that the intensity of the emitted spectra at the peak wavelengths was found to increase with decreasing pressure. More on the spectroscopic results will be discussed in Chapter 5.

Inoculated devices were placed in the vacuum chamber and powered for two fixed time intervals Δt= 60s,120s. The experiment was performed in duplicate. Figure 4-19 below shows the results from the two trials for (A) FR4 and (B) SC

In the plots below, the sterilization behavior is observed to be similar to that at atmospheric pressure for both dielectrics. It is to be noted here that unlike Figure 4-6, after plasma exposure for 2 minutes, Figure 4-19 (B) shows incomplete sterilization at all three pressures. This is to be expected. As discussed in Section 4.3, SC plasma devices show an inconsistency in sterilization behavior after 2 minutes of plasma exposure. Hence while fresh devices were used for the experimental results shown in Figure 4-6, devices that had been subjected to multiple sterilization cycles were used for results shown in Figure 4-19 (B). If a similar device were to be used to obtain a survival

curve at atmospheric pressure, complete sterilization would not be seen after 120s of plasma exposure.

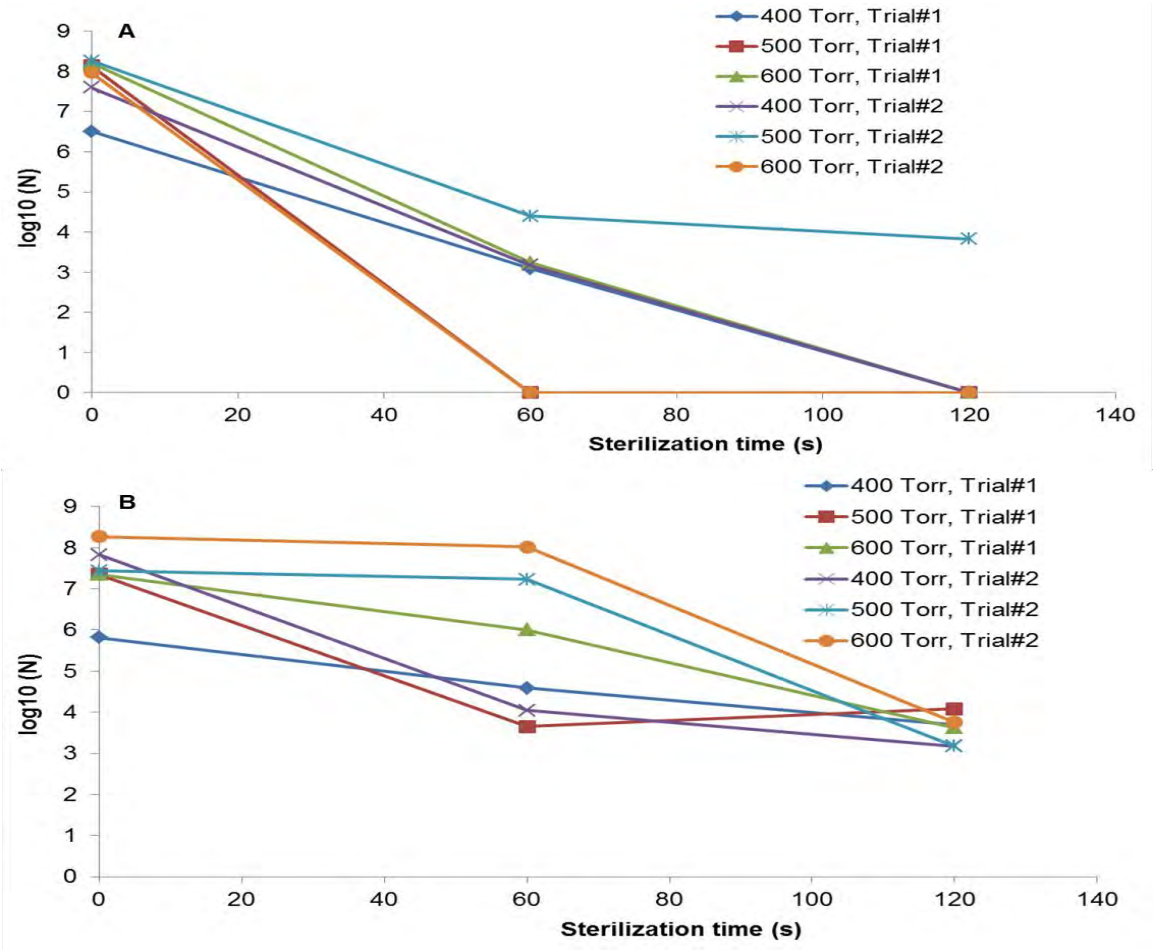

Figure 4-19. Sterilization behavior at reduced pressures for A) FR4 and B) SC plasma devices. Two sterilization times (t= 60s and 120s) were tested, using *E. coli* at the reduced pressures. Sterilization behavior at reduced pressures is found to be similar to that at atmospheric pressure.

For FR4, at 500 Torr, incomplete bacterial inactivation is achieved after 2 minutes on Trial#2. However taking into account the complete bacterial inactivation achieved for both trials at P=400 Torr, for 2 minutes, it is believed that that the observation at P=500 Torr for FR4 is an experimental outlier, rather than indicative of sterilization behavior at reduced pressure.

4.6 Discussion

This Chapter outlined a number of parametric studies, aimed at characterizing the sterilization efficiency of the AC, RF DBD surface plasma used in this study.

A variety of pathogens are subjected to plasma generated at 14 kHz, 12 kV p-p. The time taken for complete sterilization is determined in the case of each pathogen. Using FR4 plasma devices, this sterilization time is determined to be 90s-120s for *E. coli* and yeast. Using *B. subtilis* cells, this sterilization time is determined to be 4 minutes. However the medium in which *B. subtilis* cells are cultured is observed to make a difference. Using *G. stearothermophilus* spores, this sterilization time is determined to be 20 minutes. A range of other pathogens (as shown in Table 4-1) are also tested, most of which are completely sterilized within 3 minutes of plasma exposure.

Additionally doubling the volume of the *E. coli* sample deposited on the surface of the plasma device is observed to extend the sterilization time by ~30s. However, the number of CFU in 40μl (double the inoculation volume) is calculated to be almost the same as the number of CFU in 20μl (original inoculation volume). Hence it seems that the sterilization time is dependent on the volume of the liquid in the *E. coli* sample. This is an important insight into the mechanism of surface DBD plasma sterilization and will be discussed more in Chapter 5.

Two different dielectric materials (FR4 and SC) are compared in terms of sterilization efficiency. It is observed that the sterilization time in the case of SC is longer than that in the case of FR4. One hypothesis to explain this can be drawn on the basis of the

dielectric constant, which is the only differentiating parameter between both dielectric materials. The dielectric constant of FR4 is ~30% higher than the SC. The dielectric constant of a material is the ratio of amount of electrical energy stored in a material by an applied voltage, relative to that stored in vacuum. Any of the devices described in this study can be considered as a parallel plate capacitor, using a dielectric material of dielectric constant 'k'. Then, the capacitance of such a system is

$$C = \frac{k\varepsilon_0 A}{d} \quad (4\text{-}5)$$

where ε_0= absolute permittivity of air, A= surface area of the top surface of the device &'d' = the thickness of the dielectric layer. The energy stored in a parallel plate capacitor is 'U' = $\frac{1}{2}CV^2$.

Hence, for the plasma devices considered in this paper, energy stored in the device is directly proportional to the capacitance of the system, which in turn is directly proportional to the dielectric constant of the material. The FR4 device, which has a higher dielectric constant than the SC device, has more energy stored in the dielectric layer, which explains the results noted in Figure 4- 6 i.e. complete sterilization is achieved faster (t= 90s) for FR4 as compared to semi-ceramic (SC) dielectric (t= 120s). Chapter 5 will further demonstrate the differences between FR4 and SC plasma devices, all of which can be ascribed to the difference in absorbed power between both devices, which in turn can be attributed to difference in dielectric constant (as shown above).

Furthermore, it is also noticed that the SC plasma devices do not ensure consistent sterilization behavior (Figure 4-6). Prolonged sterilization cycles using the SC devices are observed to increase this inconsistency. The SEM analysis of both dielectric

substrates, for different protocols (described in Section 4.3), demonstrates that while the dielectric surface is not visibly altered by repeated plasma generation (both in the clean and inoculated cases), the electrode surface presents a highly segmented/sputtered appearance in the inoculated cases. This observation holds true for the electrodes on both FR4 and SC devices. The reason for this is not immediately apparent but can be speculated to be due to the corrosive action of salts used in the preparation of the bacterial sample. However the SEM analysis does not readily highlight why the SC plasma devices are found to demonstrate an inconsistency in terms of sterilization behavior.

Different input voltages and different input frequencies, for both FR4 and SC, are tested in order to understand the dependence of sterilization effectiveness on input power and frequency. Comparing the sterilization data for different input voltages, both for FR4 and SC, it seems that there exists a threshold value of input power density for the generated plasma, above which complete bacterial inactivation is certain. From Figure 4-15, and using the device dimensions of 2.4 x 2.3 x 0.16 cm^3, this threshold power density is calculated to be ~17-18 W/cm^3. From Figure 4-15, it is also evident, that in the case of SC, this threshold power density is not reached during plasma generation at 12 kV p-p, which may explain the sterilization uncertainty in the case of SC. What this simply means is that for the SC devices, a lesser input power density might require a longer plasma generation time in order to achieve sterilization effectiveness, similar to FR4 devices.

From Figure 4-17 (A) and (B), it is observed that plasma generation at a higher input frequency of 60 kHz and an input voltage of 9 and 10 kV p-p leads to higher input

power densities in the case of FR4 as compared to SC. Also, the increase in input power density is more rapid in the case of FR4 than SC. Consequently at 10 kV p-p, complete bacterial inactivation is observed in all three trials for FR4. In the case of SC, plasma generation at 9 kV p-p leads to very low input power densities, which explains the incomplete bacterial inactivation at this voltage. At 10 kV p-p, the input power density in the case of SC is similar to the threshold input power density, though not greater. Thus an input voltage of 10 kV p-p may be sufficient to obtain complete bacterial inactivation, but this might not be repeatable. In such a case, the SC devices need to be powered at a voltage higher than 10 kV p-p or powered at 10 kV p-p for t>2 minutes.

The dielectric heating of the substrate is directly proportional to the excitation frequency (f) and the square of the Electric Field (E) i.e. square of the input voltage (V), as described in Equation 4-3. Hence, increasing the frequency and increasing the input voltage should correspond to enhanced sterilization, which is corroborated by Figure 4-16 and 4-17 (B).

Lastly, sterilization experiments are also conducted at reduced pressures of 400, 500 and 600 Torr. The sterilization trends in these cases are found to be similar to those observed at atmospheric pressures. However comparing spectrum data at these different pressures, intensity peaks at similar wavelengths are found. These intensity values are found to increase with decreasing pressure. This increase in intensity does not seem to help sterilization, as the sterilization trends noted in Figure 4-17 are similar to those noted at atmospheric pressure. The spectra for the different pressures are described in further detail in Chapter 5, along with a discussion of the different

components involved in DBD plasma generation and their role in influencing plasma sterilization.

CHAPTER 5
UNDERSTANDING THE MECHANISM OF DBD SURFACE PLASMA STERILIZATION

Chapter 4 was aimed at varying the different parameters involved in plasma generation and studying the effect of this variation on plasma sterilization. The current chapter focuses on the fundamental question: How does DBD surface plasma sterilization work?

Diagnostic data here refers to the spectroscopic, ozone and temperature data obtained during plasma generation, both with a clean and inoculated device, in the case of both dielectrics (FR4 and SC). In the sterilization process, bacteria could be getting irradiated by the UV photons or could be chemically reacting with one or more of the reactive species produced during plasma generation. Though DBD plasma is low temperature, non-uniform average surface temperatures have been detected in the range of 300-340 K (27-67^{o}C) and 293-313 K (20-40^{o}C) for FR4 and SC respectively. The upper end of this range is harmful to many bacteria, but not bacterial spores [96]. It remains to be determined whether this also plays a role in DBD surface plasma sterilization.

The diagnostic data helps understand the concentration of reactive species and UV photons available for bacterial inactivation. Additionally experiments isolating each of these agents and examining their individual effect on bacterial concentrations are also required in order to determine the role of each agent in the plasma sterilization process. The current chapter summarizes work done in these areas.

5.1 Spectroscopic studies

The spectroscopic signature of the generated DBD plasma was determined using the Ocean Optics® USB 2000+ spectrometer. The setup of the spectrometer has been described in Chapter 3, Section 3.1.

Spectroscopic data was collected in several different scenarios. Clean and inoculated devices were fired for different time intervals Δt= 30s, 60s, 90s, 120s in the case of both FR4 and SC. The recorded spectral data in the case of a clean and inoculated FR4 device is given below in Figure 5-1. The same, for the case of a clean and inoculated SC device is given below in Figure 5-2.

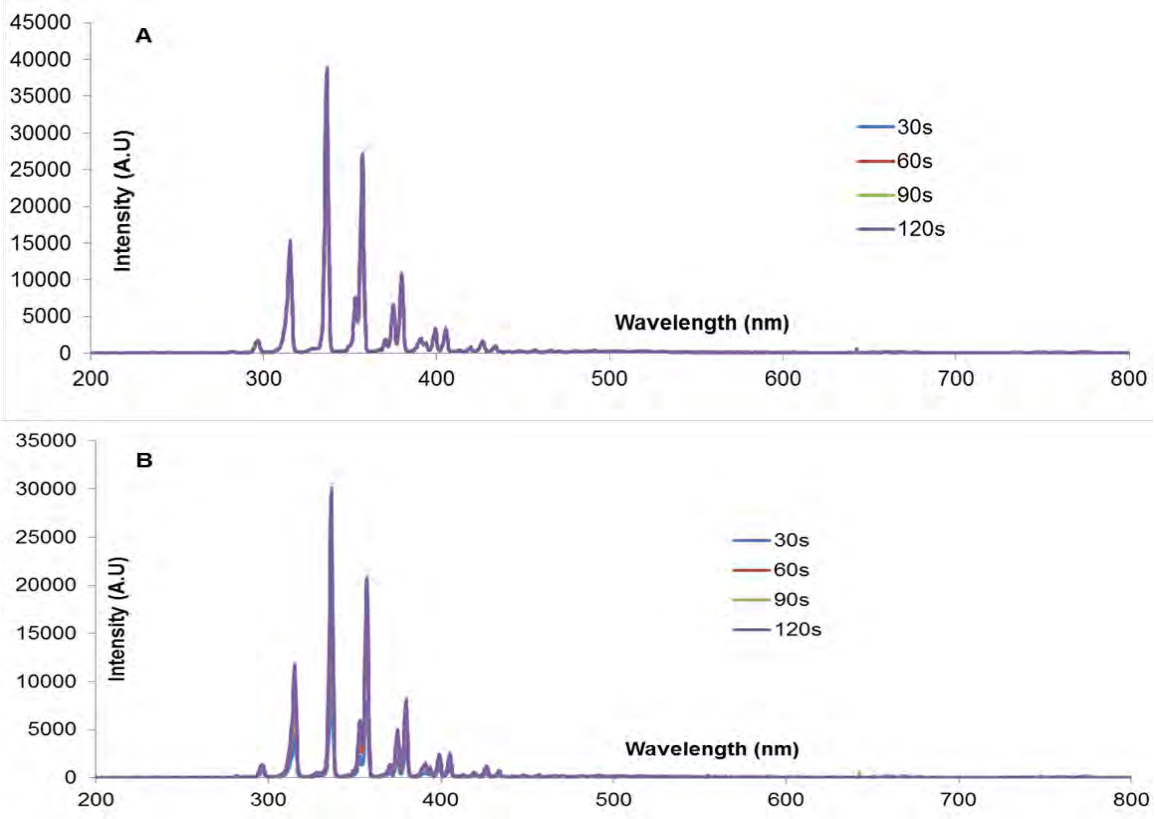

Figure 5-1. Spectral signature of A) a clean FR4 device and B) an inoculated FR4 device. Y-axis lists emission intensity in arbitrary unit.

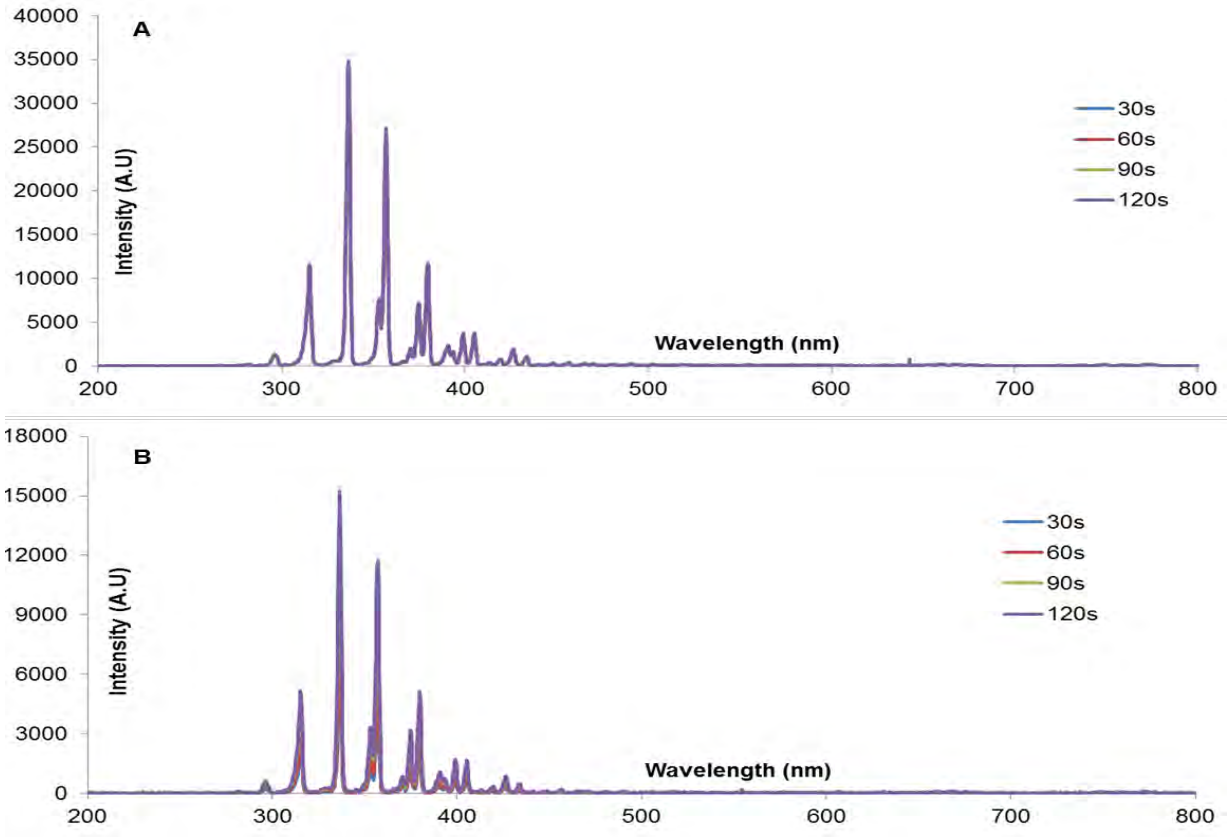

Figure 5-2. Spectral signature of A) a clean SC device and B) an inoculated SC device. Y-axis lists emission intensity in arbitrary unit.

The intensity peaks at different wavelengths correspond to photonic emission by different chemical species. Once the intensity peaks and their corresponding wavelengths are identified, the corresponding emitting chemical species can be determined [97].

Similar spectra are noted in the case of both clean and inoculated FR4 and SC devices. In Figure 5-1 and Figure 5-2, there are four principle intensity peaks: 315.25 nm, 336.67 nm, 357.24 nm and 379.52 nm. All four correspond to transitions taking place in the 2nd positive system of N_2 ($C^3\Pi_u$- $B^3\Pi_g$). The peak intensities are seen at wavelengths corresponding to N_2, which makes sense considering that N_2 makes up over 78% of air. One of the smaller peaks on the farthest right in Figure 5-1 might

indicate N_2^+, but this is uncertain due to the resolution of the spectrometer. Also, there are no reactive oxygen species produced according to the spectrum. This could simply mean that the reactive oxygen species being produced are being re-absorbed at such a high rate that they do not show up on the spectrum.

Choi et al. [98] analyzed the spectrum of a pulsed DBD discharge (volume discharge configuration at 1 kHz frequency). While they noted similar intensity peaks for N_2 in the 300-400 nm range, they also noted intensity peaks for O atoms at wavelengths higher than 394 nm. Analysis of the spectrum recorded by other authors [68] for an air plasma (in volume-discharge configuration) demonstrated no significant wavelengths below 285 nm. In Chapter 1, the lethal effects of UV radiation at 254 nm and the sterilizing effect of VUV radiation have been described in great detail. Since the spectral signature in Figure 5-1 and Figure 5-2 shows no noticeable wavelengths below 290nm, it is unlikely that shortwave UV radiation (200-300 nm) plays a major role in surface DBD plasma sterilization.

Figure 5-3 and 5-4 are expanded versions of Figure 5-1 and Figure 5-2, focusing on the spectral signature in the range 330-350 nm. This is the wavelength range in which the highest intensity peak is observed for each of the spectra in Figure 5-1 and 5-2. In Figure 5-3(A) and 5-4 (A) below, the spectral data sampled at 30s, 60s, 90s and 120s during the 2 minute interval is shown. All four plots show similar peaks i.e. plasma generated using a clean FR4 and SC device for a 2 minute time interval, shows similar intensity values at all times. However it is evident in Figure 5-3(B) and 5-4(B) that there is a temporal variation of spectroscopic intensity. Intensity at 30s is the least while intensity at 120s is the highest.

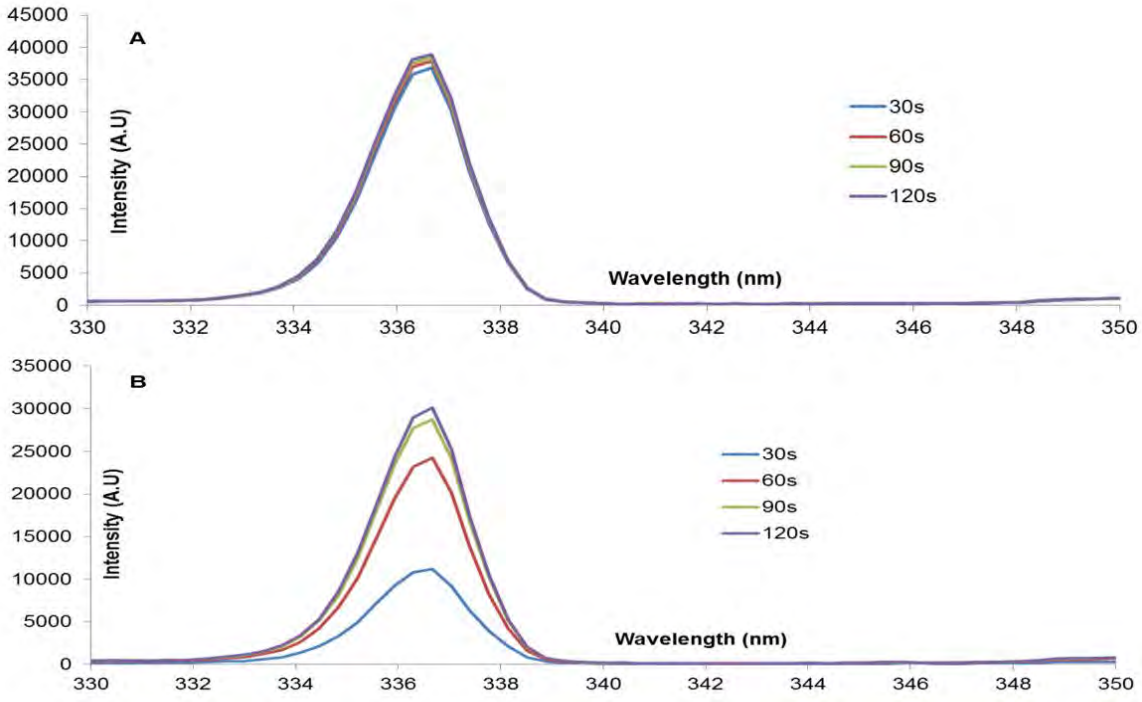

Figure 5-3. Expanded version of (A) Spectral signature of a clean FR4 device (B) Spectral signature of an inoculated FR4 device.

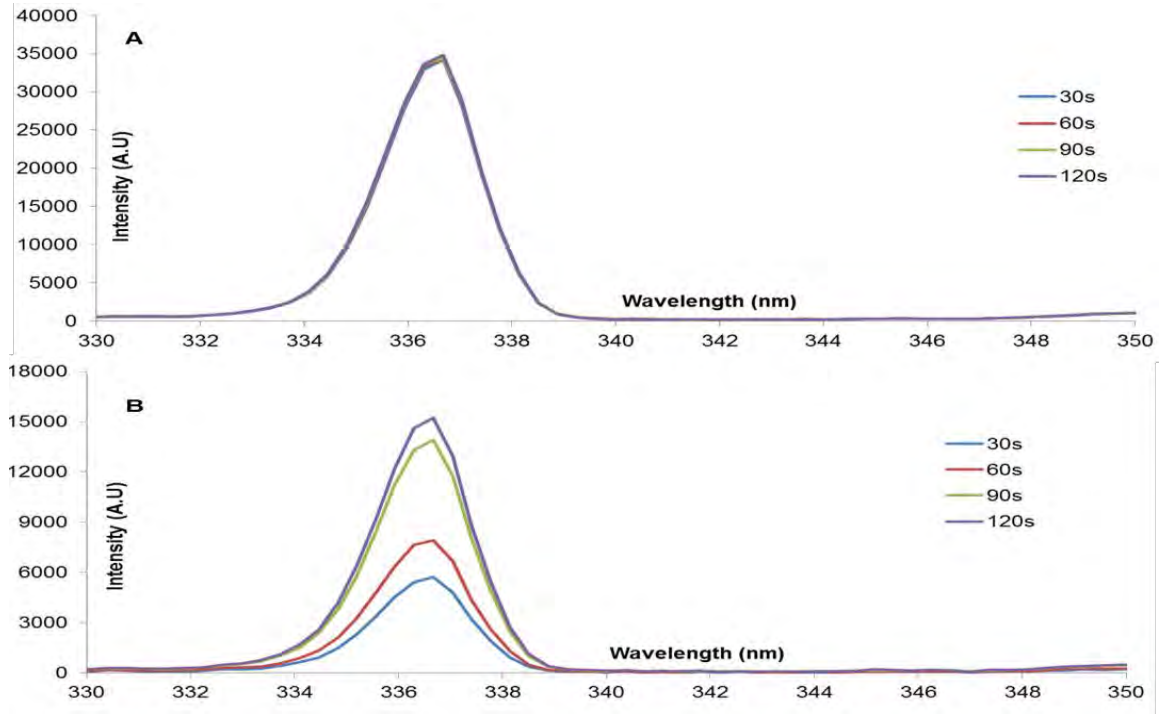

Figure 5-4. Expanded version of (A) Spectral signature of a clean SC device (B) Spectral signature of an inoculated SC device.

This gradually increasing trend in intensity mimics the gradually increasing trend observing in measured input power (discussed in Section 4.4). As with the case of the measured input power, here also, the temporal variation of intensity is observed to correspond to the gradual evaporation of the liquid sample. Also, the spectroscopic intensity in the case of the FR4 devices is far greater than that of the SC devices (both clean and inoculated). Considering the points noted above, the intensity difference in both cases raises the question of whether spectroscopic intensity plays an important role in plasma sterilization.

The spectroscopic intensity measured using a spectrometer is basically a measure of how bright the “plasma glow” is. The ratio of spectroscopic intensities can also be used to simulate rotational and vibrational plasma temperatures [99]-[100]. Thus the intensity is a measure of the concentration of excited photons in and around the area of plasma generation. Moisan et al. [16] discussed photo-desorption (etching of bacteria by the emitted UV photons) as one of the possible mechanisms in plasma sterilization. The question then is whether photodesorption plays a role in DBD surface plasma sterilization.

A set of reduced pressure experiments conducted (Section 4.5) shed some light on this matter. The objective of these experiments was simple: to study DBD surface plasma sterilization experiments at lower pressures. It has been argued that low pressures (in the mTorr range) allow the emission of VUV radiation ($\lambda<200$ nm) and reactive oxygen species, that would otherwise be immediately reabsorbed at higher pressures. Hence the reduced pressure experiments were aimed at exploring DBD surface plasma sterilization at lower pressures.

The vacuum chamber in our lab is built out of acrylic and is designed to be evacuated to pressures as low as 20 Torr. However, due to the design of the plasma device, it was only possible to operate the plasma devices at P≥ 400 Torr. Hence experiments were conducted at 400, 500 and 600 Torr.

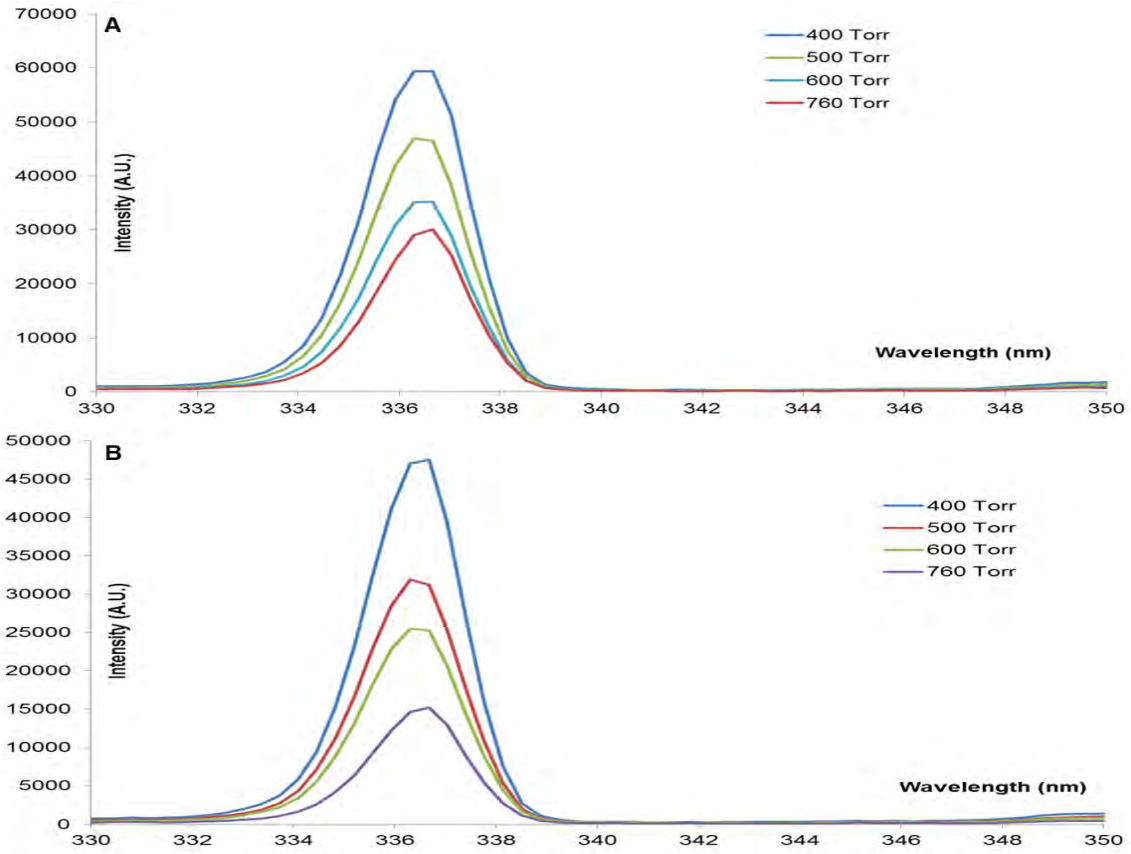

Figure 5-5. Spectroscopic comparison of (A) FR4 devices and (B) SC devices at reduced pressure

Figure 5-5 above presents the spectroscopic signature of (A) an inoculated FR4 and (B) an inoculated SC device, when powered at 14 kHz, 12 kV p-p inside the vacuum chamber at P= 400,500,600 Torr. For reference, the spectroscopic signature of a similar FR4 and SC device, powered at atmospheric pressure, is also shown. The devices were powered for a total time of 2 minutes and pectroscopic data was sampled

at every 10s. The spectroscopic signature at one particular time-point (t= 120s) is shown in Figure 5-5.

In Figure 5-5, the intensity peaks are noted at the same wavelengths for all four pressures, implying that the spectra isn't really changed much due to reduction of pressure. In particular, no new short UV wavelength peaks appear. However 400, 500 and 600 Torr correspond to 0.53, 0.66 and 0.79 atm respectively, which is still close to atmospheric pressure. Hence a drastic change in spectrum is not expected. However intensity peaks are different for the different pressures, with the intensities at 400 Torr being the highest and the intensities at atmospheric pressure, the lowest. As already discussed, this should imply that as the pressure decreases, the concentration of excited photons increases. But sterilization results at these reduced pressures (discussed in Section 4.5) demonstrate that the sterilization behavior of the FR4 and SC plasma devices at reduced pressure is the same as that at atmospheric pressure. This indicates that the excited photons may not play a major role in the sterilization process.

This section outlined spectroscopic data obtained during plasma generation using clean and inoculated FR4 and SC devices. Spectrscopic data at reduced pressures was also examined. The data shows that dominant intensity peaks are obtained at wavelengths corresponding to transitions in the N_2 2^{nd} positive system. This leads to the following questions: a) Are the reactive nitrogen species being produced the only chemically erosive species acting in the sterilization process? b) Could ozone, be acting synergistically to enhance sterilization? Section 5.2 discusses these two questions in more detail.

5.2 Ozone studies

DBDs are known ozone generators. Ozone formation is a two-step process that starts with the dissociation of O_2 molecules by the electrons in a micro-discharge [101]**:**

$$e + O_2 \rightarrow 2O + e \quad (5\text{-}1)$$

And a subsequent three-body reaction

$$O + O_2 + M \rightarrow O_3 + M \quad (5\text{-}2)$$

where M is a third reaction partner. M can be a pure oxygen species or even a nitrogen species, acting as a catalyst. Eliasson [101] hypothesized that the formation time of oxygen atoms is much smaller than that of ozone. On the other hand, ozone forms at a faster rate than the rate at which it might dissociate (equation 5-3) or its concentration might get diluted due to recombination (equation 5-4).

Ozone Dissociation: $O_3 + e \rightarrow O_2 + O + e$ (5-3)

Ozone Recombination: $O + O_3 \rightleftharpoons 2O_2$ (5-4)

If the oxygen concentration is too high (or the temperature is low), recombination (5-4) is the dominant reaction. If the temperature is too high, thermal decomposition (5-3) is the dominant chemical reaction.

As discussed in Section 1.3.2, the role of ozone or more generally, the role of reactive oxygen species in plasma sterilization is still widely debated. This section concentrates on isolating the role of ozone in DBD surface plasma sterilization. The plasma device was enclosed within a sterilization chamber made of Acrylic. Rates of ozone production/decay while operating this DBD plasma source were determined. The plasma device was also placed within sterilization chambers of different volumes and powered in order to study the dependence of ozone production/decay on chamber

volume. Additionally, the effect of exposing bacterial (*E. coli)* concentrations to the ozone thus produced was also analyzed. In doing so, the lethal amount of ozone necessary to completely inactivate *E. coli* within 7 minutes was determined. In order to prove that this inactivation effect was due to the ozone produced during DBD plasma generation, ozone production was inhibited during plasma generation. Known concentrations of *E. coli* were exposed to the ozone produced in this case too, but no significant inactivation was noted, thus leading to the conclusion that the ozone produced during plasma generation was indeed responsible for bacterial inactivation.

As previously described in Section 3.1, a 2B Tech ® Ozone monitor was used to measure the ozone levels at fixed time intervals within a closed chamber.

5.2.1 Characterization of ozone production and decay during DBD plasma generation

Sterilization chambers of four different volumes were used for the experiments in this paper. The dimensions of these are listed below:

- Chamber#1- 12”x10”x7”- 840 in^3
- Chamber#2- 12”x10”x14”- 1680 in^3
- Chamber#3- 24”x10”x14”- 3360 in^3
- Chamber#4- 48”x23.5”x24”- 27072 in^3

The volume ratio of the chambers is 1:2:4:32, with respect to Chamber#1. In order to characterize the ozone production trends during DBD plasma generation, preliminary experiments consisted of placing a plasma device in Chamber#4, powering the device over a time interval of 2 minutes and measuring the ozone levels at different locations (both along the X-axis and Y-axis) of the chamber. The various locations at which ozone was measured inside the chamber are shown in Figure 5-6. For all measurements in

Figure 5-6, the ozone probe was positioned at a height of 5” above the floor of the chamber.

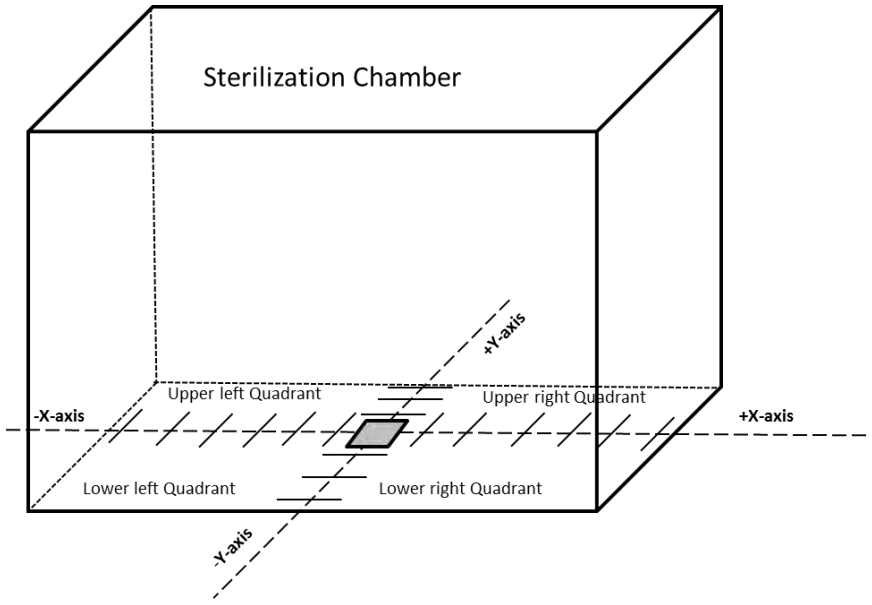

Figure 5-6. Schematic of Chamber#4. The grey square in the middle represents the plasma device. The black short lines represent the different locations at which ozone measurements are taken. These locations are uniformly spaced (4” apart), along the X- and Y- axis.

The aim of such an experiment was to get an idea of the spatial variation of ozone levels inside Chamber#4. This spatial variation is given below in Figure 5-7(A) and (B). Figure 5-7(A) shows the spatial variation of ozone production along the X-axis of the chamber while Figure 5-7(B) shows the spatial variation of ozone production along the Y-axis of the chamber. While ozone data is sampled every 10s, for the sake of simplicity only the data at 30s, 60s, 90s and 120s has been plotted and shown.

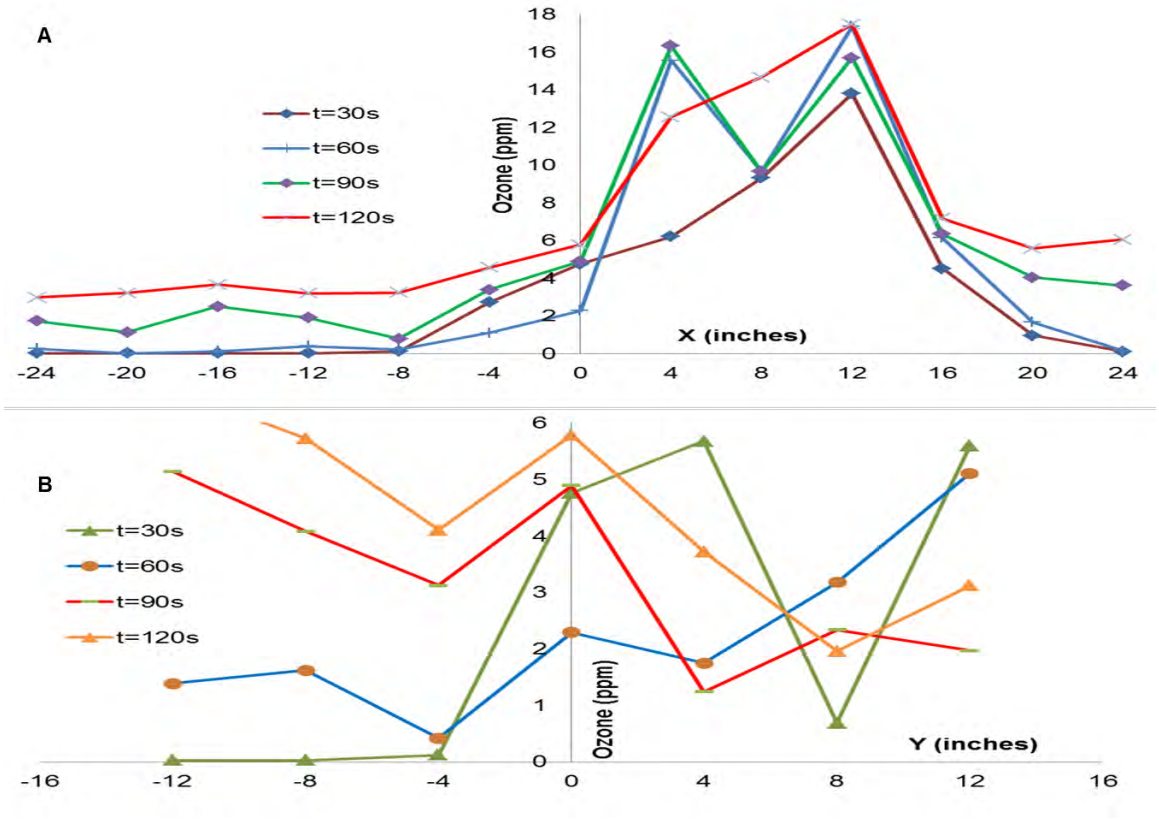

Figure 5-7. (A) Spatial variation of ozone distribution along the X-axis in the sterilization chamber (B) Spatial variation of ozone distribution along the Y-axis in the sterilization chamber

Figure 5-7(A) demonstrates that the highest amount of ozone is produced in the upper right quadrant of the chamber (as labeled in Figure 5-6). Typically the levels of ozone noted on the right hand side (RHS) of the chamber are more than those noted on the left hand side (LHS). Figure 5-7(B) indicates that the distribution of ozone produced along the Y-axis does not follow a clear-cut trend, as along the X-axis. This bias in ozone levels towards the R.H.S of the chamber can be explained due to the electrodynamic force ($\vec{F} = q\vec{E}$) produced as a result of the existent electric field during plasma generation. Previous research [102]-[103] elucidates further on the generation of this electrodynamic force and its dependence on the various plasma input parameters as well as its effect on fluid momentum. Most importantly, the direction of

this force is from the powered electrode to the grounded electrode. As a result of this electrodynamic force (from left to right), the flow is pushed to the left, as shown in Figure 5-8(A). When the configuration is flipped, as shown in Figure 5-8(B), the direction of force is from right to left. Accordingly a higher level of ozone is detected on the L.H.S of the chamber in this configuration.

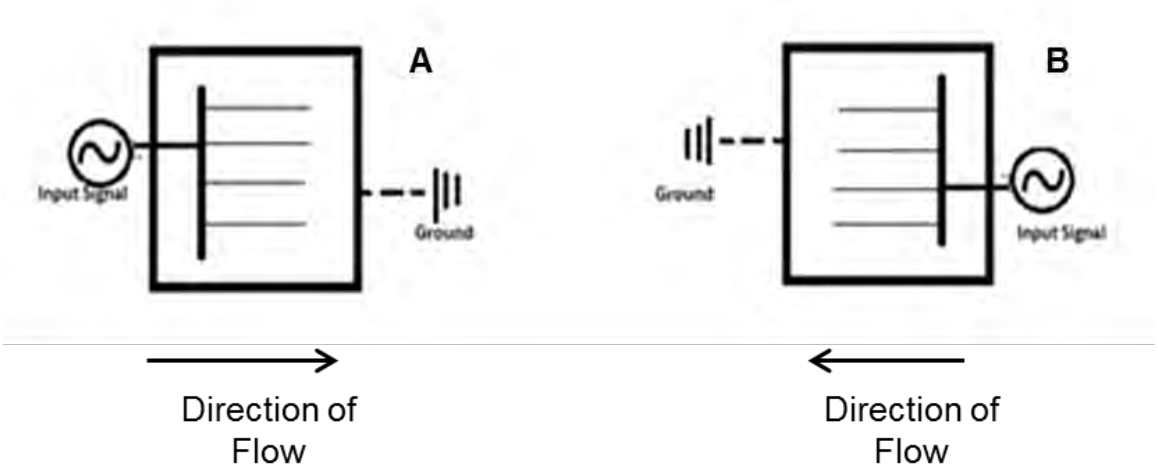

Figure 5-8 (A) and (B) showing the two different configurations in which the device is placed. It is noted that in (A), flow is “pushed” toward the right (along the X-axis). In (B), when the configuration is flipped, flow is “pushed” towards the left.

Next, the trend of ozone production and decay during DBD plasma generation and the dependence of this production/decay on chamber volume are evaluated. In order to do this, a clean FR4 device was taken and placed inside the given sterilization chamber. The ozone probe was positioned 2.5” above the chamber floor and 5” to the right of the device (measured from the center-point of the device). The device was powered for 2 minutes, turned off and the setup was allowed to rest for an additional 5 minutes, before repeating the same protocol using the same device for the next sterilization chamber. Production/decay profiles were obtained in this manner for all four sterilization chambers.

Analyzing the measured ozone data, using trend-fitting tools, Equation (5) and (6) are derived. The total ozone concentration ($[O_3]$) and time (t), during plasma generation, follow a power-law relationship, as shown below.

$$[O_3] = \begin{matrix} At_1^B, & 0 \leq t \leq 30 \\ Ct_2^D, & 30 < t \leq 120 \end{matrix} \quad (5\text{-}5)$$

where t (total time of plasma generation i.e. ozone production) = $t_1 + t_2$ and A, B, C, D are constants. In equation (5-5), total time 't' has been divided into two time segments 't_1' and 't_2', based on the biphasic ozone production trend observed within each chamber. 't_1' denotes an initial rise time for ozone production (30s) and 't_2' denotes the time during which ozone is still produced, but at a much slower rate than during t_1 (90s). Similarly, the decay of ozone in all four chambers is observed to follow a logarithmic trend of the form given below:

$$[O_3] = [O_3]_0 10^{-t/\tau} \quad (5\text{-}6)$$

where $[O_3]_0$ is the initial measured concentration of ozone and τ is the ozone-decay constant.

A, B, C, D and τ are listed in Table 5-1 below for each chamber.

Table 5-1. Values of the constants used in Equation (5-5)-(5-6)

Chamber#	A	B	C	D	$[O_3]_0$ (ppm)	τ (s)
1	7.080	0.658	8.692	0.597	174.940	909.091
2	4.999	0.557	8.735	0.408	63.958	1250
3	9.216	0.465	12.116	0.309	31.879	1250

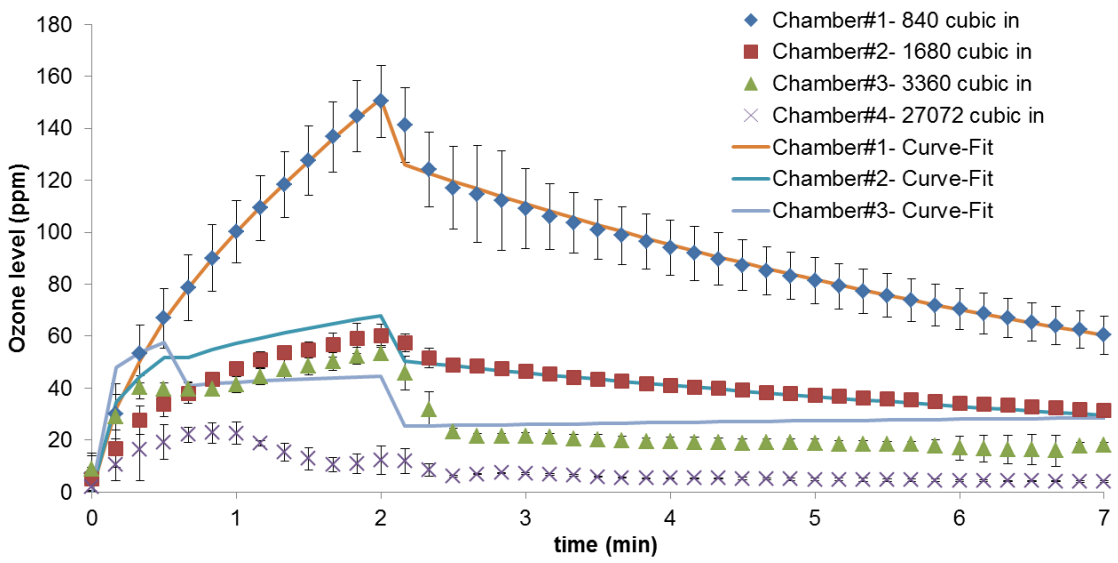

Figure 5-9. Comparison of ozone concentrations in all four chambers. The plasma device is powered at 0 min and turned off at 2 minutes, after which the setup is allowed to sit for another 5 minutes

Thus, in Figure 5-9 above, both measured ozone data as well as curve-fitted data from Equations (5-5) and (5-6) have been plotted. In the case of measured ozone data, error bars have been plotted with respect to standard deviation. In Figure 5-9, it is noticed that the plots obtained using trend-fitting tools are most accurate in the case of Chamber#1. For Chamber#2 and #3, these plots do not follow the exact same trend as the measured data. This implies that as the volume of the chamber increases, it becomes increasingly difficult to predict the rate of production/decay of ozone. It is for this reason precisely, that constants for Chamber#4 have not been listed in the above table. Owing to its comparatively larger volume, it is highly difficult to evaluate accurate trends of production/decay in Chamber#4. It must also be noted that the values of these constants apply to the ozone levels measured only at the probe position described above. These are not indicative of the ozone production/decay throughout the rest of the chamber.

Plotting the measured ozone levels with the corresponding chamber volume, at different time points during the 7 minute interval produces a correlation such as the one given below in Figure 5-10. Here 5 time points have been plotted: 60s, 120s (during plasma generation) and 240,360 and 420 s (plasma is turned off). Both chamber volume (X-axis) and ozone levels (Y-axis) have been plotted on a $\log_2$ scale for easier comparison.

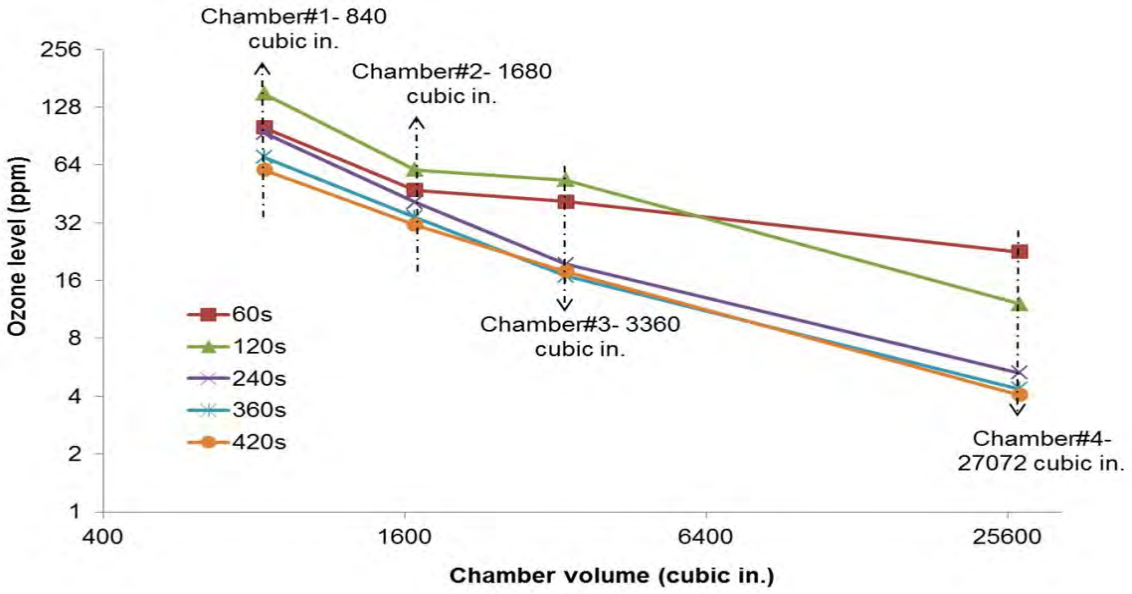

Figure.5-10. Correlation of the ozone levels with the corresponding chamber volumes. The different time points (60,120,240,360,420s) represent ozone measurements in each chamber at that particular time point.

From Figure 5-10, it is observed that ozone levels measured in Chamber#1 at any time are the highest. During the plasma generation phase (60,120s), ozone levels in Chamber#2 and #3 are almost identical. Since DBD plasma generation 'pushes' the produced ozone towards the right (as shown in Figure 5-8), it seems that the bulk of produced ozone is continuously pushed towards the right and in an upward direction during plasma generation. Since both Chamber#2 and #3 have the same height, even though the latter is twice as long as the former, the ozone produced seems to dissipate

at an identical rate in both chambers, which is why similar amounts of ozone are measured in both cases. This implies that during plasma generation (and thus, active ozone production), chamber height is the factor that determines the amount of ozone present in the chamber. This also explains why the ozone concentration in Chamber#1 is almost twice that of Chamber#2. Chamber#1 is half the height of Chamber#2 (same length and breadth), which means that the produced ozone has even less volume to dissipate in. Hence it is measured by the probe in greater concentrations.

During the decay phase, once the plasma is turned off (240,360,420s), it is observed that the rate of decay of ozone in Chamber#1 is almost double that in Chamber#2. The same trend applies to #2 , when compared with #3. This implies that larger the chamber volume, faster the rate of decay of ozone. This is reinforced by the values of $[O_3]_0$ and τ given in Table 5-1.

A small note on the different ozone concentrations noted in the different chambers has to be made. In Figures 5-7, 5-9 and 5-10, measured ozone levels have been listed in terms of ppm, for the sake of easy comparison. At any instant, these ozone levels are measured by one ozone probe, placed at the same position in each chamber. Figure 5-9 seems to indicate that Chamber#1 contains the highest ozone concentrations while Chamber#4 contains the least ozone concentrations. But it is the same FR4 plasma generator producing ozone for the same amount of time. This means that owing to the different volumes of the chambers, ozone produced during plasma generation and thereafter diffuses at different rates. Hence if we calculate the total number of molecules of ozone in each chamber, they should be identical. This is proved in Figure 5-11.

The total number of molecules of ozone in each chamber can be calculated by first converting ppm to mg/m^3, calculating the number of moles of ozone/volume in each chamber, multiplying this number by the volume of the chamber and subsequently calculating number of molecules of ozone in each chamber (1 mole= 6.023×10^{23} molecules). Figure 5-11 given below shows the total number of molecules of ozone (calculated) in each chamber at t= 60,120,240,360 and 420 s .

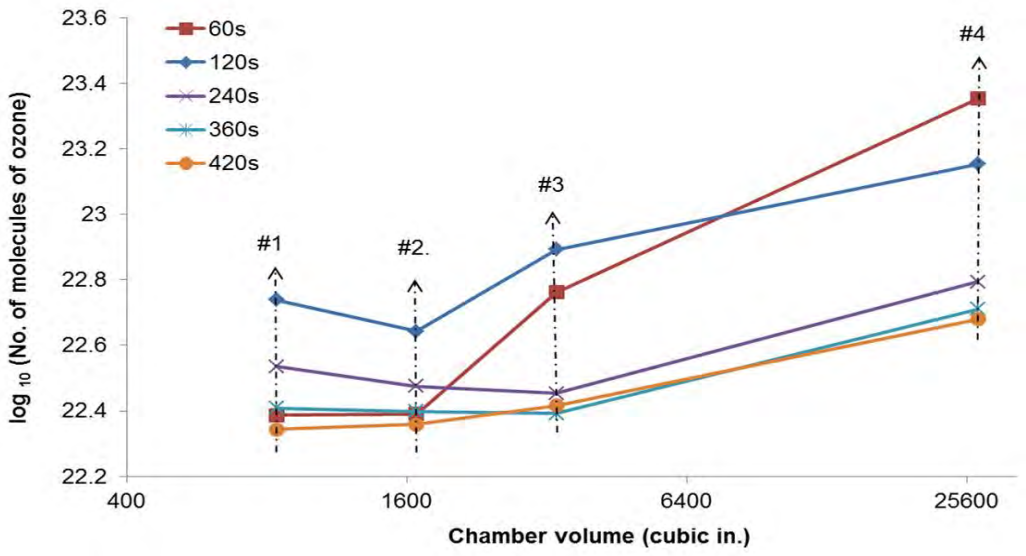

Figure 5-11. Correlation of the total number of ozone molecules present in each chamber at t= 60,120,240,360,420s) to the respective chamber volumes. The X-axis is plotted on a $\log_2$scale for easier comparison. #1-#4 represents the different chambers.

At first glance, it seems that total number of ozone molecules in each chamber varies. However, keep in mind, that the Y-axis is plotted on a $\log_{10}$ scale. Thus at any given time point, the total number of ozone molecules in any chamber range between 10^{22}- 10^{24}. The minute variation in number of molecules can be attributed to differences in probe measurements.

When the ozone production of the two dielectric materials compared for sterilization purposes, FR4 and SC, was examined during plasma generation, it was observed that the ozone production in the case of FR4 was marginally higher than that in the case of SC. This comparison is shown below in Figure 5-12.

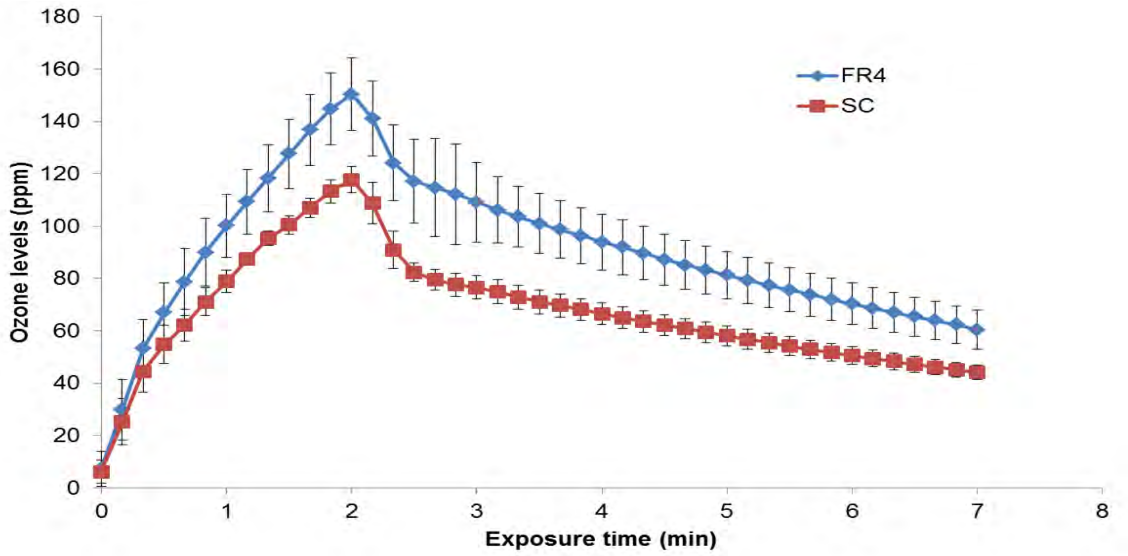

Figure 5-12. Comparison of ozone production during 7 minutes for FR4 versus SC. The plasma device is powered at 0 min and turned off at 2 minutes, after which the setup is allowed to sit for another 5 minutes

In Figure 5-12, it is observed that the rates of production and decay of ozone in the case of SC is similar to that in the case of FR4. Comparing the ozone concentration at different times for FR4 and SC, it is noted that on an average, the ozone concentration in the case of FR4 is ~25.8% higher than in the case of SC.

In this section, an overview of the trends in ozone production and decay during DBD plasma generation was provided. Owing to the volume of the sterilization chamber, the ozone produced dissipates at different rates. This also means that if an inoculated device were to be placed at one constant position in each chamber, it would be exposed

to varying concentrations of ozone. This helps determine the maximum level of ozone needed in order to completely inactivate *E. coli*. The effect of exposing *E. coli* to this produced ozone was studied. The results of such a study are listed in the next section.

5.2.2 The effect of ozone produced during DBD plasma generation on *E. coli*

As mentioned before, DBD plasma generation produces UV photons, charged particles and neutrals. Since DBD plasma produces high concentrations of ozone, the effect of exposing *E. coli* concentrations to this produced ozone was tested.

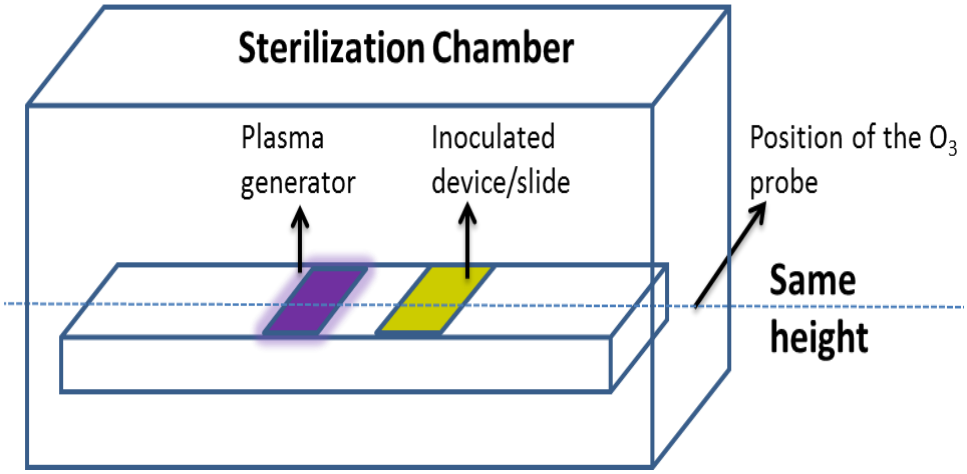

Figure 5-13. Experimental schematic for the ozone exposure tests. On the left is the plasma generator, which is used to generate plasma and produce ozone inside the chamber. On the right is the inoculated device/glass slide, which is inoculated with 20 µl of E. coli and exposed to the ozone produced by the plasma generator

The schematic for the ozone exposure experiments is given above in Figure 5-13. The ozone probe is positioned ~1” away from the inoculated device, at the same height as the devices so as to accurately capture the ozone levels that the inoculated device is subject to. Judging by the ozone distribution in Figure 5-8, the ozone probe was placed on the RHS of the chamber, in order to measure the maximum amount of ozone in the chamber.

For these tests, a clean FR4 device is selected as the plasma generator or ozone generator. Three kinds of inoculated substrates (having equal surface areas) are tested: FR4, SC and glass coverslips. For each test, the substrate is inoculated with 20 µl of E. coli (corresponding to a concentration of 10^{6-8} CFU). Once the inoculated substrate is placed next to the ozone generator, the chamber is closed. The inoculated substrate is allowed to sit in the chamber for total time 't' which consists of a plasma generation time (t_3) and a resting time (t_4). Hence $t_{EXP}= t_3+t_4$. At the end of t_{EXP}, the chamber is opened, the inoculated substrate removed and subjected to the post-processing protocol described in Section 3.5.2. Experiments are triplicated to ensure reproducibility.

Using Sterilization Chamber#1, FR4 plasma generator and three kinds of inoculated substrates, three exposure times (t_{EXP}= 2, 7, 32 min) were tested. Each exposure time 't_{EXP}' consists of t_3= 2 min and t_4= 0, 5 and 30 minutes respectively. Figure 5-14 given below depicts the results of such a test. Error is listed in terms of the standard deviation from the mean of measurements.

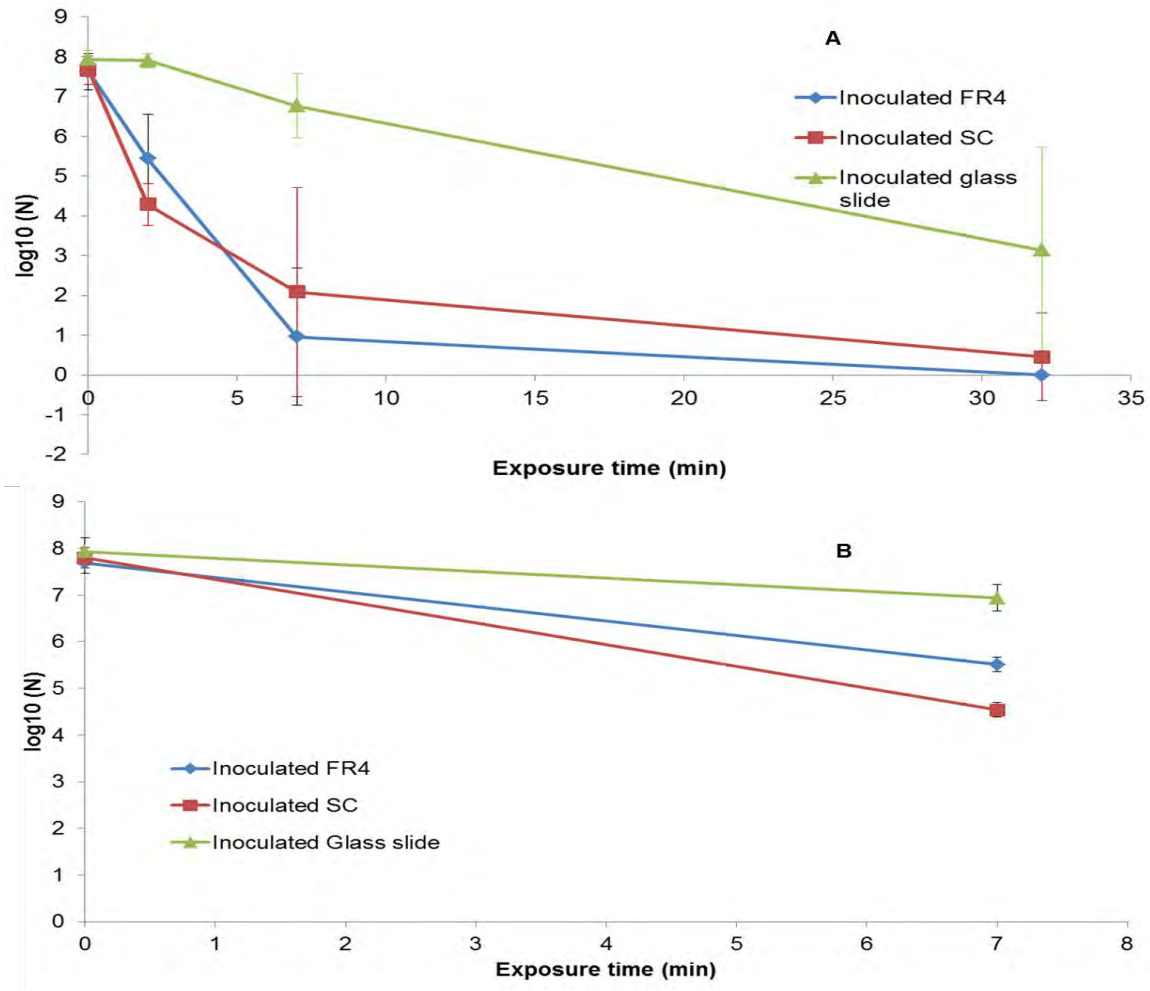

Figure 5-14: Inactivation plots due to ozone exposure with (A) FR4 plasma generator and (B) SC plasma generator

In Figure 5-14(A), it is evident that in the case of FR4 plasma generator, ozone exposure is highly lethal to *E. coli.* In the case of inoculated FR4 substrate, starting from an initial *E. coli* concentration of 10^8 CFU, a ~3 $\log_{10}$ reduction, ~6 $\log_{10}$ reduction and complete reduction in *E. coli* concentration is noted at 2, 7 and 32 minutes respectively. A single $\log_{10}$ implies a $1/10^{th}$ decrease in bacterial concentration i.e. 10^7 CFU reduces to 10^6 CFU. In the case of inoculated SC substrate, similar $\log_{10}$ reduction is noted at 2, 7 and 32 minutes, although complete inactivation is not noted at 32 minutes. However in the case of inoculated glass slides, incomplete inactivation is noted in all three cases.

In Figure 5-14(B) i.e. in the case of SC plasma generator, ozone exposure causes incomplete inactivation of *E. coli* in the case of all three inoculated substrates. From the ozone concentrations noted for the FR4 Plasma generator and the SC plasma generator in Figure 5-12 and the sterilization data noted for both in Figure 5-14, it is evident that 120-150 ppm of O_3 is sufficient to cause a major reduction in *E. coli* concentration after 7 minutes of ozone exposure. It is conjectured that the 7 minute interval is a 'threshold' time interval i.e. if the *E. coli* concentration was exposed to the same level of ozone for t_{EXP} slightly longer than 7 minutes, complete bacterial inactivation could be seen. This conjecture is made in light of the fact that for the inoculated FR4 substrate, after 7 minutes of O_3 exposure, 4 out of 6 trials showed complete bacterial inactivation.

It must be noted here that in the case of the inoculated glass slides, exposure to ozone produced using either a FR4 plasma generator or SC plasma generator does not seem to make a difference. This indicates that there is a substrate dependence that determines the effect of ozone on *E. coli*. When glass slides are inoculated with 20 µl of *E. coli*, it is visibly evident that the bacterial sample deposited on the glass slide clumps into random droplets on the surface of the glass slide. This is because glass is a far less hydrophilic surface than FR4 or SC, thus making it difficult for liquid to adhere to it. Hence this uneven clumping of *E. coli* on the glass slide might be leading to shielding of the underlying bacteria, which would explain reduced killing in the case of glass slides.

The results of exposing *E. coli* ozone in Chambers#2-#4 are shown below in Figure 5-15. Owing to the similar levels of inactivation noted in the case of inoculated FR4 and SC substrate in Figure 5-14, for the following cases, only an inoculated FR4

substrate is considered. As is evident, after 7 minutes, a nearly complete inactivation is noted in the case of Chamber#1. In Chambers#2-#4, after 7 minutes, only a reduction of 1-4 $\log_{10}$ is noted.

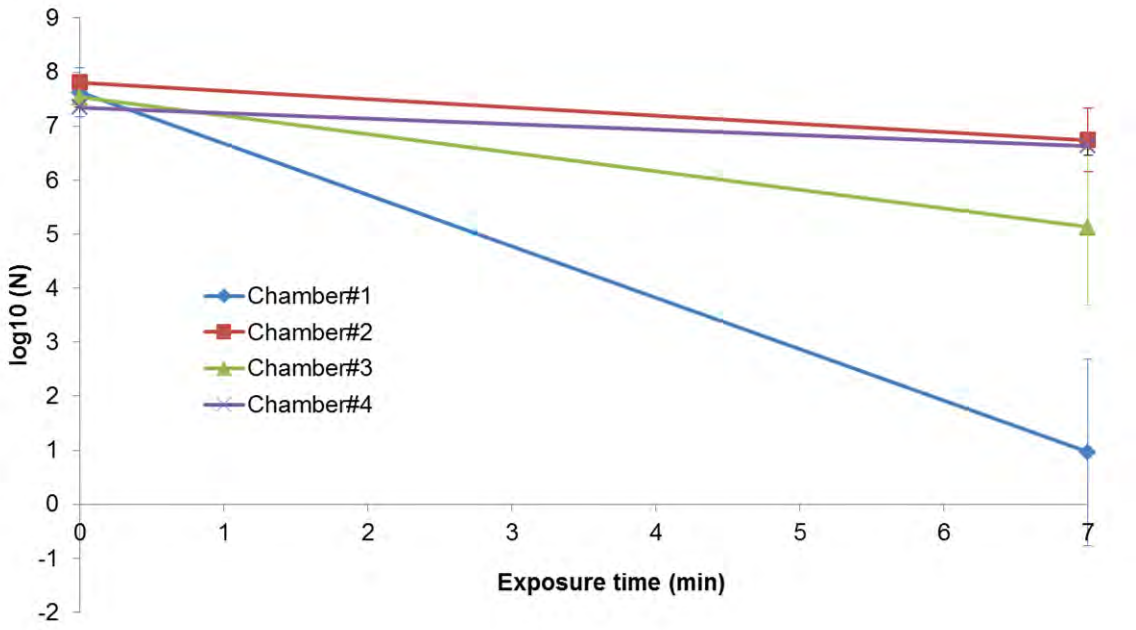

Figure 5-15. Inactivation plots due to ozone exposure in the different chambers using a FR4 plasma generator and an inoculated FR4 substrate

This reduction is further dependent on chamber volume. While in Chamber#4 and #2, the reduction in *E. coli* concentration, due to 7 minutes of ozone exposure is only 1-2 $\log_{10}$, varied results are observed in Chamber#3. In Chamber#3, the reduction in *E. coli* concentration, due to 7 minutes of ozone exposure, is more like 3-4 $\log_{10}$. It is not immediately clear as to why this difference is observed in Chamber#3, as compared to Chamber#2 and #4.

The next step was to evaluate whether ozone produced during plasma generation is truly responsible for the almost complete bacterial inactivation noted in Figure 5-14(A). In order to evaluate this, ozone produced was inhibited in the following

two ways 1) Using activated charcoal to inhibit ozone production 2) Generating plasma using Nitrogen (N_2) as the discharge gas

A fixed amount of Activated charcoal (MarineLand Black Diamond ®) was placed on the plasma generator and the plasma generator subsequently operated. In doing so, the produced ozone was directly adsorbed by the charcoal and ozone levels were immediately reduced by around 98%. For subsequent tests, care was taken to adjust this amount of activated charcoal on the plasma device to maintain the same reduced levels of ozone.

This comparison of levels of ozone produced with and without charcoal for Chamber#1 is shown below in Figure 5-16. For both cases, a clean FR4 plasma device was placed in Chamber#1, powered at 0 min and turned off at 2 minutes, after which the setup was allowed to rest for another 5 minutes**.** Since there is a huge difference between ozone levels in both cases, for the sake of simplicity, ozone concentration (on the Y-axis) is shown on a $\log_{10}$ scale.

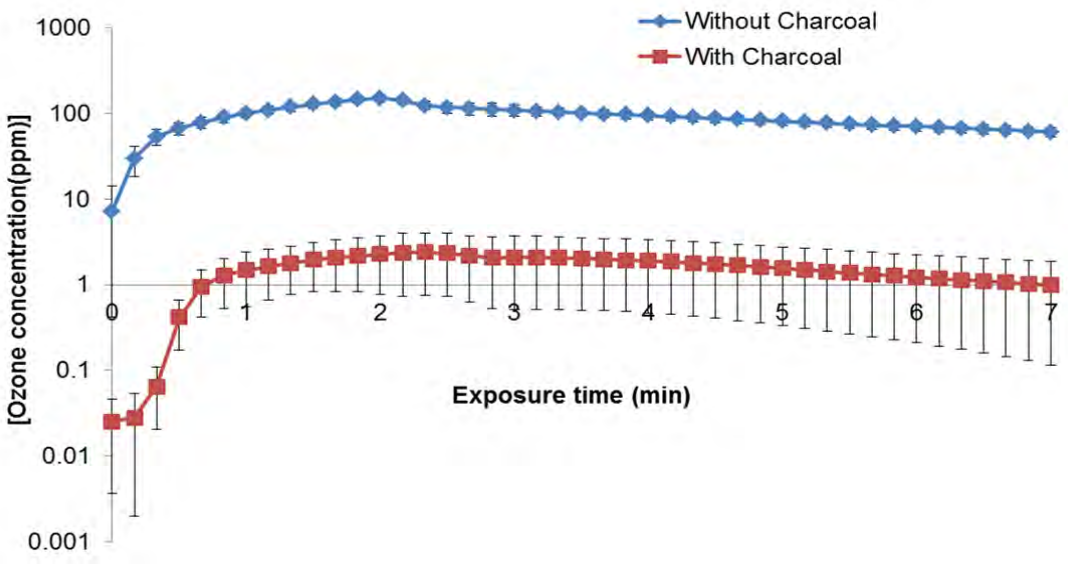

Figure 5-16. Comparison of ozone production with and without charcoal for Chamber#1. Plasma is turned off at 2 min.

As is evident from Figure 5-16, the addition of charcoal on top of the device during plasma generation leads to a reduction of ozone concentration by a factor of 100. For all the sterilization tests testing the effect of exposing *E. coli* concentrations to ozone produced in cases with and without charcoal, the amount of charcoal on the device was adjusted so as to maintain the reduced ozone concentration as shown in Figure 5-16. For the purpose of this study, such a configuration will be referred to as a 'modified plasma generator'. Chamber#1 was used for these tests and FR4 devices were used as the modified plasma generators.

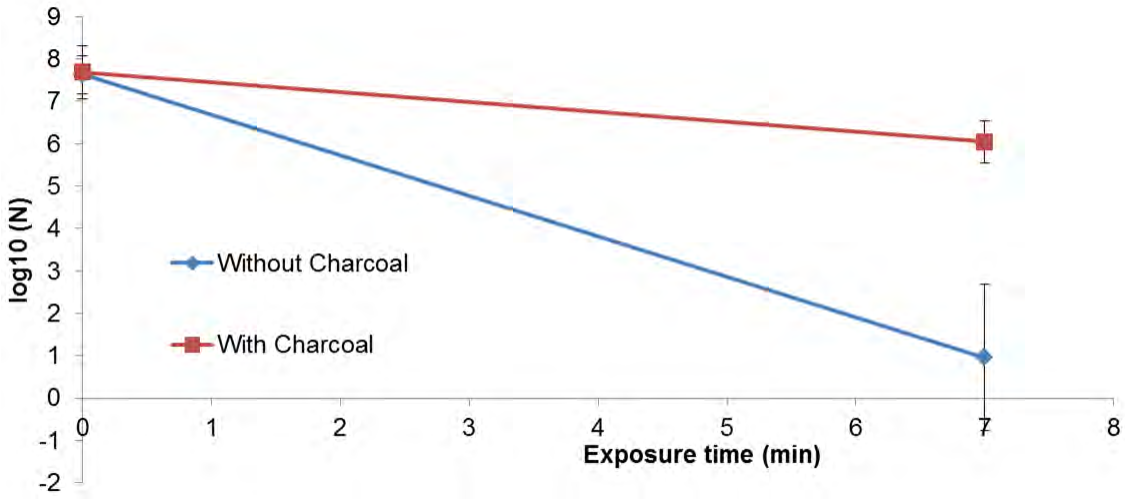

Figure 5-17. Inactivation plots due to ozone exposure in Chamber#1 with and without charcoal. A clean FR4 device was used as the ozone generator and covered with charcoal when needed. The device was powered for 2 minutes.

When the inoculated substrate is exposed to this modified plasma generator for 7 minutes and then post-processed, negligible reduction in *E. coli* concentration is observed, thus proving that the ozone produced during plasma generation is responsible for inactivation of *E. coli*. This inactivation effect with and without charcoal, in the case of an inoculated FR4 substrate, is shown above in Figure 5-17. The wide disparity in bacterial inactivation is immediately evident and proves that the reduced

ozone concentrations due to adsorption by activated charcoal do not effectively kill *E. coli*, when compared to the case of no charcoal. While Figure 5-17 demonstrates that ozone produced during DBD plasma generation is responsible for bacterial inactivation, an alternative experiment to prove this was also conducted.

DBD Plasma was generated using Nitrogen (N_2) as the working gas. A smaller vacuum chamber (9.3”x7.4”x5.6”) was used as the sterilization chamber. The chamber was then evacuated to an absolute pressure of 0.0978 atm, following which Nitrogen gas (Airgas Inc., UN1066, 99.0% N_2) was introduced into the chamber until the pressure in the chamber rose to 1 atm. This process was repeated four times to maintain a majority N_2 environment. The aim of such an intensive method of flushing out all the air and filling the chamber with nitrogen was to ensure that very low oxygen levels remain in the chamber in order to inhibit ozone production during DBD plasma generation. Using laws of partial pressures, this percentage of nitrogen, at the end of 4 flushes was calculated to be 99.998 ± 0.78 %. Hence the aim of maintaining a pure N_2 environment was accomplished fairly well.

The experimental protocol in these tests, unlike the previous ozone exposure tests, consisted of inoculating select FR4 devices with 20 µl of *E. coli* (initial concentration= 10^8 CFU), placing them in the sterilization chamber, sealing the chamber, flushing the chamber with N_2 four times and then powering the device for the requisite time interval (Δt). Owing to the rigorous nature of these tests, only FR4 substrate was tested. The time intervals tested were Δt= 60s, 120s. Each time interval test was replicated thrice, using the same *E. coli* sample to ensure repeatability. The

comparison of sterilization results from plasma generation using discharge gas as air versus N_2 are given below in Figure 5-18.

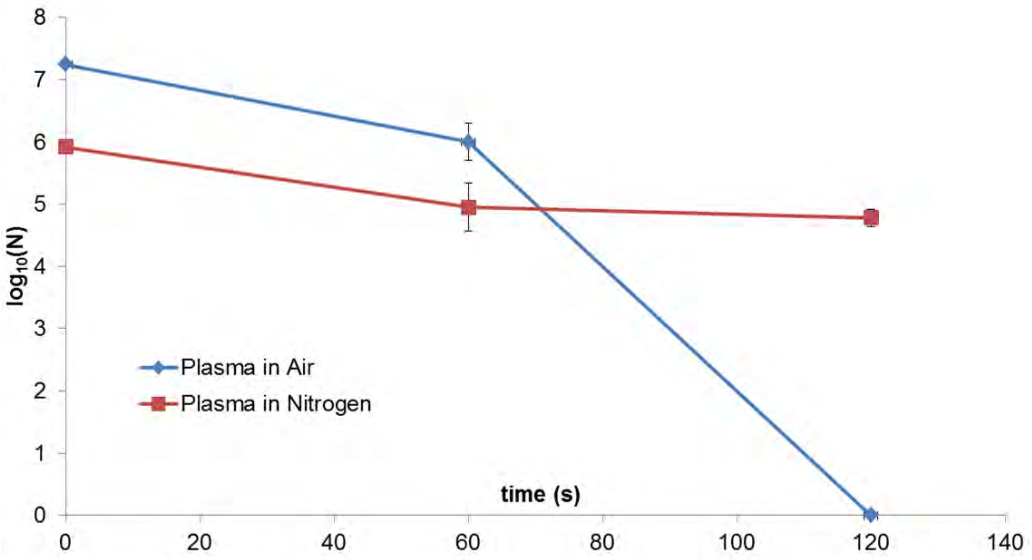

Figure 5-18. DBD Surface Plasma Sterilization, comparing air and nitrogen as the discharge gas. Two sterilization times (60s and 120s) are tested, using *E, coli* as the test pathogen.

In Figure 5-18 above, in the case of air, complete bacterial inactivation is noted within 120s. In the case of N_2, starting from an initial concentration of 10^6 CFU, at the end of 120s of plasma generation, only a 1 $\log_{10}$ reduction in *E. coli* concentration is noted. However, the initial concentration of *E. coli* used was 10^8 CFU, which implies that the flushing of the chamber four times as well as evacuation of the chamber to extremely low pressure causes a 2 $\log_{10}$ reduction in *E. coli* concentration. Nevertheless, even with a pre-plasma concentration of 10^6 CFU, it is evident that plasma generation in Nitrogen (hence, plasma generation in the absence of ozone) does not cause much of a reduction in *E. coli* concentration. Thus from the results of the Charcoal tests as well as Nitrogen tests, we conclude that ozone produced during plasma generation is capable of inactivation of *E. coli*, on prolonged exposure times.

5.3 Temperature Studies

Section 1.2 discusses the classification of laboratory plasmas into two categories: high temperature plasmas and low-temperature plasmas. In high temperature plasmas, the high temperature serves to equilibrate the high temperature of the electrons, hence establishing local thermal equilibrium (LTE). But in low-temperature plasmas, the heavy particles in plasma (ions, neutrals) are at a much lower temperature than the electrons, which are typically high-energy particles. Hence these plasmas are classified as non-LTE and are typically used for low-temperature applications, such as plasma sterilization.

The effect of heating of the surface due to plasma generation and its subsequent contribution to sterilization has been examined [53]. Using a CO_2 plasma in the low-pressure regime, they observed a higher destruction efficiency at 60^{o}C as compared to that at 15^{o}C. A more fundamental analysis of the rotational and vibrational temperatures during plasma generation was conducted by Ayan et al. [104], who analyzed the relationship between rotational and vibrational temperatures and the plasma power density. They conclude that the gas temperature depends only on average power, which means that increasing the average power might increase the average temperature, resulting in an increase in surface temperature of the treated tissue. However, they do not explicity evaluate the effect of surface temperature on sterilization.

Hence for the DBD plasma setup used for sterilization in this thesis, it was necessary to (a) understand the kind of surface temperatures attained during plasma generation (b) examine the effect of temperature only on *E. coli*, in order to determine the role temperature plays in the plasma sterilization process.

In order to do this, an infrared camera (FLIR A320®) was used to measure the temperature of the surface during plasma generation. FLIR A320® The infrared camera uses an uncooled micro-bolometer to detect infrared radiation and converts it into an electronic signal, which is then processed to produce a thermal image that can be processed to obtain surface temperature.

In order to obtain the thermographic image of each plasma device, while it was being operated, the plasma device was powered for 2 minutes, during which thermographic images of the plasma device were obtained by the Infrared camera at a sampling rate of 0.5 Hz. After turning off the plasma device, the camera continued to record images for another 2 minutes, thus yielding a total of 48 frames. These images are transferred in real-time to a computer, wherein they are subjected to additional data processing.

Since the IR camera works by detecting the heat radiated off the surface, the temperatures obtained depend on the thermal emissivity coefficient, which needs to be calculated accurately. This is done by placing thermocouples on the device and heating up the device on a VWR Scientific ® hot plate. Data from the thermocouple is sampled via a LabView ® interface. The hot plate is allowed to heat up to a fixed , known temperature, after which it is switched off and allowed to cool down. While it is cooling down, temperature is sampled via the thermocouple attached to the device on the hotplate and the IR camera simultaneously. Thus, the temperature detected by the thermocouple is the known, actual temperature (T_a) and the temperature detected by the IR camera is the detected temperature (T_{IR}). Emissivity coefficient ‘e’ is calculated,

via the software provided by the IR Camera (ExaminIR) using the Stefan-Boltzmann law:

$$P = e\sigma(T^4 - T_{amb}^4) \quad (5\text{-}7)$$

The LHS of this equation remains the same while the RHS varies for the temperature measured by the thermocouple versus the temperature measured by the IR camera. Hence, by a process of comparison, the emissivity coefficient is calculated and applied to correct for T_{IR}. For FR4 and SC, this emission coefficient was calculated as 0.9097±0.03 and 0.929±0.03 respectively.

Once the emissivity coefficients for temperature correction were obtained, a number of different scenarios were tested in order to obtain temperature data. First a set of three different clean FR4 and SC devices was powered for a 2 minute interval, wherein temperature was sampled every 5s for each device. Secondly, a set of three different FR4 and SC devices, each inoculated with 20 µl of *E. coli*, were powered for a 2 minute interval, wherein temperature was sampled for each device again. For each of these devices, once plasma is turned off at 2 minutes, the device was allowed to rest for another 2 minutes. Temperature was sampled during these 2 minutes also.

Figure 5-19 below shows two sets of images. (A)-(D) is a depiction of the temperature of the electrode surface area at four different times (t= 30s,60s,90s,120s). (E)-(H) is a depiction of the same for an inoculated FR4 device. From Figure 5-19, it is observed that for a clean FR4 device, the surface temperature at 120s is marginally higher than that at 30s.The average surface temperature at 120s is observed to be ~16^{o}C higher than that at 30s. The highest temperatures are noted at the edge of the electrodes. However, for an inoculated device at 30s (5-19(E)), the temperature is fairly

low (average surface temperature= 28°C- 34°C) due to the presence of the liquid bacterial sample on the surface. By 60s, this liquid has evaporated and temperature slowly starts increasing, reaching the maximum value at 120s. However this temperature profile does not resemble the one for a clean device at 120s. The difference between average surface temperature at 30s and 120s for the inoculated case is calculated to be ~25°C.

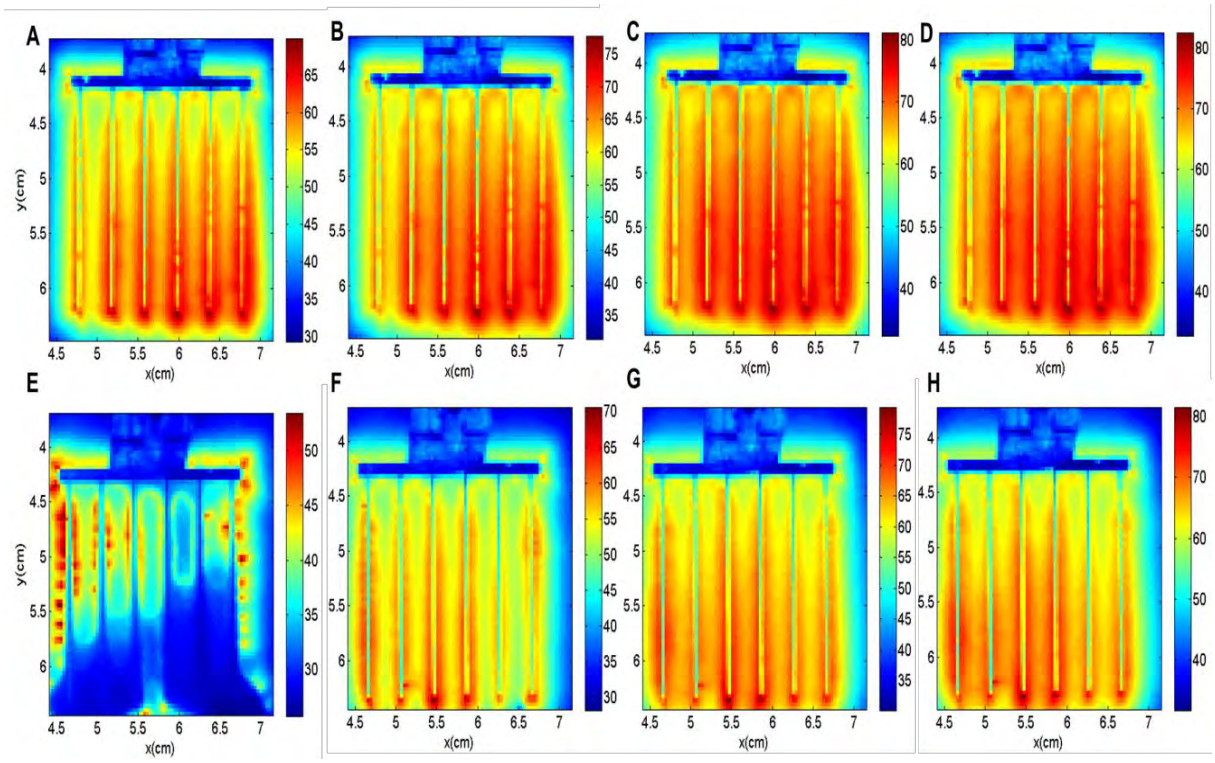

Figure 5-19. Variation of temperatures at t= 30s, 60s,90s, 120s for Clean FR4 device (A-D) and Inoculated FR4 device (E-H)

Figure 5-20 below shows the same two sets of images for a clean and inoculated SC device respectively. Surface temperatures are considerably lower in the case of SC, as compared to FR4. In the case of the inoculated device, the effect of liquid bacterial sample on the surface is demonstrated very clearly. In the case of the inoculated SC device, the liquid sample does not evaporate until the very end of the 2 minute interval.

This is depicted in Figure 5-20 (E)-(H), where surface temperature remains on the lower side even at 90s. The difference between average surface temperature at 30s and 120s for the clean and inoculated SC cases is calculated to be ~11^{o}C and 22^{o}C respectively.

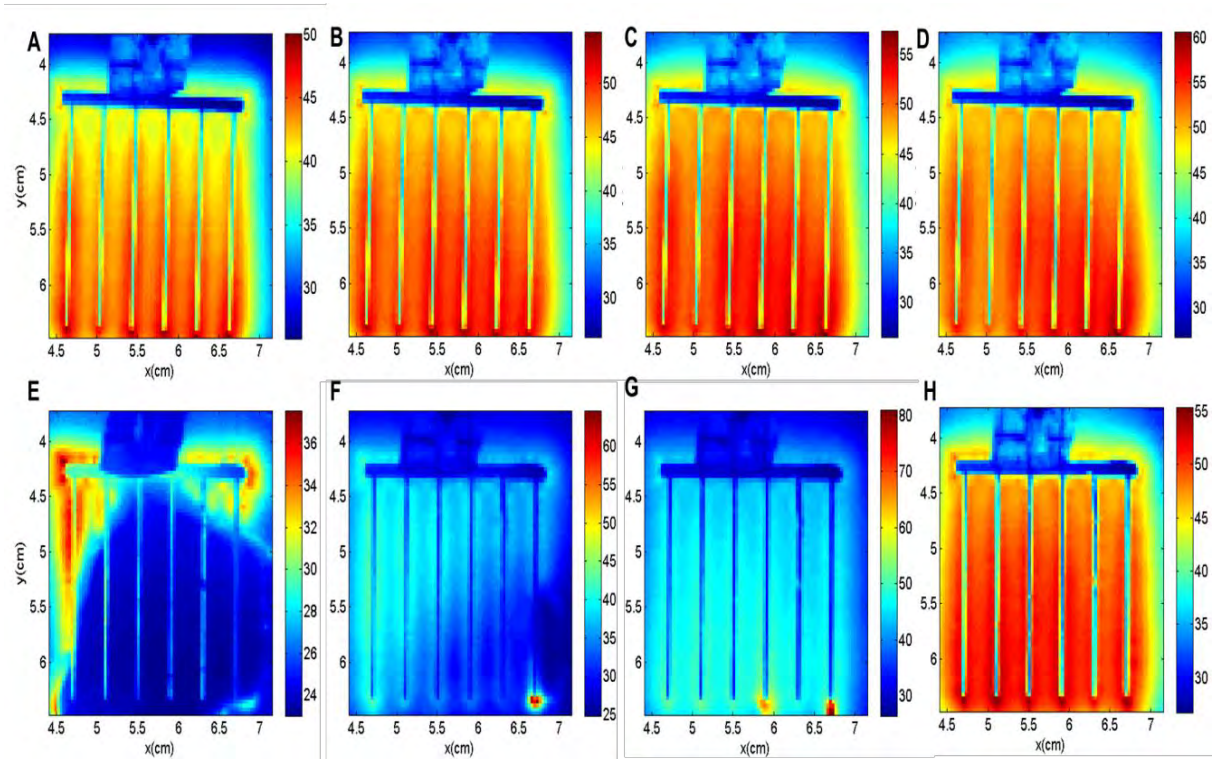

Figure 5-20. Variation of temperatures at t= 30s, 60s,90s, 120s for Clean SC device (A-D) and Inoculated SC device (E-H)

To get a better idea of the variation of temperature over time for the two configurations (clean and inoculated), the average temperature over the entire electrode surface area at every 5s, over a total of 2 minutes was calculated. Figure 5-21 below shows this variation of average temperature for a clean and inoculated device (FR4 & SC). The variation of temperature thus shown in Figure 5-21 is a clearer graphical representation of the temperature trends noted in Figure 5-19 and Figure 5-20.

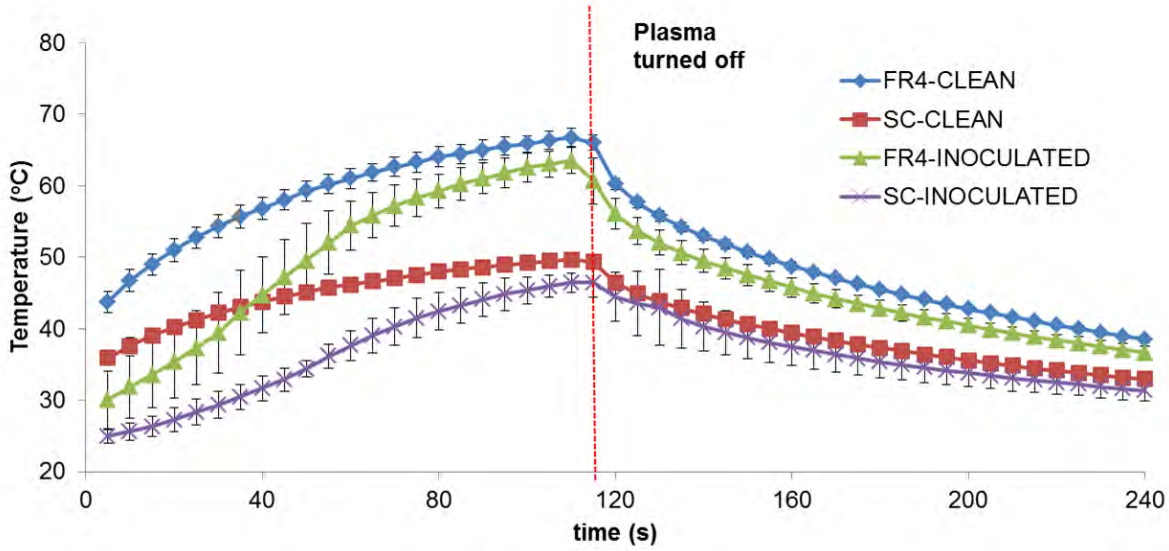

Figure 5-21. Comparison of average surface temperatures during plasma generation for clean and inoculated FR4 and SC devices, measured using an infrared camera.

A clean FR4 device has the highest average surface temperature. An inoculated FR4 device has very low surface temperatures initially. However as has been demonstrated in Figure 5-19, after the first 30s, this temperature rises rapidly. The rise in temperature is less steep than in the case of the inoculated SC device, as corroborated by the images in Figure 5-20.

In order to determine the role of temperature in sterilization, a separate set of experiments was conducted wherein the devices were heated up to fixed temperatures, inoculated with 20 µl of *E. coli* and allowed to rest on the hot plate for 2 minutes. The thermal conductivity of FR4 material used in this study is not readily available (although literature sources commonly cite a value of 0.25-0.3 W/m.K) while manufacturer specifications cite the thermal conductivity of SC as 0.71 W/mK. Accordingly the SC devices were seen to heat up faster than the FR4 devices. Once the device reached the required temperature, the bacterial sample was deposited on it and the heating of the

device was continued for another 2 minutes. Following this, each of the devices was subjected to standard post-processing protocols and incubated for 48 hours. Colony counts were performed to estimate the number of surviving organisms.

Two types of temperatures were tested using each dielectric. The average and maximum surface temperatures during plasma generation were measured both for FR4 and SC. Average and maximum temperatures measured in the case of FR4 were ~54^{o}C and ~77^{o}C respectively. Average and maximum temperatures measured in the case of SC were ~39^{o}C and ~72^{o}C respectively. Thus in order to test the effect of temperature alone on *E. coli,* the inoculated FR4 and SC devices were first heated up to their respective average temperatures The results of such a test, using the average temperature in each case, are given below in Figure 5-22.

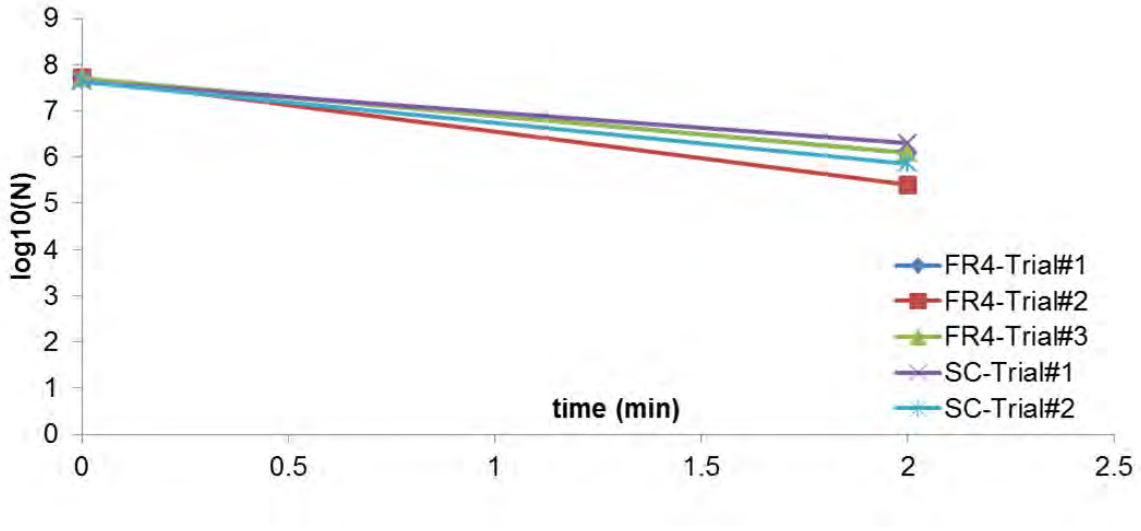

Figure 5-22. Sterilization plots analyzing the effect of temperature on inoculated FR4 and SC devices. In each case, the inoculated devices were heated up to the average temperature measured during plasma generation.

Figure 5-23 below shows the results of the same test, using the maximum temperature in each case. For the sake of simplicity, results for both inoculated FR4 and SC devices are shown on the same plot.

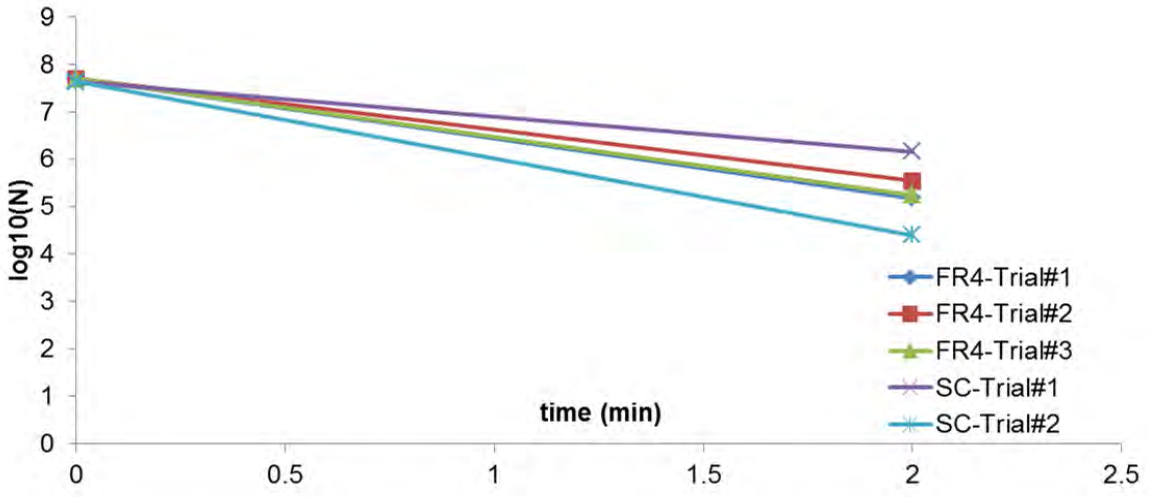

Figure 5-23. Sterilization plots analyzing the effect of temperature on inoculated FR4 and SC devices. In each case, the inoculated devices were heated up to the maximum temperature measured during plasma generation.

Inoculated FR4/SC devices were heated to average and maximum temperatures in each case so as to subject the bacterial concentration to surface temperatures measured during plasma generation. This was done in order to mimic the role of temperature during plasma generation. Of course, due to the design of the hotplate, variability is introduced in terms of maintaining a constant temperature for the 2 minute interval. However care was taken to maintain the temperature within 2^{o}C-3^{o}C of the desired temperature. It must also be noted that during plasma generation, the surface temperature is non-uniform, which means that the whole surface is not at the same temperature at any given point during plasma generation. However, by heating up an inoculated device on a hot-plate, the whole device is heated to a uniform temperature. Hence, bacterial samples in these tests are actually being subjected to a much more uniform (and hence greater) heating effect than they would be subject to during plasma generation.

As is evident from Figure 5-22 and Figure 5-23, subjecting the bacterial concentrations to even such uniform high temperatures does not seem to produce a significant reduction in bacterial concentrations. This implies that temperature does not play a major role in plasma sterilization. However it is possible that temperature could be acting synergistically with another plasma component to influence the sterilization process.

From the spectroscopic, ozone and temperature data discussed above, there seems to be a critical point during the sterilization cycle i.e. the complete evaporation of the liquid bacterial sample deposited on the dielectric surface. Once complete evaporation occurs, the spectroscopic intensity, emitted ozone levels and surface temperatures all increase significantly. Corresponding to this, a rapid drop in bacterial concentrations, leading to complete inactivation, is also observed The next section discusses the significance of this critical point more elaborately.

5.4 Microbiological analysis

The previous sections concentrated on characterizing the DBD plasma being used for sterilization in this study and analyzing how the different plasma components might play a role in the mechanism of plasma sterilization. The current section takes a different approach in understanding this mechanism. The interaction of plasma with cells is explored through a number of different microbiological techniques in order to obtain insight into which cell component might be affected by plasma exposure. These techniques include microscopic analysis of plasma-treated cells, fluorescence measurements etc.

5.4.1 Evaluation of membrane damage by Live/Dead® BacLight™ Assay

The plate counts provide information about the number of viable microorganisms remaining on the sterilization device, but do not give information about the fate of individual cells. Ozone and other oxidative species target unsaturated lipids and lipopolysaccharides (LPS) in G- cell membranes resulting in lethal damage and leakage of cell contents before complete destruction of vegetative cells is seen [105]-[106]. To examine membrane damage, LIVE/DEAD® BacLight™ bacterial viability kits (Life Technologies, Carlsbad, California) were used. These kits use a two-color fluorescence assay to determine the integrity of bacterial membranes. The two dyes both stain nucleic acids, but differ in their spectral range and ability to penetrate cells. SYTO®9, a green fluorescent dye that penetrates both damaged and intact cell membranes, and propidium iodide, a red fluorescent dye that cannot penetrate intact membranes and thus only stains cells with lethal membrane damage. The propidium iodine reduces the fluorescence seen from SYTO®9 when both are present. If cells are damaged to the point of lysis and thus lose their nucleic acids, they will not stain with either dye [70], [52]. These stained bacterial suspensions can then be observed under a fluorescence microscope or fluorescence can be measured in microtiter plates.

In order to visualize the *E. coli* effect of plasma exposure on *E. coli* cells, different inoculated FR4 devices were plasma-treated for t= 0,30,60,90 and 120s and sealed into sterile bags containing 1 ml of phosphate-buffered saline (PBS). Each device was agitated thoroughly for 20s, after which the supernatant from each bag was removed and subjected to a fluorescent staining protocol. For each time point, 5 μl of

the stained bacterial suspension, was then trapped between a slide and a coverslip and examined using a Leica® DM4000 fluorescence microscope.

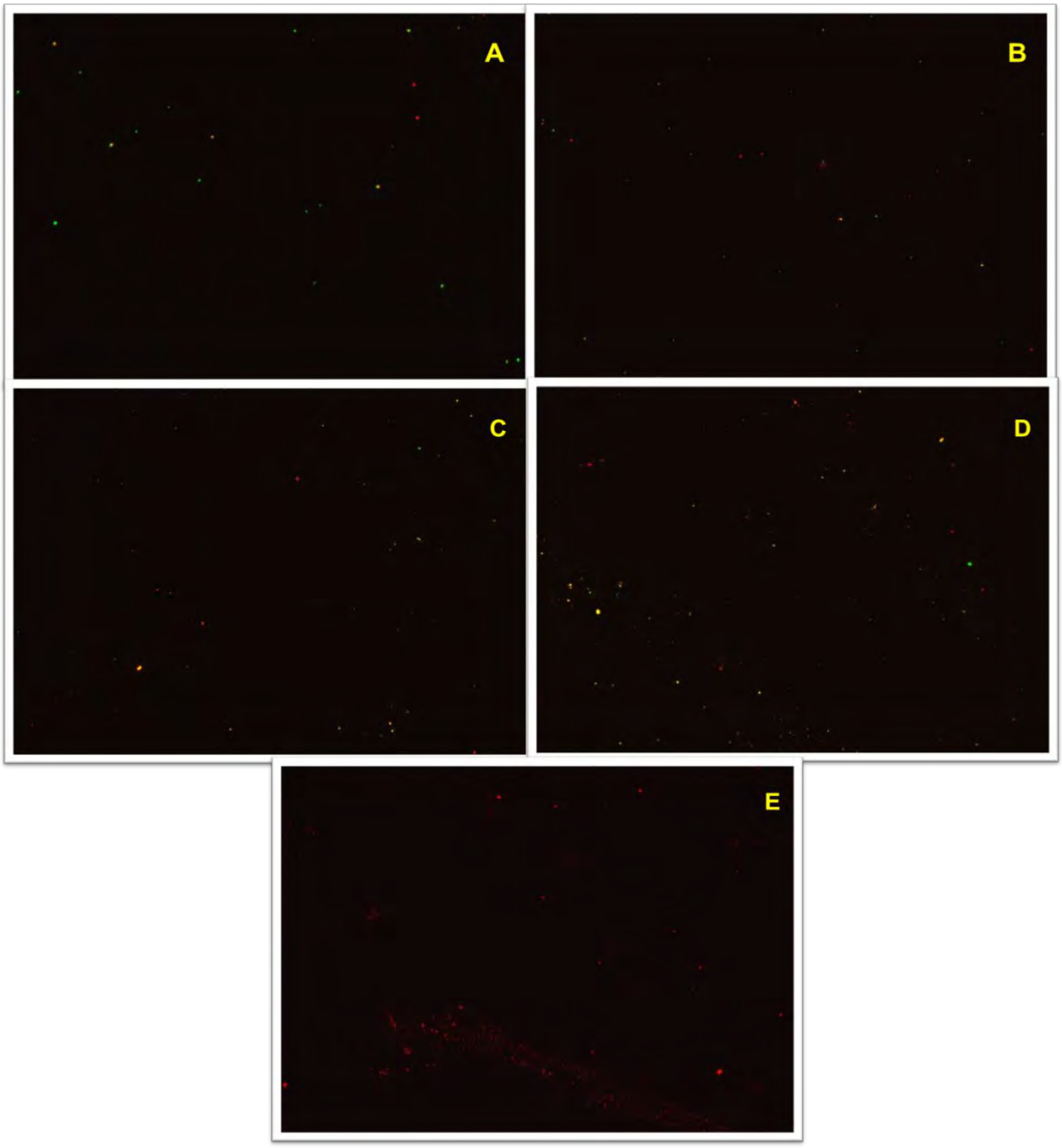

Figure 5-24. Fluorescence Images obtained of the different cell suspensions after exposure to plasma for t= 0,30,60,90 and 120s respectively. A-E correspond to t= 0-120s respectively.

The excitation/emission maxima for the SYTO 9 stain and propidium iodide are 480/500 nm and 490/635 nm respectively. The corresponding set of images is given

above in Figure 5-24 (A)-(E). The different images A-E correspond to t= 0,30,60,90 and 120s respectively. The fluorescent images confirm what is expected: at: no bacterial inactivation at 0s (the picture is filled with green mostly), negligible inactivation at 30s (minimal red flecks are observed), followed by partial inactivation at 60s and 90s (similar concentrations of red and green) and complete inactivation at 120s (all red on the slide)From Figure 5-24, very little concentration of cells is noticed on each individual fluorescence image. This is due to the fact that the initial concentrations of cells were very low, to start out with. Additionally the lag time between plasma treatment of cells and fluorescence imaging was 3-5 hours, owing to time taken for preparation protocols. When cell suspensions are allowed to rest for such a long time, a portion of the cells tends to lyse, which is why lower cell concentrations are noted.

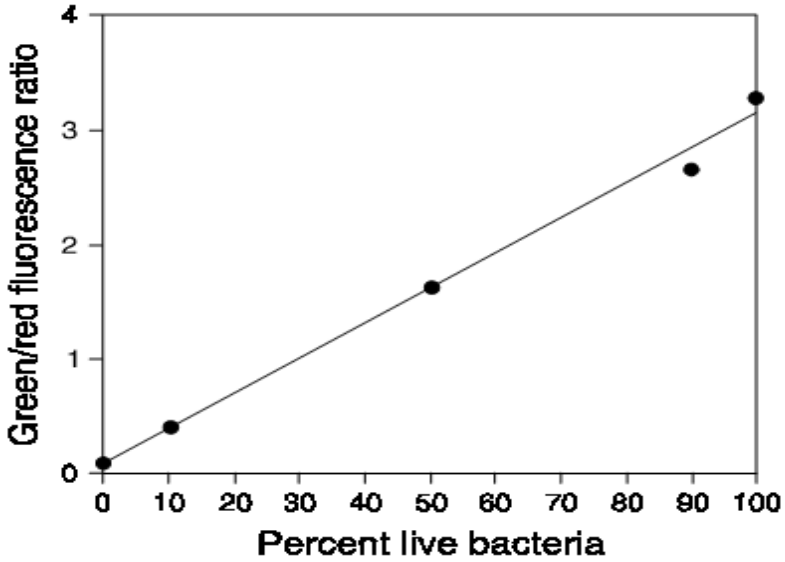

Figure 5-25. An example of the calibration curve calculated by measuring $Ratio_{G/R}$ for cell suspensions with different proportions of live/dead cells.

The ratio of live/dead cells can also be calculated using the measurement of fluorescent intensity of the cell suspension at each time point and correlating it to the percentage of live cells in the suspension (using a calibration curve like the one shown

above in Figure 5-25). This calibration curve is used to determine the proportion of live/dead cells in the cell suspensions obtained after different plasma exposure times.

This is accomplished via measurement of the fluorescence in a micro-plate reader. The same protocol as before is followed, except that the supernatant at each time point, after being treated with a fluorescent staining protocol, is subsequently mixed with filter-sterilized dH_2O. 100 μl of this prepared cell suspension is pipetted into separate wells of a 96-well flat-bottom microplate. Three such sets of wells are prepared to account for standard deviation.

With the excitation wavelength centered at about 485 nm, the fluorescence intensity at an emission wavelength corresponding to green (~530 nm) is measured for each well of the entire plate. Similarly, using the same excitation wavelength, the fluorescence intensity at an emission wavelength corresponding to red (λ_R ~ 630 nm) is measured for each well again. The ratio of intensities ($Ratio_{G/R}$) is derived by dividing the fluorescence intensity measured at λ_G by the fluorescence intensity measured at λ_R. This ratio is then compared to existing calibration curves, in order to calculate the proportion of live bacteria. An example of this calibration curve is shown above in Figure 5-25.

Thus, calculating $Ratio_{G/R}$ for the different cells suspensions obtained after plasma exposure times t= 0,30,60,90 and 120s, and plotting this $Ratio_{G/R}$ for the different time points, Figure 5-26 below is obtained. In this figure, data from all three replicates of microplate readings is shown. Figure 5-26 shows similar phasic behavior, as observed in survival curves for *E. coli* (Figure 4-1). There exists a slight decrease in $Ratio_{G/R}$ at 30s (implying that a small population of the cells is dead), followed by a

larger reduction in this ratio at 60,90 and 120s. It is also evident from this figure, that the majority of the cells are killed between 30-60s, thus corroborating the D-values (time taken for 90% reduction in cell population) obtained in Figure 4-4

Since the cell suspensions used at different time points here were obtained after plasma exposure using inoculated FR4 devices, the below values of $Ratio_{G/R}$ make sense. If inoculated SC devices were used instead, a much less phasic behavior would be expected in Figure 5-26 with the major drop in $Ratio_{G/R}$ occurring between 100-120s.

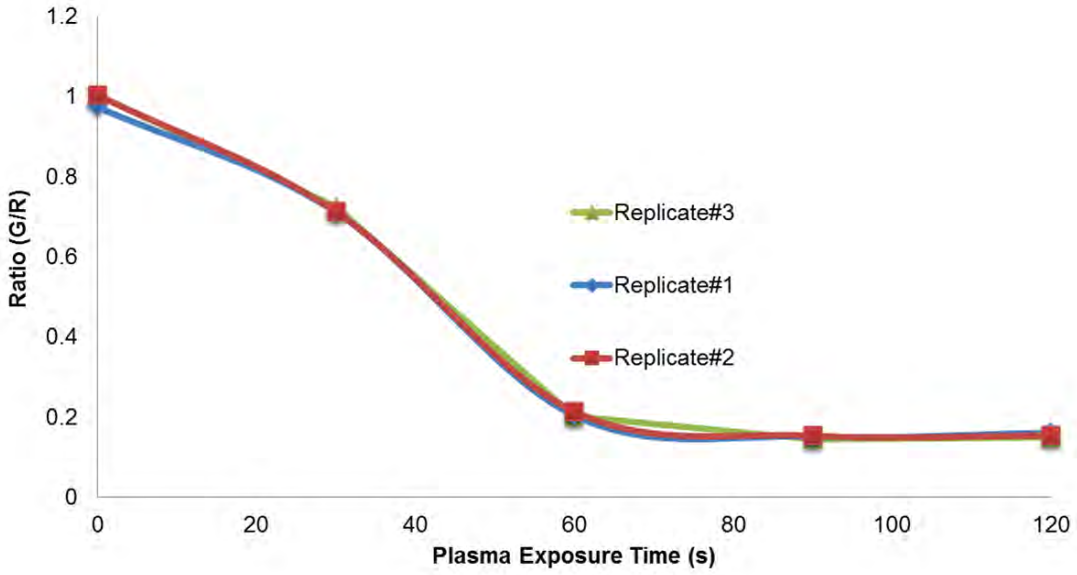

Figure 5-26. Plot of the $Ratio_{G/R}$ calculated after different plasma exposure times

Comparing Figure 5-25 and 5-26, the percentage of live cells at 60,90 and 120s seems to be ~0%. Notice that $Ratio_{G/R}$ at t= 0s is ~1, which implies 10% live bacteria in the cell suspension. As reiterated before, this is due to the relatively lesser concentration of cells in the original cell suspensions used for fluorescence imaging.

The presence of both red and green staining cells indicates that damage to cell membranes is contributing to overall cell mortality. If the cells were ruptured due to electrostatic tension or were completely etched away from the plasma treatment, then

$Ratio_{G/R}$ would have been difficult to determine at t=60-120s, since ruptured cells cannot be stained by either dye. Thus it is likely that the cells treated by plasma are inactivated due to damage to the cell-membrane or one of the cell-organelles, rather than cell-rupture by plasma treatment. Further analysis in this direction would require SEM imaging of the plasma-treated cells

5.4.2 Mutation Studies.

Section 5.1 demonstrates that the spectral signature of the generated DBD plasma does not contain any lethal UV radiation, specifically UV-C radiation (Figure 1-10). UV-C radiation is especially important as it can cause dimerization of DNA strands in cells, thus affecting base pairings and causing mutations during DNA replications. The objective of the mutation studies was to definitively determine whether damage due to UV-C radiation is a factor during DBD plasma sterilization.

Rifampin is a bactericidal antibiotic drug of the *rifamycin* group. Media containing Rifampin is known to select for the growth of rifampin-resistant (Rif (r)) mutants [107]. Rifampin resistant cells arise at about 1 in 10^{14} cells from naturally occurring point mutations. DNA damage due to UV light exposure increases the rate at which resistance mutations occur. Hence *E. coli* cells treated with plasma for the sterilization times cited in Figure 4-1 were cultured both on regular LB agar as well as agar containing Rifampin. The expectation was that if the *E. coli* cells were being damaged by UV-C radiation during plasma generation, then a higher percentage of Rifampin resistant colonies would be seen on the Rifampin plates, as compared to unexposed cultures. However this was not observed. Instead the CFU concentration on both sets of plates appeared to be similar. This proved that damage to the *E. coli* cells was not due

to DNA damage, which in turn proved that shortwave UV radiation was likely not responsible for cell death due to DBD plasma exposure.

5.4.3 Microscopic analysis of plasma interaction with *B. subtilis* biofilms

A biofilm is an architecturally complex community of bacterial cells. Biofilms harbor multiple cell types i.e. in the same biofilm, individual cells can follow different developmental pathways, resulting in heterogeneous populations. Hence one group of cells can perform one distinct function and localize to a separate region within the biofilm, while another can perform another distinct function and localize to a different regions. This property of biofilms makes them very popular for laboratory research. Research in plasma interaction with biofilms picked up pace, as recently as 2007 onwards (discussed further in Section 1.3.3).

The differentiation in cell function can be highlighted by the use of different fluorescence proteins [108]. Two different cell phenotypes are monitored for changes due to plasma interaction: the motile cell phenotype (‘swimming’ genes) and the matrix-producing cell phenotype. Changes in the motile phenotype are determined by monitoring the expression of the *hag* operon, which encodes flagellin, a major protein component of flagella (responsible for locomotion in cells). Changes in the matrix-producing phenotype are determined by monitoring the expression of the *tapA* operon, which encodes the primary protein component of the extra-cellular matrix [93]-[94], [109]. A dual reporter strain for both of these genes was used in which genes en-coding fluorescent proteins are fused to promoters of the *tapA* and *hag* genes. A $_{tapA}$-YFP (yello fluorescent protein) fluorescence reporter construct was integrated into the *amy*E locus and a $_{hag}$-CFP (cyan fluorescent protein) was integrated into the *lacA* operon.

The objective of microscopically examining the biofilm exposed to plasma was to determine which cell phenotype is affected due to plasma exposure: the motile cells or the matrix-producing cells. Since fluorescent reporter strains of *B. subtilis* NCIB360 were readily available, these were used for the microscopic analysis.

B. subtilis cells were stored at -80^{o}C and streaked directly from frozen stocks to LB agar. After 12 hours of incubation at 37^{o}C, 3 ml of LB liquid medium was inoculated with cells from an isolated colony. This inoculated medium was incubated in a shaker at 37^{o}C for 3 hours, until OD was approximately 1. A 3 μl drop of this culture was then deposited at the center of a 60 mm MSgg (minimal salts, glycerol glutamate) agar plate and incubated at 37^{o}C for 24-48 hours. This led to the formation of a biofilm. The biofilm thus grown was transferred to an inverted microscope system (*Nikon Eclipse Ti)* for brightfield and fluorescence imaging. Then, a plasma device was inverted (comb-like electrode inverted face-down) and plasma generated at 40-50 kHz, 9-10 kV p-p for 2 minutes. Both the input frequency and voltage varied because of the additional impedance introduced due to the device resting face down on the surface of the MSgg agar. However care was taken to ensure that the frequency and input voltage remained within the stated limits.

The biofilm was imaged before, during and after plasma exposure using a 4x objective. Images were taken along the equatorial slice of the agar plate and are shown below in Figure 5-27. The imaging order is (A) before plasma exposure (B) immediately after plasma exposure for 1 minute (C) before Plasma exposure for the 2nd time (D) immediately after plasma exposure for 1 minute (2nd time) (E) 50 minutes after plasma exposure for 1 minute (2nd time).

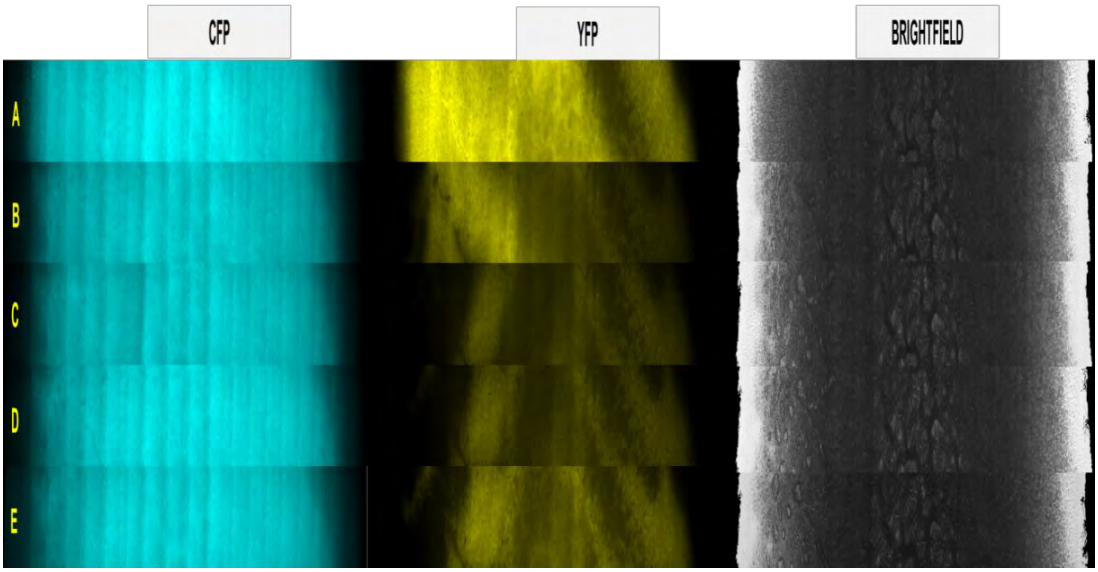

Figure 5-27. Images of bio-films before, during and after plasma exposure. CFP indicates motile cells and YFP indicates matrix-producing cells. A-E indicates the imaging order of the biofilms.

Thus the *B. subtilis* biofilm was exposed to plasma for 2 minutes in 1 minute intervals. As is observed from Figure 5-27, the CFP images do not show a significant variation in intensity, whereas the YFP show a gradual decrease in intensity from A-E,

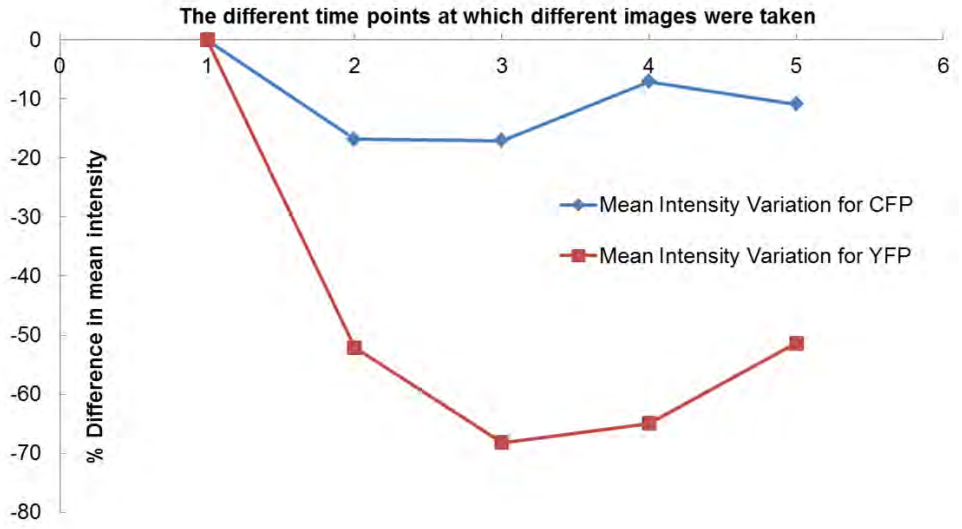

Figure 5-28. Mean intensity variation in CFP and YFP modes for imaging order A-E. On the Y-axis is plotted the % reduction in intensity (-ve because of the reduction). Points 1-5 correspond to frames A-E.

signaling cell injury/death. When this intensity variation from A-E is plotted graphically, Figure 5-28 above is obtained.

In Figure 5-28, the % reduction in mean intensity values in frames B-E, as compared to frame A is plotted both for CFP and YFP modes. As is evident, there is a drastic reduction in intensity values for the YFP mode, which implies further that the matrix-producing cells are more damaged than the motile cells after 2 minutes of plasma exposure.

This result also matches the results seen with the *B. subtilis* sterilization experiments, describe in Figure 4-2. DBD plasma is observed to be more lethal to the *B. subtilis* strain cultured in MSgg media (complete inactivation in 4 minutes) rather than the one cultured in LB media (incomplete inactivation in 6 minutes). MSgg media promotes the growth of the matrix-producing phenotype while LB media promotes the growth of the motile phenotype. Hence both the sterilization tests and the microscopic biofilm analysis confirm that plasma exposure is more lethal to cells expressing the matrix-forming phenotype. This is an important insight into determining the cell breakdown mechanism due to plasma exposure.

5.5 Discussion

In this chapter, many different features of DBD plasma generation are discussed in an effort to understand their role in plasma sterilization. The different features discussed are the spectroscopic signature, ozone levels and surface temperatures measured during plasma generation. Additionally, an insight into the cell state after plasma exposure is also gained via microbiological studies.

Spectroscopic data obtained highlights intensity peaks at wavelengths corresponding to transitions in the 2^{nd} positive system of N_2. No intensity peaks are

obtained at λ< 300 nm, thus making it unlikely that UV-C radiation plays a major role in DBD plasma sterilization at atmospheric pressure. This observation is further confirmed by the Rifampin studies, which do not show an increase in mutation rates.

The levels of ozone produced during DBD plasma generation and the dependence of the decay of this produced ozone on volume of the sterilization chamber is discussed in detail in Section 5.2.1. Such a comprehensive dataset helps understand and predict the rates of produced ozone and the time taken for the produced ozone to dissipate using a surface DBD plasma device.

Ozone exposure tests, in which an initial concentration of *E. coli* is exposed to ozone produced during plasma generation, demonstrate that this initial concentration is almost completely inactivated after 7 minutes of ozone exposure (in the case of an inoculated FR4/SC substrate). Additionally, it is determined that a threshold value (120-150 ppm) of ozone-concentration is required for ~99.99% reduction in bacterial concentrations.

Activated charcoal is used to inhibit ozone production. Reducing *E. coli* concentrations to these reduced ozone concentrations leads to negligible reduction in bacterial concentrations (Figure 5-17). This implies that the reduction in ozone levels due to activated charcoal is what causes the reduced degree of lethality due to ozone exposure. However the protocol for testing ozone exposure consists of inoculating a clean plasma device with *E. coli* and placing it next to a clean plasma device (which acts as the plasma generator). Thus while the latter is being powered, the former is being exposed to the plethora of reactive species being produced. It is not being exposed to the direct action of the plasma, but rather to the ‘afterglow’. This afterglow,

as described before, contains a number of reactive species, especially reactive oxygen species like ozone (O_3),O_2*($a^1\Delta_g$), O(^{1}D), O(^{3}P). It is also possible that the activated charcoal responsible for inhibition of ozone production is also responsible for the inhibition of other reactive species. However, keeping in mind that the average residence times for most of these reactive species is on the order of seconds and that the inoculated device is ~1" away from the plasma generator, it is considered highly likely that bacterial inactivation in such a case is due to the produced ozone.

In order to further explore this theory, plasma is also generated in a pure nitrogen (N_2) atmosphere. A smaller vacuum chamber is used as the sterilization chamber and before each experiment, the chamber is flushed with nitrogen sufficiently so as to maintain a ~99.98% N_2 environment. Survival curves obtained using such a setup (using a protocol similar to that used for Figure 4-1) show that plasma exposure in a Nitrogen (N_2) environment does not produce significant bacterial inactivation (Figure 5-18). This further supplements the idea that ozone produced during DBD plasma generation is likely responsible for bacterial inactivation. Of course, the way to confirm this would be to use additional reagents designed to detect reactive oxygen species in bacterial cell suspensions [110].

Temperature studies, conducted using an FLIR® A320 IR camera are useful in determining the surface temperature distribution for the dielectric substrate during plasma generation. It is noted that surface temperatures are greater in the case of FR4 , compared to SC. Additionally, experiments are also conducted in which the bacterial concentrations were heated to surface temperatures, similar to those observed during plasma generation. Survival curves obtained from these experiments demonstrated that

pathogen inactivation due to effect of temperature alone was negligible (Figure 5-22 and 5-23).

The physiological state of cells after plasma exposure is examined using a LIVE/DEAD bacterial viability kits, which helps visualize the proportion of live/dead cells after different intervals of plasma exposure. The proportion of the live/dead cells measured corresponds to the inactivation rates observed in Figure 4-1. This information also helps conjecture that a possible mechanism of plasma sterilization is damage to the cell membrane rather than rupture of the cells due to electrostatic tension.

Finally the effect of liquid on the dielectric surface is examined. The evaporation of the liquid *E. coli* sample deposited upon the device surface follows a pattern. Initially the bacterial sample deposited covers the entire electrode surface area, and plasma is visible only around the edges of the electrode. As time progresses, the sample begins to evaporate around the outer edges of the electrode. Gradually, this evaporation begins to spread to other parts of the electrode, until eventually plasma covers the entire electrode surface area. This usually occurs at around t= 60s for the FR4 dielectric and at t= 120s for the semi-ceramic (SC) dielectric. These two times are also the times at which a steep drop in pathogen concentration is noted from the sterilization plots (Figure 4-1).

Spectroscopic, ozone, temperature and power data uniformly show that plasma is repressed while visible bacterial sample is present on the plasma devices. Absorbed input power plots (Figure 4-13) shows the correspondence of the temporal variation of absorbed input power to the amount of bacterial sample on the plasma device. The spectroscopic intensity peaks are noted at the same wavelengths at each time point;

however, their intensities increase as the liquid evaporates (Figure 5-3 and 5-4). Similarly, it was observed that as the liquid sample evaporated, rate of production of ozone remained low until the entire liquid sample evaporated. Thereafter ozone production increases. Similarly surface temperature plots show the sudden increase in temperature once the entire sample evaporates (Figure 5-19-5-21).

When the same number of organisms was deposited in a 40µl volume instead of the standard 20µl inoculation volume, the “passive phase” wherein there is little or no loss of viability, that was noted in Figure 4-1 was extended by about 30s in Figure 4-5 i.e.the rapid drop in *E. coli* concentration occurs at t>120s, as opposed to 90s in the case of the lower inoculation volume (20 µl). This further promotes the theory that the amount of liquid bacterial sample deposited on the plasma device affects the sterilization time.

Oehmigen et al. [111] reported experiments wherein they examined the role of acidification in influencing antimicrobial activity due to DBD plasma exposure. They concluded that plasma treatment of non-buffered liquids by indirect surface DBD results in acidification and thus, inactivation of suspended bacteria. When they tested the same theory with buffered solutions, they noted that pH decrease is avoided and therefore, antimicrobial plasma activity is reduced. It is suggested that reactive species from the plasma generation are the cause of liquid acidification and bactericidal activity.

Along similar lines, plasma devices inoculated with 20 µl of *E. coli* and plasma activated for Δt= 30,60,90,120s were placed in sterile bags and thoroughly rinsed with 1 ml of Type 1 (ultrapure) Milli-Q® water. For each sample, the pH of the corresponding volume of water was measured using an Accumet® AB 15 pH meter, which has an

accuracy of ± 0.01. This process was repeated for both FR4 and SC dielectric devices. Before measuring the pH, the meter was standardized using pH buffer solution. The pH of LB broth used to make the *E. coli* sample was measured as 7.16 and that of the *E. coli* sample itself was measured to be 6.77. The variation of pH is given below in Figure 5-29.

Figure 5-29 indicates that the reduction of pH is greater in the case of FR4 as compared to SC. However unlike the strong reduction in pH values noted by Oehmigen et al. [111], there is not a strong pH change in our results (both FR4 and SC). Thus it is most likely that rapid acidification plays some role but not a major one in bacterial cell death. Note that the pH value does not vary much, except during the last 30s (for FR4) and not at all for SC.

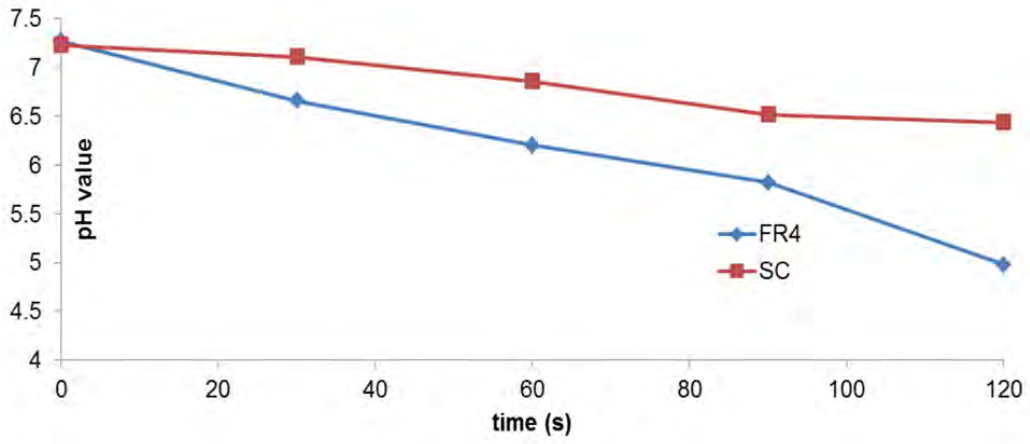

Figure 5-29. Plot of pH values, obtained by rinsing devices with Millipore water after plasma generation and measuring the pH value of this water in each case. Both FR4 and SC dielectrics are compared.

This is again indicative of the effect of the liquid on the dielectric surface. Since the liquid bacterial sample deposited on the dielectric substrate does not evaporate until the very end of the sterilization time interval (for both FR4 and SC) the pH does not

change very much until the very end. This confirms that the liquid deposited on the dielectric substrate inhibits plasma generation.

Hence, the point at which all the liquid covering the electrode evaporates and plasma covers the entire electrode surface area is the point at which there is a steep rise in input power, emitted ozone levels and spectroscopic intensity. It is also at this point, where the steep drop in pathogen concentration occurs, thus indicating that there is a threshold time-point after which complete sterilization occurs. Dobrynin et al. [63] explore the plasma dosage required for bacterial inactivation in cases with and without water. Their results show that the plasma dosage required for complete bacterial inactivation in cases with water is lower than that required for cases without water. They also conclude that the presence of water and direct plasma are both required to achieve fast inactivation and that this inactivation is highly dependent on the amount of water. In the present cases, it is found that as long as the liquid bacterial sample is present on the surface of the plasma device, plasma generation and therefore, sterilization is hampered.

One way to explain this adverse effect is in terms of capacitance. If the FR4/SC plasma device is considered as a capacitor of capacitance (C_1), then the liquid layer spread uniformly on top of the device can be considered as a second capacitor of capacitance (C_2), connected in 'series' with C1. Thus the combined capacitance of this system would be

$$C = \frac{C_1 C_2}{C_1 + C_2} = \frac{C_2}{1 + \frac{C_2}{C_1}} \quad (5\text{-}8)$$

The impedance, Z_1 of the liquid layer varies inversely with the amount of liquid present on the surface of the device i.e. as the liquid evaporates, impedance Z_1 decreases. Since Z_1 is inversely proportional to capacitance, C_1 ($Z = \frac{1}{j\omega C}$), it follows that as Z_1 decreases, C_1 increases. Following this, as C_1 increases, the capacitance of the overall system (C) increases and thus, the energy stored in the system ($U= \frac{1}{2}CV^2$) increases, proving that the amount of the liquid on the surface of the plasma device is actually detrimental to the performance of the plasma device as a sterilizer. This is mirrored in Figure 4-5 i.e. more the inoculation volume, more the amount of liquid covering the electrode surface and hence more the sterilization time.

CHAPTER 6
CONCLUDING REMARKS & RECOMMENDATIONS FOR FUTURE WORK

Using a FR4 plasma device to generate DBD surface plasma, it is determined that a sterilization time of 2-3 minutes is required for complete inactivation of vegetative pathogens (*E. coli, Yeast)*. Sterilization tests with *G. stearothermophilus* spores required a sterilization time of 20 minutes for complete inactivation [112].

Two types of dielectric materials are investigated: FR4 (dielectric constant= 4.29) and semi-ceramic (dielectric constant= 3.00). Both kinds of substrate materials have not been investigated before in terms of plasma sterilization. It is observed that sterilization times are shorter and more reliable in the case of FR4 as compared to semi-ceramic. Diagnostic data measured during plasma generation in both cases (spectral signature, emitted ozone levels, surface temperature, absorbed RF input power) also highlighted FR4 as the superior dielectric, when compared to SC.

It is also found that a higher input voltage led to a higher absorbed input power, thus leading to a complete sterilization. For the plasma devices used, the threshold input power density required for complete sterilization is calculated to be ~2.71 W/cm^2. At a higher input frequency, it is found that a lower input voltage (10 kV p-p) is required for complete sterilization.

Lastly, in terms of parameter analysis, the effect of reduced pressures on sterilization effectiveness is also examined. Sterilization effectiveness is examined at P= 400,500 and 600 Torr, for plasma exposure times of 1 and 2 minutes. The sterilization effectiveness at the reduced pressures is found to be similar to that at atmospheric pressure. Spectroscopic studies showed that the spectral pattern characteristic of the generated DBD plasma shows intensity peaks at wavelengths characteristic of the 2nd

positive system of N_2. FR4 and SC plasma devices showed intensity peaks at same wavelengths, although they differ in intensity values shown at each wavelength. Since no notable wavelengths below λ= 300 nm are observed, it is concluded that UV irradiation is likely not a mechanism in surface plasma sterilization at atmospheric pressure. This is also confirmed by the Rifampin studies.

The dissipation rates of ozone, during and after plasma generation using the different FR4/SC substrates as well as using sterilization chambers of different sterilization volumes, are determined. It is observed that the FR4 substrate used produces greater levels of ozone as compared to the SC substrate, during plasma generation. It is also observed that the chamber volume determines the dissipation of produced ozone inside the chamber.

Ozone exposure tests, in which an initial concentration of *E. coli* is exposed to ozone produced during plasma generation, demonstrated that this initial concentration is ~99.99% inactivated after 7 minutes of ozone exposure (in the case of an inoculated FR4/SC substrate). The required levels of ozone for this inactivation are determined to be 120-150 ppm.

In order to prove that bacterial inactivation on exposure to air excited by plasma generation is due to the produced ozone, two independent tests areconducted. Activated charcoal is used to adsorb the produced ozone, following which an exposure test demonstrated no significant bacterial inactivation. Also plasma treatment of inoculated devices in a nitrogen-rich environment also produced negligible reduction in bacterial concentration, which proved that when plasma was generated in a nitrogen-

rich environment (i.e. an environment low in ozone), sterilization efficiency was significantly reduced.

Measurement of surface temperatures during plasma generation demonstrates average non-uniform surface temperatures of 320-340 K in the case of FR4 and 310-315 K in the case of SC. Sterilization tests in which bacterial concentrations are heated to these observed surface temperatures, using a hot plate, showed that the effect of temperature alone was not enough for complete bacterial inactivation.

Bacterial samples deposited on the dielectric surface and exposed to plasma possess a liquid component due to the culture broth used for bacterial growth. It is noted that as plasma is generated, the liquid sample slowly evaporates. The point at which the liquid completely evaporates has been observed to be the point at which an increase in spectroscopic intensity, ozone concentration, surface temperatures and absorbed input power is noticed. It is also at this point that a steep drop in pathogen concentration is observed. Thus it appears that the presence of liquid on the surface also determines the sterilization efficiency.

Microscopic analysis of *B. subtilis* biofilms exposed to plasma demonstrated that plasma exposure affected one particular cell function (matrix-production) as compared to another cell function (motility). This is important to know in order to determine the mechanism of cell death due to plasma exposure. On that note, fluorescence measurements also demonstrate that cell death is likely not due to rupturing of the cells due to electrostatic tension caused by charge accumulation on the cell membranes.

In understanding the mechanism of plasma sterilization, different factors have been examined and tested separately to determine their role in affecting sterilization

effectiveness. While the spectroscopic data implies that UV radiation is not a major factor in plasma sterilization and the spectroscopic data would have us believe that intensity is not important, it is prudent to exercise caution before eliminating their roles, especially the latter, completely. It is possible that even the photons emitted during plasma generation might be etching the bacterial species (photo-desorption), though probably in a minor capacity.

Similarly, ozone exposure tests indicate that exposure to highest concentrations of generated ozone for 2 minutes produces a ~4 $\log_{10}$ reduction in bacterial concentrations. The lethal effect of ozone has been proved. Considering that the bacterial sample resting on the surface absorbs most of the ozone produced initially during plasma generation , it is very possible that ozone plays a major role in plasma sterilization.

From the temperature studies, it is noted that heating an inoculated plasma device to an average surface temperature (noted during plasma generation) produces only 1-2 $\log_{10}$ reduction in bacterial concentrations. Hence temperature and ozone tests point to the fact that surface temperature and ozone might be playing a synergistic role in the sterilization process.

The volume of research discussed in this thesis has provided a substantial amount of information about the processes of surface plasma sterilization. It has also raised an additional number of interesting research avenues.

6.1 Scope of Technology

Work outlined in this study has already proved the effectiveness of DBD surface plasma in sterilizing pathogens. However only single plasma devices were tested. In order to further the scope of this technology, sterilization testing has to be conducted

using larger sterilization arrays. These arrays could be embedded with a grid-like arrangement of the current plasma devices. In testing these arrays, the inherent problem to be dealt with will be the huge amount of ozone being produced during plasma generation. While a single plasma device can produce 120-150 ppm of ozone during a 2 minute interval in an enclosed space, a larger array made up of several of these devices will definitely produce more ozone. Thus the volume of the chamber in which such an array is enclosed will be important.

Additionally, in testing for sterilization, the entire array will be inoculated with the bacterial sample. The devices themselves will be arranged on the array in a grid-like fashion, with a small gap between each row and each column of devices. During plasma generation, this gap will be inoculated, but not covered by plasma. This poses a problem in terms of sterilization and should be kept in mind, while designing the sterilization array.

In fact, work is currently underway in building such an array and testing it for sterilization purposes.

6.2 Further analysis of the mechanism of plasma sterilization

The microbiological information gained has highlighted that plasma exposure affects one cell function primarily. It has also highlighted a possible cause of cell death due to plasma exposure. In order to view the damage to the cells up-front, SEM analysis of the cells exposed to plasma is required.

Additionally, the direction of research afforded by plasma interaction with biofilms, wherein it has been observed that plasma affects a particular type of cell function, seems to be a very interesting direction of research to pursue. In this aspect, knockouts (cell types with a particular gene subtracted) can be studied further to

understand whether the lack of a particular gene affects the cell's reaction to plasma exposure.

On the plasma-side, an important research avenue to pursue would be to determine the rotational, vibrational and translational temperatures attained during plasma generation. These temperatures can be simulated using spectroscopic information or measuring using a more rigorous optical emission spectroscopy (OES) setup. Measurement of the rotational and vibrational temperatures during plasma generation helps determine the energy densities of the different species produced in plasma generation, thus providing further insight into the sterilization mechanism. Additionally, in this study, the role of ozone in bacterial inactivation has been discussed extensively. The effect of exposing bacterial concentrations to different ozone concentrations produced during plasma generation has been discussed. However owing to the highly coupled nature of the problem, it is a little harder to understand the role of ozone in the process of plasma sterilization itself. However, plasma generation also produces other reactive oxygen species (O, O^-, O_2^+). Due to the short reaction times of these species, it is much more difficult to detect these and analyze their role in plasma sterilization. However certain assays do exist that detect the oxidation of certain proteins that are integral to the cell structure [110]. Using these assays, it is possible to analyze the role of other reactive species in the process of plasma sterilization.

6.3 Numerical modeling in plasma sterilization

Abundant literature exists in the domain of numerical modeling of dielectric barrier discharge (DBD) plasma. The concentration of different chemical species emitted in a plasma discharge can be numerically modeled using chemical reactions and plasma transport parameters [113]. There also exists an abundance of literature in

the modeling of cell breakdown- the microbiological parameters involved, different mechanisms that can cause breakdown, threshold voltages that can irreversibly damage a cell. What is required is a coupling between the two problems: a single numerical model that simulates the penetration of plasma species into a bacterial cell, causing cellular breakdown. This numerical model should be able to map the cellular breakdown also, via chemical destruction of integral components of the bacterial cell or electrophoretic rupture of the cell wall.

For a numerical model resembling the structure of the cell wall, Dobrynin et al. [63] suggest the lipid peroxidation model as a valid model. Given below, in Figure 6-1 is a skeleton of chemical reactions that make up the lipid peroxidation model.

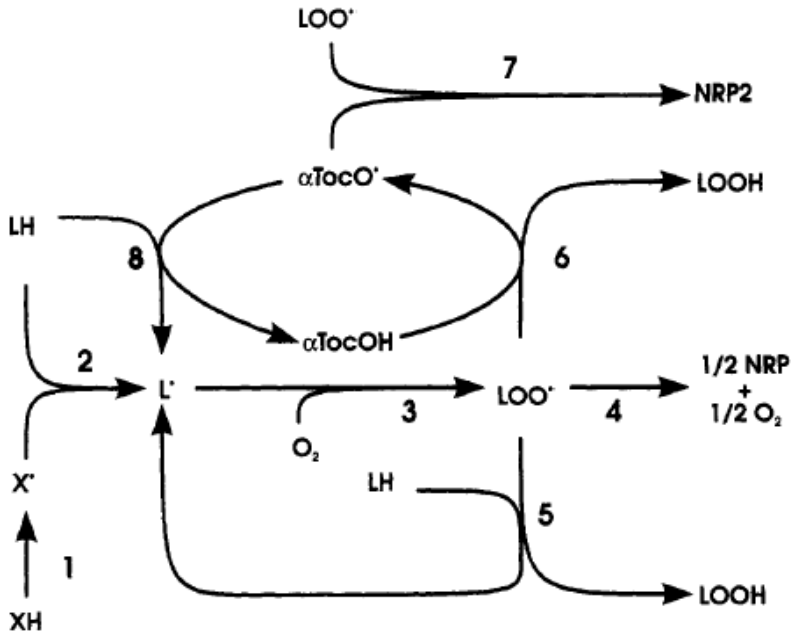

reaction no.	reaction	rate constant ($M^{-1} s^{-1}$)	ref/comment
1	$XH \rightarrow X^{\cdot}$		constant rate v_1 (radical influx) = 2.0×10^{-6} M s^{-1}
2	$X^{\cdot} + LH \rightarrow L^{\cdot}$		not rate-limiting; a value of 3.0 $M^{-1} s^{-1}$ was used
3	$L^{\cdot} + O_2 \rightarrow LOO^{\cdot}$	3×10^8	ref 9
4	$2LOO^{\cdot} \rightarrow NRP + O_2$	1×10^5	ref 5
5	$LOO^{\cdot} + LH \rightarrow LOOH + L^{\cdot}$	31	ref 14
6	$LOO^{\cdot} + TocOH \rightarrow LOOH + TocO^{\cdot}$	1×10^6	ref 6
7	$LOO^{\cdot} + TocO^{\cdot} \rightarrow NRP2$	2.5×10^6	ref 8
8	$TocO^{\cdot} + LH \rightarrow TocOH + L^{\cdot}$	7×10^{-2}	ref 7; this reaction is not included in the base case model

Figure 6-1. Scheme of reactions used for Lipid Peroxidation [114]

This scheme consists of seven coupled reactions. Reaction#1 is not used in the model, but is more of a starter reaction that sparks off the other reactions. Note that that coupling factor between this model and plasma air chemistry is oxygen. More complex lipid peroxidation models exist, that employ reactions with other reactive oxygen species, which are again common to plasma air chemistry models.

Thus, a combination of such a model as shown in Figure 6-1 and a numerical plasma-air chemistry model would have numerous coupled chemical reactions, all happening at the same instant, thus adding to computational complexity and time. The ionization rate is definitely dependent on other plasma parameters such as driving voltage, driving frequency, biological species being tested, electrode geometry etc. There is a huge dependency on biological species being tested because different species take different times for complete inactivation to be achieved. However this is estimated by the factor ‘t’ , which is the sterilization time.

Thus numerically simulating such a model poses a hefty challenge. In an earlier work [115] an attempt was made to correlate the rate of ionization during plasma generation to the sterilization pattern noted in a stamp test. However more work is needed in trying to understand the relation between the rate of ionization during plasma generation and its effect on influencing the sterilization time.

The road ahead is full of interesting questions to answer. With further research, the day is not too far off, when surface plasma sterilization will be implemented as a viable technology, promising safe, portable and fast sterilization.

REFERENCES

1. Tietjen L, Cronin W, McIntosh N (1992) Infection Prevention Guidelines for Family Planning Service Program. Durant, OK: Essential Medical Information Systems Inc.

2. Setlow P (2006) Spores of B.subtilis: their resistance to and killing by radiation, heat and chemicals. Journal of Applied Microbiology 101: 514-525.

3. Russell AD (1990) Bacterial spores and chemical sporicidal agents. Clinical Microbiology Reviews 3: 99-119.

4. Walker JT, Dickinson J, Sutton JM, Raven NDH, Marsh PD (2007) Cleanability of dental instruments- implication of residual protein and risks from Creutzfeldt-Jakob disease. British Dental Journal 203: 395-401.

5. Lee CH, Montville TJ, Sinskey AJ (1979) Comparison of the efficacy of steam sterilization indicators. Applied and Environmental Microbiology 37: 1113-1117.

6. Palenik CJ, Riggen SD, Celis LJ, Miller CH (1991) Effectiveness of steam autoclaving on the contents of sharps containers. American Journal of Infection Control 19: 103.

7. Prolo DJ, Pedrotti PW, White DH (1980) Ethylene oxide sterilization of bone, dura mater and fascia lata for human transplantation. Neurosurgery 6: 529-539.

8. Spaulding EH, Emmons EK, Guzara ML (1958) Ethylene Oxide Sterilization. The American Journal of Nursing 58: 1530-1531.

9. Borneff-Lipp M, Okpara J, Bodendorf M, Sonntag HG (1997) Validation of low-temperature plasma (LPT) sterilization systems: Comparison of two technical versions, the Sterrad 100, 1.8 and the 100 S. Hygiene und Mikrobiologie 3: 21-28.

10. Jacobs P, Kowatsch R (1993) Sterrad Sterilization System: A new technology for instrument sterilization. Endoscopic surgery and allied technologies 1: 57-58.

11. Jacobs PT, Lin SM (1987) Hydrogen Peroxide Plasma Sterilization System.

12. Aquino KAdS (2012) Sterilization by Gamma Irradiation. In: Adrovic F, editor. Gamma Radiation: InTech.

13. Kowlaski WJ, Bahnfleth WP (2000) UVGI design basics for air and surface disinfection. Heating/Piping/AirConditioning Engineering. 100-110 p.

14. Lerouge S, Wertheimer MR, Yahia LH (2001) Plasma sterilization: a review of parameters, mechanisms and limitations. Plasmas and Polymers 6: 175-188.

15. Graham GS (1998) Industrial Applications of Plasma Sterilization. In: Booth AF, editor. Sterilization of Medical Devices: CRC Press.

16. Moisan M, Barbeau J, Moreau S, Pelletier J, Tabrizian M, et al. (2001) Low Temperature Sterilization using gas plasmas: A review of the experiments and an analysis of the inactivation mechanism. International Journal of Pharmaceutics 226: 1-21.

17. Laroussi M (1996) Sterilization of Contaminated Matter with an Atmospheric Pressure Plasma. Plasma Science, IEEE Transactions on 24: 1188-1191.

18. Koulik P, Begounov S, Goloviatinskii S (1999) Atmospheric Plasma Sterilization and Deodorization of Dielectric Surfaces. Plasma Chemistry and Plasma Processing 19: 311-326.

19. Kelly-Wintenberg K, Hodge A, Montie TC, Deleanu L, Sherman D, et al. (1999) Use of a one atmosphere uniform glow discharge plasma to kill a broad spectrum of microorganisms. Journal of Vacuum Science & Technology A: Vacuum, Surfaces and Films 17: 1539-1544.

20. Kalghatgi S, Kelly CM, Cerchar E, Torabi B, Alekseev O, et al. (2011) Effects of Non-Thermal Plasma on Mammalian Cells. PLoS ONE 6: e16270.

21. Fridman A (2008) Plasma Chemistry: Cambridge University Press.

22. Bogaerts A, Neyts E, Gijbels R, van der Mullen J (2002) Gas discharge plasmas and their applications. Spectrochimica Acta Part B: Atomic Spectroscopy 57: 609-658.

23. Conrads H, Schmidt M (2000) Plasma generation and plasma sources. Plasma Soures SciTechnol 9: 441-454.

24. Kogelschatz U (2003) Dielectric-barrier Discharges: Their History, Discharge Physics and Industrial Applications. Plasma Chemistry and Plasma Processing 23: 1-46.

25. Gaunt LF, Beggs CB, Georghiou GE (2006) Bactericidal action of the reactive species produced by gas-discharge non-thermal plasma at atmospheric pressure: A Review. Plasma Science, IEEE Transactions on 34: 1257-1269.

26. Haverkamp RG, Miller BB, Free KW (2002) Ozone Production in a High Frequency Dielectric Barrier Discharge Generator. Ozone: Science & Engineering 24: 321-328.

27. Chu PK, Chen JY, Wang LP, Huang N (2002) Plasma-surface modification of biomaterials. Materials Science and Engineering: R: Reports 36: 143-206.

28. Shiloh J, Rosenberg A, Wurzberg E (2001) Modular Dielectric Barrier Discharge device for pollution abatement.

29. Kalghatgi SU, Fridman G, Fridman A, Friedman G, Clyne AM. Non-thermal Dielectric Barrier Discharge Plasma Treatment of Endothelial Cells; 2008. pp. 3578-3581.

30. Fridman G, Friedman G, Gutsol A, Shekhter AB, Vasilets VN, et al. (2008) Applied Plasma Medicine. Plasma Processes and Polymers 5: 503-533.

31. Fridman G, Peddinghaus M, Balasubramanian M, Ayan H, Fridman A, et al. (2006) Blood Coagulation and Living Tissue Sterilization by Floating-Electrode Dielectric Barrier Discharge in Air. Plasma Chemistry and Plasma Processing 26: 425-442.

32. Fridman G, Shereshevsky A, Jost MM, Brooks AD, Fridman A, et al. (2007) Floating Electrode Dielectric Barrier Discharge Plasma in Air promoting Apoptotic Behaviour in Melanoma Skin Cancer Cell Lines. Plasma Chemistry and Plasma Processing 27: 163-176.

33. Cooper M, Fridman G, Staack D, Gutsol AF, Vasilets VN, et al. (2009) Decontamination of surfaces from Extremophile Organisms using Nonthermal Atmospheric-Pressure Plasmas. Plasma Science, IEEE Transactions on 37: 866-871.

34. Klampfl TG, Isbary G, Shimizu T, Li YF, Zimmermann JL, et al. (2012) Cold Atmospheric Air Plasma Sterilization against Spores and Other Microorganisms of Clinical Interest. Applied and Environmental Microbiology 78: 5077-5082.

35. Heinlin J, Morfill G, Landthaler M, Stolz W, Isbary G, et al. (2010) Plasma medicine: possible applications in dermatology. Journal der Deutschen Dermatologischen Gesellschaft 8: 968-976.

36. Jiang C, Chen MT, Gorur A, Schaudinn C, Jaramilo DE, et al. (2009) Nanosecond Pulsed Plasma Dental Probe. Plasma Processes and Polymers 6: 479-483.

37. Sladek REJ, Stoffels E, Walraven R, Tielbeek PJA, Koolhoven RA (2004) Plasma Treatment on Dental Cavities: A Feasibility Study. Plasma Science, IEEE Transactions on 32: 1540-1543.

38. Menashi WP (1968) Treatment of Surfaces.

39. Boucher RM (1980) Seeded gas plasma sterilization method.

40. Bithell RM (1982) Package and sterilizing process for same.

41. Ratner BD, Chilkot A, Lopez GP (1990) Plasma Deposition, Treatment and Etching of Polymers. San Diego, CA.

42. Baier RE, Carter JM, Sorensen SE, Meyer AE, McGowan BD, et al. (1992) Radio-frequency gas plasma (glow discharge) disinfection of dental operative instruments, including handpieces. JOralImplantol: 236-242.

43. Park BJ, Lee DH, Park JC, Lee IS, Lee KY, et al. (2003) Sterilization using a microwave-induced argon plasma system at atmospheric pressure. Physics of Plasmas 10: 4539.

44. Trompeter FJ, Neff WJ, Franken O, Heise M, Neiger M, et al. (2002) Reduction of Bacillus subtilis and Aspergillus niger spores using nonthermal atmospheric gas discharges. Plasma Science, IEEE Transactions on 30: 1416-1423.

45. Lee K-Y, Park BJ, Lee DH, Lee I-S, Hyun SO, et al. (2005) Sterilization of E.coli and MRSA using microwave-induced argon plasma at atmospheric pressure. Surface & Coatings Technology 193: 35-38.

46. Nelson CL, Berger TJ (1989) Inactivation of micro-organisms by oxygen gas plasma. Curr Microbiol: 275-276.

47. Roth JR (1995) Steady-state glow discharge plasma.

48. Yu H, Xiu ZH, Ren CS, Zhang JL, Wang DZ, et al. (2005) Inactivation of yeast by Dielectric Barrier Discharge Plasma in Helium at Atmospheric Pressure. IEEE Transactions on Plasma Science.

49. Sun Y, Qiu Y, Nie A, Wang X (2007) Experimental Research on Inactivation of Bacteria using Dielectric Barrier Discharge. IEEE Transactions on Plasma Science 35.

50. Tanino M, Xilu W, Takashima K, Katsura S, Mizuno A (2007) Sterilization using Dielectric Barrier Discharge at Atmospheric Pressure. Intl Journal of Plasma Environmental Science & Technology 1.

51. Deng S, Cheng C, Ni G, Meng Y, Chen H (2008) Bacterial Inactivation by Atmospheric Pressure Dielectric Barrier Discharge Plasma Jet. Japanese Journal of Applied Physics 47: 7009.

52. Joshi SG, Paff M, Friedman G, Fridman G, Fridman A, et al. (2010) Control of MRSA in planktonic form and biofilms: A biocidal efficacy study of non-thermal dielectric barrier discharge plasma. American Journal of Infection Control 38: 293-301.

53. Hury S, Vidal DR, Desor F, Pelletier J, Lagarde T (1998) A parametric study of the destruction efficiency of bacillus spores in low pressure oxygen-based plasmas. LettAppl Microbiol 26: 417-421.

54. Lerouge S, Wertheimer MR, Marchand R, Tabrizian M, Yahia LH (1999) Effect of gas composition on spore mortality and etching during low-pressure plasma sterilization. Journal of biomedical materials research 51: 128-135.

55. Ying J, Chunsheng R, Zhilong X, Dezhen W, Younian W, et al. (2006) Comparison of yeast inactivation treated in He, Air and N2 DBD Plasma. Plasma Science & Technology 8: 720.

56. Wrobel AM, Lamontagne B, Wertheimer MR (1988) Large-area microwave and radiofrequency plasma etching of polymers. Plasma Chemistry and Plasma Processing 8: 315-329.

57. Chau T, Kao K, Blank G, Madrid F (1996) Microwave plasmas for low-temperature dry sterilization. Biomaterials 17: 1273-1277.

58. Bol'shakov AA, Cruden,B.A., Mogul,R., Rao,M.V.V.S., Sharma,S.P., Khare,B.N., Meyyappan,M., (2004) Radio-Frequency Oxygen Plasma as a Sterilization Source. AIAA Journal 42: 823-832.

59. Lerouge S, Fozza AC, Wertheimer MR, Marchand R, Yahia LH (2000) Sterilization by low-pressure plasma: the role of Vacuum-UV radiation. Plasma and Polymers 5: 31-46.

60. Moreau S, Moisan M, Tabrizian M, Barbeau J, Pelletier J, et al. (2000) Using the flowing afterglow of a plasma to inactivate B.subtilis spores: influence of the operating conditions. Journal of Applied Physics 88: 1166-1174.

61. Sohbatzadeh F, Colagar AH, Mirzanejhad S, Mahmodi S (2010) E.coli, P.aeruginosa and B.cereus Bacteria Sterilization using Afterglow of Non-Thermal Plasma at Atmospheric Pressure. Applied Biochemistry and Biotechnology 160: 1978-1984.

62. Philip N, Saoudi B, Crevier M-C, Moisan M, Barbeau J, et al. (2002) The Respective Roles of UV Photons and Oxygen Atoms in Plasma Sterilization at Reduced Gas Pressure: The Case of N2-O2 mixtures. Plasma Science, IEEE Transactions on 30: 1429-1436.

63. Dobrynin D, Fridman G, Friedman G, Fridman A (2009) Physical and biological mechanisms of direct plasma interaction with living tissue. New Journal of Physics 11: 115020.

64. Kong MG, Kroessen G, Morfill G, Nosenko T, Shimizu T, et al. (2009) Plasma medicine: an introductory review. New Journal of Physics 11: 115012.

65. Rastogi RP, Kumar A, Tyagi MB, Sinha RP (2010) Molecular mechanisms of ultraviolet radiation-induced DNA damage and repair. Journal of nucleic acids.

66. Halfmann H, Denis B, Bibinov N, Wunderlich J, Awakowicz P (2007) Identification of the most efficient VUV/UV radiation for plasma based inactivation of Bacillus atrophaeus spores. Journal of Physics D: Applied Physics 40: 5907.

67. Moisan M, Barbeau J, Crevier MC, Pelletier J, Philip N, et al. (2002) Plasma Sterilization. Methods and Mechanisms. Pure Appl Chem 74: 349-358.

68. Laroussi M, Leipold F (2004) Evaluation of the roles of reactive species, heat and UV radiation in the inactivation of bacterial cells by air plasmas at atmospheric pressure. International Journal of Mass Spectrometry 233: 81-86.

69. Laroussi M, Mendis DA, Rosenberg M (2003) Plasma interaction with microbes. New Journal of Physics 5: 41.41-41.10.

70. Stoffels E, Sakiyama Y, Graves DB (2008) Cold Atmospheric Plasma: Charged Species and Their Interactions with Cells and Tissues. Plasma Science, IEEE Transactions on 36: 1441-1457.

71. Laroussi M (2005) Low temperature Plasma-based sterilization: Overview and State of the Art. Plasma Processes & Polymers 2: 391-400.

72. Broadwater WT, Hoehn RC, King PH (1973) Sensitivity of Three Selected Bacterial species to Ozone. Applied Microbiology 26: 391-393.

73. Sweet F, Kao M-S, Lee SC, Hagar WL, Sweet WE (1980) Ozone selectively Inhibits Growth of Human Cancer Cells. Science 209: 931-933.

74. Efremov NM, Adamiak BY, Blochin VI, Dadashev SJ, Dmitriev KI, et al. (2000) Action of a Self-Sustained Glow Discharge in Atmospheric Pressure Air on Biological Objects. Plasma Science, IEEE Transactions on 28: 238-241.

75. Ohkawa H, Akitsu T, Tsuji M, Kimura H, Kogoma M, et al. (2006) Pulse-modulated high frequency plasma sterilization at atmospheric pressure. Surface and Coatings Technology 200: 5829-5835.

76. Mastanaiah N, Saxena U, Johnson J, Roy S (2010) Inactivation of Yeast cell using Dielectric Barrier Discharge. In 48th AIAA Aerospace Sciences Meeting, Orlando.

77. Brelles-Marino G (2010) Bacterial Biofilm Inactivation by Gas-Discharge Plasmas. Biological and Environmental Applications of Gas Discharge Plasmas: Nova Science Publisher.

78. Sladek REJ, Filoche,S.K., Sissons,C.H., Stoffels,E., (2007) Treatment of Steptococcus mutans biofilms with a nonthermal atmospheric plasma. Letters in Applied Microbiology 45: 318-323.

79. Vandervoort KG, Abramzon,N., Brelles-Marino,G., (2008) Plasma Interactions with bacterial biofilms as visualized through Atomic Force Microscopy. Plasma Science, IEEE Transactions on 36: 1296-1297.

80. Lee MH, Park BJ, Jin SC, Kim D, Han I, et al. (2009) Removal and sterilization of biofilms and planktonic bacteria by microwave-induced argon plasma at atmospheric pressure. New Journal of Physics 11: 115022.

81. Kumar R, Saurav S, Titov EV, Levin DA, Long RF, et al. (2011) Thermo-structural studies of spores subjected to high temperature gas environments. International Journal of Heat and Mass Transfer 54: 755-765.

82. Gallagher MJ, Vaze N, Gangoli S, Vasilets VN, Gutsol AF, et al. (2007) Rapid Inactivation of Airborne Bacteria using Atmospheric Pressure Dielectric Barrier Grating Discharge. Plasma Sciences, IEEE Transactions on 35: 1501-1510.

83. Akishev Y, Grushin M, Karalnik V, Trushkin N, Kholodenko V, et al. (2008) Atmospheric Pressure Nonthermal Plasma sterilization of microorganisms in liquids and on surfaces. Pure and Applied Chemistry 80: 1953-1969.

84. Pintassilgo CD, Loureiro J, Guerra V (2005) Modelling of a N2-O2 flowing afterglow for plasma sterilization. Journal of Physics D:Applied Physics 38: 417-430.

85. Kutasi K, Pintassilgo CD, Coelho PJ, Loureiro J (2006) Modeling of a post-dischare reactor used for plasma sterilization. Journal of Physics D: Applied Physics 39: 3978.

86. Babaeva NY, Kushner MJ (2010) Intracellular electric fields produced by dielectric barrier discharge treatment of skin. Journal of Physics D: Applied Physics 43: 185206.

87. Tripathi P, Beaussart A, Andre G, Rolain T, Lebeer S, et al. (2012) Towards a nanoscale view of lactic acid bacteria. Micron 43: 1323-1330.

88. Antifungals (http://www.sigmaaldrich.com/technicaldocuments/articles/biofiles/antifungals.html.

89. Lectures on Microbial Growth. Rutgers University.

90. Niemela S (2003) Uncertainty of quantitative determinations derived by cultivation of microorganisms: Centre for Metrology and Accreditation.

91. Kearns DB, Chu F, Branda SS, Kolter R, Losick R (2005) A master regulator for biofilm formation by Bacillus subtilis. Molecular Microbiology 55: 739-749.

92. Kearns DB, Losick R (2003) Swarming motility in undomesticated B.subtilis. Molecular Microbiology 49: 581-590.

93. Branda SS, Gonzalez-Pastor JE, Dervyn E, Ehrlich D, Losick R, et al. (2004) Genes involved in the formation of structured multicellular communities by Bacillus subtilis. Journal of Bacteriology 186: 3970-3979.

94. Branda SS, Gonzalez-Pastor JE, Ben-Yehuda S, Losick R, Kolter R (2001) Fruiting body formation by Bacillus Subtilis. ProcNatlAcadSci 98: 11621-11626.

95. Gordon R, Haynes W, Pang C (1989) The genus bacillus. US Department of Agriculture handbook. pp. 109-126.

96. Mackey BM, Miles CA, Parsons SE, Seymour DA (1991) Thermal denaturation of whole cells and cell components of Escherichia coli examined by differential scanning calorimetry. Journal of General Microbiology 137: 2361-2374.

97. Pearse RWB, Gaydon AG (1976) The Identification of Molecular Spectra. London: Chapman and Hall.

98. .Choi JH, Han I, Baik HK, Lee MH, Han DW, et al. (2006) Analysis of Sterilization Effect by pulsed dielectric barrier discharge. Journal of Electrostatics 64: 17-22.

99. Staack D, Farouk B, Gutsol AF, Fridman A (2006) Spectroscopic studies and rotational and temperature measurements of atmospheric pressure normal glow plasma discharges in air. Plasma Sources Science and Technology 15: 818-827.

100. Staack D, Farouk B, Gutsol A, Fridman A (2007) Spatially resolved Temperature Measurements of Atmospheric Pressure Normal Glow Microplasmas in Air. Plasma Science, IEEE Transactions on 35: 1448-1455.

101. Eliasson B, Hirth M, Kogelschatz U (1987) Ozone synthesis from oxygen in dielectric barrier discharges. Journal of Physics D: Applied Physics 20: 1421-1437.

102. Singh KP, Roy S (2007) Modeling plasma actuators with air chemistry for effective flow control. Journal of Applied Physics 101: 123308.

103. Singh KP, Roy S (2008) Force approximation for a plasma actuator operating in atmospheric air. Journal of Applied Physics 103: 013305.

104. Ayan H, Fridman G, Staack D, Gutsol AF, Vasilets VN, et al. (2009) Heating Effect of Dielectric Barrier Discharge for Direct Medical Treatment. Plasma Science, IEEE Transactions on 37: 113-120.

105. Cho M, Kim J, Kim J, Yoon J, Kim J (2010) Mechanisms of Escherichia coli inactivation by several disinfectants. Water Research 44: 3410-3418.

106. Zhang Y, Wu Q, Zhang J, Yang X (2011) Effects of ozone on membrane permeability and ultrastructure in Pseudomonas aeruginosa. Journal of Applied Microbiology 111: 1006-1015.

107. Norton M, Spilkia A, Godoy VG (2013) Antibiotic resistance acquired through a DNA damage-inducible response in Acinetobacter baumannii. Journal of Bacteriology 195: 1335-1345.

108. Vlamakis H, Aguilar C, Losick R, Kolter R (2008) Control of cell fate by the formation of an architecturally complex bacterial community. Genes & Development 22: 945-953.

109. Kearns DB, Chu F, Rudner R, Losick R (2004) Genes governing swaming in Bacillus subtilis and evidence for a phase variation mechanism controlling surface motility. Molecular Microbiology 52: 357-369.

110. Joshi SG, Cooper M, Yost A, Paff M, Ercan UK, et al. (2011) Nonthermal Dielectric-Barrier Discharge Plasma-Induced Inactivation involves oxidative DNA damage and Membrane Lipid Peroxidation in Escherichia coli. Antimicrobial Agents and Chemotherapy 55: 1053-1062.

111. Oehmigen K, Hahnel M, Brandenburg R, Wilke C, Weltmann KD, et al. (2010) The role of Acidification for Antimicrobial Activity of Atmospheric Pressure Plasma in Liquids. Plasma Processes & Polymers 7: 250-257.

112. Mastanaiah, N., Johnson, JA., Roy, S., “Effect of Dielectric and Liquid on Plasma Sterilization using Dielectric Barrier Discharge Plasma”. PLoS One (In Press), July 2013.

113. Singh KP, Roy S (2007) Modeling plasma actuators with air chemistry for effective flow control. Journal of Applied Physics 101.

114. Abuja PM, Esterbauer H. (1995) Simulation of lipid peroxidation in low-density lipoprotein by a basic" skeleton" of reactions. Chemical research in toxicology 8(5): 753-763

115. Mastanaiah N, Wang CC, Johnson JA, Roy S (2011) A computational diagnostic tool for understanding plasma sterilization. In 49th AIAA Aerospace Sciences Meeting, Orlando.

BIOGRAPHICAL SKETCH

In 2003, Navya began her undergraduate studies at the Indian Institute of Technology (IIT), Madras, India, where she went on to receive her bachelors degree in Aerospace Engineering. After finishing her undergraduate curriculum in 2007, Navya received a partial scholarship from the University of Florida, to pursue a Master of Science (M.S.) degree in Aerospace Engineering. Under the guidance of Dr.Subrata Roy, she began working towards her doctoral degree in Aerospace Engineering in 2008.